LONG-TERM INVESTIGATION OF THE LUNAR TIDE IN THE EQUATORIAL ELECTROJET DURING STRATOSPHERIC SUDDEN WARMINGS

Kumulative Dissertation
zur Erlangung des akademischen Grades
"doctor rerum naturalium"
(Dr. rer. nat.)
in der Wissenschaftsdisziplin "Geophysik"

eingereicht an der
Mathematisch-Naturwissenschaftlichen Fakultät
der Universität Potsdam

von

TARIQUE ADNAN SIDDIQUI

Institut für Erd- und Umweltwissenschaften

Mai 2017

SUPERVISORS:
Hauptbetreuer : Prof. Dr. Claudia Stolle
Zweitbetreuer : Prof. Dr. Jorge L. Chau

Published online at the
Institutional Repository of the University of Potsdam:
URN urn:nbn:de:kobv:517-opus4-406384
http://nbn-resolving.de/urn:nbn:de:kobv:517-opus4-406384

In memory of my grandparents . . .

ABSTRACT

The ionosphere, which is strongly influenced by the Sun, is known to be also affected by meteorological processes. These processes, despite having their origin in the troposphere and stratosphere, interact with the upper atmosphere. Such an interaction between atmospheric layers is known as vertical coupling. During geomagnetically quiet times, when near-Earth space is not under the influence of solar storms, these processes become important drivers for ionospheric variability. Studying the link between these processes in the lower atmosphere and the ionospheric variability is important for our understanding of fundamental mechanisms in ionospheric and meteorological research.

A prominent example of vertical coupling between the stratosphere and the ionosphere are the so-called stratospheric sudden warming (SSW) events that occur usually during northern winters and result in an increase in the polar stratospheric temperature and a reversal of the circumpolar winds. While the phenomenon of SSW is confined to the northern polar stratosphere, its influence on the ionosphere can be observed even at equatorial latitudes. During SSW events, the connection between the polar stratosphere and the equatorial ionosphere is believed to be through the modulation of global atmospheric tides. These tides are fundamental for the ionospheric E-region wind dynamo that generates electric fields and currents in the ionosphere. Observations of ionospheric currents indicate a large enhancement of the semidiurnal lunar tide in response to SSW events. Thus, the semidiurnal lunar tide becomes an important driver of ionospheric variability during SSW events

In this thesis, the ionospheric effect of SSW events is investigated in the equatorial region, where a narrow but an intense E-region current known as the equatorial electrojet (EEJ) flows above the dip equator during the daytime. The day-to-day variability of the EEJ can be determined from magnetic field records at geomagnetic observatories close to the dip equator. Such magnetic data are available for several decades and allows to investigate the impact of SSW events on the EEJ and, even more importantly, helps in understanding the effects of SSW events on the equatorial ionosphere. An excellent long-term record of the geomagnetic field at the equator from 1922 onwards is available for the observatory Huancayo in Peru and is extensively utilized in this study.

The central subject of this thesis is the investigation of lunar tides in the EEJ during SSW events by analyzing long time series. This is done by estimating the lunar tidal amplitude in the EEJ from the magnetic records at Huancayo and by comparing them to measurements of the po-

lar stratospheric wind and temperature, which led to the identification of the known SSW events from 1952 onwards. One goal of this thesis is to identify SSW events that predate 1952. To this end, superposed epoch analysis (SEA) is employed to establish a relationship between the lunar tidal power and the wind and temperature conditions in the lower atmosphere. A threshold value for the lunar tidal power is identified that is discriminative for the known SSW events. This threshold is then used to identify lunar tidal enhancements, which are indicative for any historic SSW events prior to 1952. It can be shown, that the number of lunar tidal enhancements and thus the occurrence frequency of historic SSW events between 1926 and 1952 is similar to the occurrence frequency of the known SSW events from 1952 onwards.

Next to the classic SSW definition, the concept of polar vortex weakening (PVW) is utilized in this thesis. PVW is defined for higher latitudes and altitudes ($\approx$ 40km) than the classical SSW definition ($\approx$ 32km). The correlation between the timing and magnitude of lunar tidal enhancements in the EEJ and the timing and magnitude of PVW is found to be better than for the classic SSW definition. This suggests that the lunar tidal enhancements in the EEJ are closely linked to the state of the middle atmosphere.

Geomagnetic observatories located in different longitudes at the dip equator allow investigating the longitudinally dependent variability of the EEJ during SSW events. For this purpose, the lunar tidal enhancements in the EEJ are determined for the Peruvian and Indian sectors during the major SSW events of the years 2006 and 2009. It is found that the lunar tidal amplitude shows similar enhancements in the Peruvian sector during both SSW events, while the enhancements are notably different for the two events in the Indian sector.

In summary, this thesis shows that lunar tidal enhancements in the EEJ are indeed correlated to the occurrence of SSW events and they should be considered a prominent driver of low latitude ionospheric variability. Secondly, lunar tidal enhancements are found to be longitudinally variable. This suggests that regional effects, such as ionospheric conductivity and the geometry and strength of the geomagnetic field, also play an important role and have to be considered when investigating the mechanisms behind vertical coupling.

ZUSAMMENFASSUNG

Die Ionosphäre, die hauptsächlich durch Prozesse solaren Ursprungs beeinflusst wird, wird auch durch meteorologische Prozesse beeinflusst. Obwohl diese Prozesse ihren Ursprung in der Troposphäre und Stratosphäre haben, wechselwirken sie mit der oberen Atmosphäre. Eine solche Wechselwirkung zwischen atmosphärischen Schichten wird als vertikale Kopplung bezeichnet. Bei magnetisch ruhigen Bedingungen, wenn der erdnahe Weltraum nicht durch solare Stürme beeinflusst wird, werden diese Prozesse zu wichtigen Einflussfaktoren für die ionosphärische Variabilität. Für unser Verständnis von fundamentalen Mechanismen im Forschungsfeld der Ionosphäre und der Meteorologie ist es wichtig, die Verbindung zwischen diesen Prozessen in der unteren Atmosphäre und der ionosphärischen Variabilität zu ermitteln.

Ein wichtiges Beispiel für die vertikale Kopplung zwischen Stratosphäre und Ionosphäre sind die sogenannten plötzlichen stratosphärischen Erwärmungsereignisse (sudden stratospheric warming, SSW), die üblicherweise im Winter stattfinden und zu einer Erhöhung der stratosphärischen Temperatur und einer Umkehrung der zirkumpolaren Winde führen. Während das Phänomen des SSW auf die nördliche polare Stratosphäre beschränkt ist, kann sein Einfluss auf die Ionosphäre sogar in äquatorialen Breiten beobachtet werden. Bei SSW - Ereignissen wird vermutet, dass die Verbindung zwischen der polaren Stratosphäre und der äquatorialen Ionosphäre durch die Modulation globaler atmosphärischer Gezeiten erfolgt. Diese Gezeiten sind grundlegend für den Wind-Dynamo in der ionosphärischen E-Region, der dort elektrische Felder und Ströme erzeugt. Beobachtungen ionosphärischer Ströme zeigen, dass die semidiurnalen lunaren Gezeiten als Reaktion auf ein SSW - Ereignis eine starke Erhöhung erfahren. Damit werden die semidiurnalen lunaren Gezeiten zu einem wichtigen Faktor für die ionosphärische Variabilität während eines SSW - Ereignis.

In dieser Dissertation wird der äquatoriale ionosphärische Effekt von SSW-Ereignissen untersucht. In der E-Region über dem magnetischen Äquator fließt tagsüber ein schmaler aber intensiver Strom, der als äquatorialer Strahlstrom oder Elektrojet (EEJ) bekannt ist. Der von Tag zu Tag unterschiedlich ausgeprägte EEJ kann aus Magnetfeldregistrierungen von geomagnetischen Observatorien nahe dem magnetischen Äquator abgeschätzt werden. Solche Magnetfeldregistrierungen stehen über mehrere Jahrzehnte zur Verfügung und erlauben es, den Einfluss der SSW-Ereignisse auf den EEJ zu untersuchen, und, noch wesentlicher, helfen sie, den Einfluss von SSW-Ereignissen auf die äquatoriale Ionosphäre zu verstehen. Eine ausgezeichnete, im Jahre 1922 beginnende Langzeit-Registrierung des Ma-

gnetfeldes am Äquator gibt es für das Observatorium Huancayo in Peru. Sie wird in der vorliegenden Arbeit intensiv genutzt.

Das zentrale Thema der Dissertation ist die Analyse von Langzeit - Registrierungen zur Untersuchung der lunaren Gezeiten des EEJ bei SSW - Ereignissen. Dazu wird die Amplitude der lunaren Gezeiten des EEJ aus den Magnetfeldregistrierungen des Observatoriums Huancayo bestimmt und mit den Messungen des polaren stratosphärischen Windes und der Temperatur verglichen, die zur Identifizierung der bekannten SSW - Ereignisse seit 1952 geführt haben. Ein Ziel der vorliegenden Arbeit ist es, auch SSW - Ereignisse vor 1952 zu identifizieren. Dahingehend wird eine Superposed Epoch Analysis (SEA) benutzt, und damit wird eine Beziehung zwischen die Leistung der lunaren Gezeiten und den Wind- und Temperaturbedingungen in der unteren Atmosphäre hergestellt. So wird ein Grenzwert für die Leistung der lunaren Gezeiten für die bekannten SSW - Ereignisse ermittelt. Dieser Grenzwert wird dann benutzt, um eine Verstärkung der lunaren Gezeiten zu identifizieren, die historische SSW-Ereignisse vor 1952 anzeigt. Es zeigt sich, dass die Häufigkeit der Verstärkung der lunaren Gezeiten, und damit die Häufigkeit der historischen SSW-Ereignisse zwischen 1926 und 1952, ähnlich ist zu der Häufigkeit der bekannten SSW-Ereignisse seit 1952 ist.

Neben der klassischen SSW - Definition wird in dieser Dissertation das Konzept des Polar Vortex Weakening (PVW) genutzt. Das PVW ist für höhere Breiten und Höhenlagen (40 km) festgelegt als die klassische SSW - Definition (32 km). Die Korrelation zwischen dem Zeitpunkt und der Stärke der Verstärkung der lunaren Gezeiten des EEJ einerseits und dem Zeitpunkt und der Stärke des PVW andererseits ist besser als die entsprechende Korrelation bei Anwendung der klassischen SSW - Definition. Dies lässt darauf schließen, dass die Verstärkung der lunaren Gezeiten des EEJ eng mit dem Zustand der mittleren Atmosphäre verknüpft ist.

Geomagnetische Observatorien, die bei verschiedenen Längengraden am magnetischen Äquator liegen, erlauben es, die längengradabhängige Variabilität des EEJ bei SSW - Ereignissen zu untersuchen. Zu diesem Zweck wird die Verstärkung der lunaren Gezeiten fär zwei ausgeprägte SSW - Ereignisse in den Jahren 2006 und 2009 im peruanischen und im indischen Sektor bestimmt. Es zeigt sich, dass die Amplitude der lunaren Gezeiten im peruanischen Sektor bei beiden Ereignissen eine ähnliche Verstärkung aufweist, während die Verstärkung im indischen Sektor für die zwei Ereignisse deutliche Unterschiede aufweist.

Zusammenfassend kann gesagt werden, dass die Verstärkung der lunaren Gezeiten des EEJ in der Tat mit dem Auftreten von SSW - Ereignissen korreliert ist und dass sie als wichtiger Einflussfaktor auf die Variabilität der Ionosphäre der niederen Breiten berücksichtigt werden muss. Außerdem konnte gezeigt werden, dass die Verstärkung der lunaren Gezeiten eine längengradabhängige Variabilität aufweist. Dies legt nahe, dass regio-

nale Gegebenheiten, wie die Leitfähigkeit der Ionosphäre und die Geometrie und Stärke des Erdmagnetfeldes, bei der vertikalen Kopplung auch eine wichtige Rolle spielen und bei der Untersuchung der dabei zugrundeliegenden Mechanismen berücksichtigt werden müssen.

ACKNOWLEDGEMENTS

It is rightly said that a journey is always more important than the destination. While continuing along the path during this doctoral journey, I must say that I've been quite fortunate to come across deeply motivated individuals who not only provided me with an excellent scientific guidance but were equally wonderful mentors.

First and foremost I'd like to express my sincere gratitude towards Prof. Dr. Hermann Lühr for continuously supporting me throughout my graduate and doctoral journey. I've been very fortunate to continue my research endeavors under his guidance. The countless discussions I've had with him have massively contributed to my understanding of the subject.

I am also deeply indebted to my doctoral supervisor Prof. Dr. Claudia Stolle for her immeasurable contributions in my development during these last three years. I would like to thank her for giving me the freedom to explore topics of my own interest and then continuously backing me towards success. This dissertation would have been practically impossible without her interminable support.

Much gratitude is also owed to my second doctoral supervisor Prof. Dr. Jorge L. Chau for his numerous feedbacks and motivating discussions that helped me to broaden my horizon and gain different perspectives on the subject. I also gratefully acknowledge the support of Dr. Jaeheung Park for his guidance and suggestions that led to significant improvement in the paper that he co-authored. I would also like to thank Dr. Yosuke Yamazaki for providing me helpful feedbacks on a draft version of this thesis. Major thanks goes to Dr. Jürgen Matzka for his scientific inputs that have been extremely valuable during my stay here at GFZ. I'd also especially thank him for helping me in writing the thesis's abstract and its translation.

I also greatly appreciate the discussions during the ISSI team meetings led by Dr. Nick Pedatella. I wish to express my appreciation to all the ISSI team members for their critical suggestions that have been very important during this work.

During my time in Potsdam, I was fortunate to make numerous friends both at workplace and outside. Their role in motivating me during difficult times cannot be quantified. I want to particularly thank Dr. Foteini Vervelidou, Robin Senftleben, Leonie Pick, Juan Rodriguez-Zuluaga, Juan Sebastian Cervantes, Nikita Aseev, Irina Zhelavskaya, Dr. Chao Xiong, Dr. Guram Kervalishvili, Dr. Maxwell Brown, Dr. Stefanie Weege and Huang-Tao in Section 2.3 at GFZ. Heartfelt thanks are due to Martina Krüger and Alex Jordan for their administrative and technical assistance during all these times.

Studying away from home and in a different culture can be a daunting task for anyone. Thankfully, I was able to meet a lot of fellow PhDs and post-docs from India and together we were able to make our stay in Potsdam quite productive and enjoyable. I'd especially acknowledge Dr. K. M. Bhatt, Dr. Sanjay Bora, Dr. Praveen K. Mishra, Dr. Prashant Pavashe, Dr. Naeem Khan, Dr. Rahul Lathe, Vikas, Namrata, Chiranjit, Tapas and Saurabh for being an important part of this journey. I also want to thank Dr. Subhadeep Paul for encouraging me to pursue doctoral studies after we graduated.

I'd like to acknowledge the support of GFZ Potsdam for funding my doctoral studies and sponsoring my travel grants. A big thanks to André Miede for providing his template `classicthesis` for LaTeX which was used to typeset this thesis.

Lastly, I'd like to thank my parents and my siblings for without their constant support this journey would not have been possible.

CONTENTS

LIST OF FIGURES

LIST OF TABLES

Part I

INTRODUCTION

1 INTRODUCTION

1.1 THE EARTH'S IONOSPHERE

The ionosphere is the part of the Earth's atmosphere that extends from about 60 to 1,000 km in altitude and contains a relatively large number of ions and electrons. The ionization of atmosphere at these altitudes is largely due to collisions between the incoming solar photons and neutral gaseous molecules or atoms that result in the removal of electrons from these atmospheric constituents. Although less than 1% of the upper atmosphere becomes ionized, the generation of charged particles make the gas electrically conducting, which completely changes its characteristics. The ionosphere can be basically seen as a by-product of the interaction between the Sun and the Earth's atmosphere. Closer to the surface of the Earth, the incoming solar photons have insufficient energy for ionizing the neutral gases and away from the Earth's surface there are fewer neutral components for collision, due to a decrease in the atmospheric density with increasing altitude. The combination of these two factors result in the creation of the Earth's ionosphere within a limited region of the atmosphere.

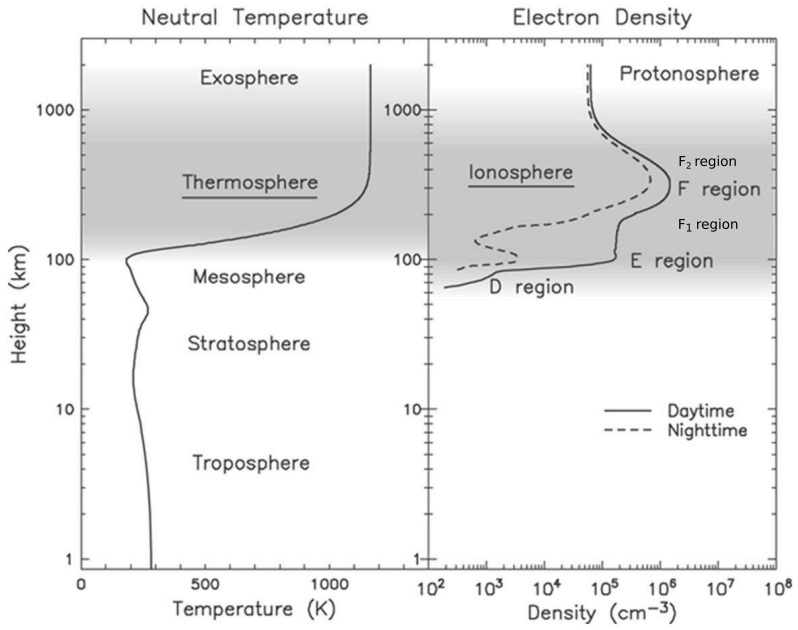

Figure 1.1: Vertical temperature profile of the atmosphere from ground to space (left) and the vertical profile of electron density in the day and night time ionosphere (right) (courtesy of NICT-Japan, Figure 1).

The sources of ionization in the atmosphere include photons and energetic particle precipitation. Ionizing photons primarily come from the Sun while precipitating energetic electrons can also produce additional ionizing photons in the atmosphere through a process called as bremstrahlung, or braking radiation (e.g., Kivelson and Russell, 1995). Ionization takes place in the neutral atmosphere if the energies of photons and precipitating particles exceed the binding energy of electrons in the gaseous constituents. The solar photons in the extreme ultraviolet (EUV) and ultraviolet (UV) range constitute the dominant source of daytime atmospheric ionization.

The ionosphere is historically classified as the region of the atmosphere that can affect the propagation of radio waves. The existence of highly electrically conducting ionosphere was independently postulated in 1902 by Heaveside and Kennelly to explain Marconi's transatlantic radio transmissions. Appleton used the letter E to denote the first ionospheric layer that was observed by experimental measurements and subsequently he used the letter F and D when the reflections from higher and lower layers, respectively, were observed. Based on the peak electron density profile the ionosphere can be divided into three regions: the D-region (between 60 - 90 km), the E-region (between 90 - 140 km), and the F-region (above 140 km). The F-region is usually further divided into F1- and F2-regions. More than one maximum region of electron density is found because the upper neutral atmosphere is composed of different gaseous constituents and they interact differently with the UV and EUV radiation. Figure 1.1 shows the vertical neutral temperature profile in the layers of the atmosphere along with the vertical profile of electron density in the ionosphere. The variation of day and night time electron densities with altitude in the ionospheric regions can be seen in this figure.

The major source of ionization in the atmosphere is the solar EUV photoionization and photoelectron impact ionization of O, O_2, and N_2. Photoionization of an atom or molecule (X) can be represented as

$$X + h\nu \longrightarrow X^+ + e^* \tag{1.1}$$

where e^* is a photoelectron. For molecules XY, photoionization can be represented as

$$XY + h\nu \longrightarrow XY^+ + e^* \tag{1.2}$$

Photoelectrons produced from these reactions can acquire sufficient energy to carry out further ionization through photoelectron impact ionization

$$X + + e^* \longrightarrow X^+ + e + e^{'} \tag{1.3}$$

where e represents the electron with reduced energy and $e^{'}$ is a secondary electron.

Photoelectron impact ionization constitutes 25–30% of the total source of ionization above 200 km but becomes the dominant source below 150 km (e.g., Richards and Voglozin, 2011). The major ions produced in the ionosphere between 60-600 km as a result of photoionization of major neutral constituents are N_2^+, O_2^+ and O^+. Below 200 km, the ionosphere is dominated by ionized components of heavier gases such as N_2 and O_2. N_2^+ is the major source of NO^+ below 200 km and is produced in large quantities throughout most of the ionosphere, but it is a minor species as it reacts very quickly with electrons and atomic oxygen through charge-transfer reactions as seen in the following example:

$$N_2^+ + O \longrightarrow NO^+ + N \tag{1.4}$$

Between 200 km and 600 km, the atomic ions such as O^+ become the dominating species and above this altitude, the ions of lighter atoms such as H and He start dominating. The daytime composition of ion species below 1000 km during solar minimum conditions is presented in Figure 1.2 that has been adapted from Johnson (1966).

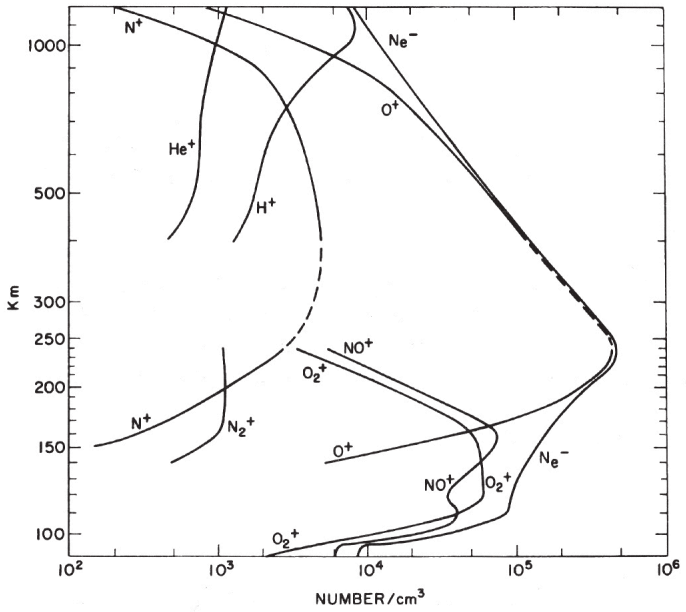

Figure 1.2: Ionic composition of solar minimum daytime ionosphere (adapted from Johnson, 1966, Figure 1).

The D-region of the ionosphere lies approximately between 60-90 km altitude and consists mostly of NO^+ and O_2^+ ions. Only the most energetic ionization sources can penetrate to D-region altitudes and the X-rays and Lyman α emission line are mainly responsible for ionization in this region. The electron concentration in this region remains at low values (below 10^4

$cm^{-}3$) and the dynamics is controlled by the neutral atmosphere. The D-region is also important for its role in commercial radio communication. Due to relatively higher atmospheric density as compared to E- and F-regions, the radio signals get more attenuated due to increased collision between the electrons and the neutrals. It is found that the low frequency signals are unable to reach the higher ionized regions within the ionosphere due to attenuation, except at night when the D-region disappears.

The E-region of the ionosphere is considered to be located between 90-140 km altitude. Ionization in this region is mainly due to X-rays and UV radiation. The dominating ions in this region also consists of NO^+ and O_2^+. The production of these molecular ions is essentially balanced by recombination reactions with electrons. The E-layer in this region fairly approximate the behaviour of a Chapman layer with daily maximum at local noon, seasonal maximum in summer, and solar cycle dependence. The maximum free electron density in the E-region occurs at an altitude of about 110 km and is between 100 - 1000 times larger than the D-region densities, which leads to the E-region becoming much more important than the D-region as a reflector of radio waves. Unlike the D-region, the E-region does not disappear completely at night and remains weakly ionized.

The F-region constitutes a major segment of the ionosphere and extends above 140 km altitude. During daytime, it contains two separate layers called F1 and F2 while during night time, the F1 layer usually vanishes and only the F2-region is present. The average electron density in the F-region is about 10 times greater than the E-region. The F1-layer lies at an altitude of approximately 140-210 km with the maximum electron density in this layer occurring near 170 km. Ionization in this region is mainly due to EUV radiation. The F1-region is dominated by NO^+ and O_2^+ and O^+ ions. Above 200 km, the atomic ions start becoming dominant species in the ionosphere and the F2-region is dominated by O^+ ions. The F2-layer achieves its maximum electron density at altitudes between 250-400 km. The origin of the F2-layer is not a result of chemical balance as seen in the case of D- and E- layers but in this layer, the O^+ ion production is balanced by diffusion of this ion through the neutral atmosphere as the recombination rate in this layer is significantly reduced due to extremely low atmospheric air density. The F2-layer peak arises due to a faster decrease in the recombination reaction rates with height as compared to the ion production rates. The F2-region above the maximum electron density peak is called the topside F2-layer of the ionosphere. The F-region is very important for High Frequency (HF) radio wave propagation.

The Earth's ionosphere is a weakly ionized plasma in which the motion of electrons and ions is determined by the combined effects of collisions and magnetization. Below 90 km in the D-region, the ionosphere can be considered to be unmagnetized and the motions of ions and electrons are dominated by collisions with neutrals. In this region, the collision frequen-

cies of ions and electrons with neutrals are much greater than their respective gyrofrequencies, which means the magnetic field doesn't influence the motion of electrons and ions, resulting in their flow being in the direction of neutral wind.

In the E-region, the electrons are trapped in the magnetic field lines while the motion of ions are still dominated by collisions with neutrals. The gyrofrequencies of electrons are much greater than their collision frequencies while ions still collide with neutrals at a rate greater than their gyrofrequencies at these altitudes. Thus, the electrons predominantly drift across both the geomagmagnetic and electric fields and the ions primarily move with the neutral wind. This differential motion between the ions and the electrons produces currents and electric fields in the ionosphere.

Above 150 km, both the electrons and ions are magnetized as their respective collision frequencies with neutrals become much smaller due to decreasing atmospheric density and the geomagnetic field controls the motion of the electrons and ions. In the presence of an electric field, the electrons and ions move together in the direction perpendicular to both electric (**E**) and magnetic (**B**) fields at a velocity,

$$v_i = v_e = \frac{E \times B}{B^2} \tag{1.5}$$

and the lack of differential motion between the ions and electrons prevents the generation of currents at these altitudes.

Between 90 and 150 km altitude, the currents are produced by the wind dynamo mechanism. Analogous to a mechanical dynamo in which the rotation of a conducting coil normal to the magnetic field induces electric field and leads to the flow of current, in the ionospheric dynamo, tidal winds move the conducting ionosphere across the Earth's magnetic field and generate currents. The neutral wind motions in the low and middle latitude ionosphere are driven by tidal oscillations that are generated by in situ heating and also by waves that propagate from below (e.g., Forbes, 1995). The upper propagating waves are greatly affected by the state of background atmosphere and contribute to the day-to-day variability of the ionosphere. This lower atmospheric influence on the ionosphere is discussed in greater detail in the next section.

1.2 LOWER ATMOSPHERIC FORCING INTO THE IONOSPHERE

The ionosphere displays a significant day-to-day variability. Knowledge about the phenomena that are responsible for ionospheric variabilities and their understanding is important in today's modern age, as much of our communication and navigation capabilities rely on satellite signals that penetrate these regions. Ionospheric monitoring and development of forecasting capabilities will be of crucial importance in the coming future.

Therefore it becomes imperative to continue our experimental and theoretical investigations of the ionosphere.

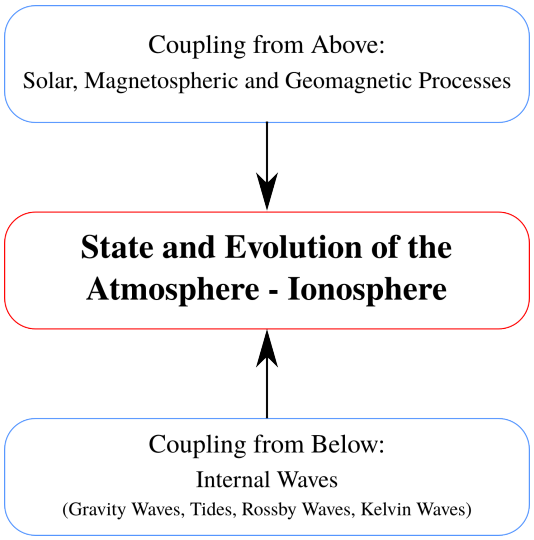

Figure 1.3: Vertical coupling: the atmosphere-ionosphere system is under the influence of lower atmospheric forces (internal waves) from below and external forcings (solar, magnetospheric, and geomagnetic) from above (adapted from Yiğit et al. (2016), Figure 1, reprinted with kind permission from publisher Elsevier.).

The major drivers responsible for ionospheric variability include solar ionizing flux, geomagnetic activity and lower atmosphere meteorological processes. The first two factors are solar controlled and are associated with ionospheric forcing from above. The ionosphere is, however, also forced from below through different meteorological processes that also contribute to its variability (e.g., Forbes et al., 2000; Rishbeth and Mendillo, 2001). The meteorological influence on the ionosphere is realized through atmospheric waves which include tides, planetary waves and gravity waves (e.g., Kazimirovsky et al., 2003). The atmosphere-ionosphere coupling is illustrated in Figure 1.3 taken from Yiğit et al. (2016).

Atmospheric tides refer to those large-scale oscillations of the atmosphere whose periods are integral fractions of a lunar or solar day (e.g., Chapman and Lindzen, 1970). Atmospheric tides are primarily forced by periodic absorption of solar radiation in the atmosphere and to a lesser degree by the lunar gravitational force. Dominant solar tidal components occur at 24-hour (diurnal) and 12-hour (semidiurnal) periods. The lunar tide is also composed of different modes, but the lunar semidiurnal tide (12.420 solar or 12 lunar hours) is the most important, because it reaches the largest amplitudes.

The term planetary waves is often used as a synonym of Rossby waves, which appear in the atmosphere due to the latitudinal gradient of the Coriolis force that balances variations of the pressure gradient force (e.g.,

Holton and Hakim, 2012). Gravity waves refers to disturbances in which the restoring force is buoyancy which acts to restore the fluid parcels displaced from hydrostatic equilibrium (e.g., Andrews et al., 1987).

The atmospheric waves can be classified according to their temporal and spatial scales. Planetary waves and tides have horizontal scales comparable to the Earth's radius while the horizontal wavelengths of gravity waves can easily extend up to several hundred km. In terms of temporal scales, gravity waves can vary between a few minutes to several hours whereas the tidal periods are subharmonics of a solar or a lunar day. The time periods of planetary waves can vary between 2-30 days. Atmospheric waves are excited through meteorological processes and propagate upward while growing in amplitude due to the decreasing background air density. Therefore the amplitudes of even small wave disturbances can reach significant values at higher altitudes. The upward propagating atmospheric waves from the lower atmosphere deposit energy and momentum at ionospheric altitudes thus modulating the temperature and wind fields and driving polarization electric fields and currents in the ionosphere.

Vertical coupling between the troposphere and ionosphere has been explored for a long time (e.g., Beynon and Brown, 1951; Martyn, 1952). One of the earliest evidence for tropospheric-ionospheric coupling was shown by Schödel et al. (1973) using total electron content data which showed variations with the same period as ground pressure recordings. This coupling is also seen during severe tropospheric phenomenon such as thunderstorms and tornadoes during which the excited gravity waves are seen to propagate up to the ionospheric F-region heights (e.g., Hung and Smith, 1979). Ionospheric effects have also been related to tropical tropospheric disturbances such as typhoons and thunderclouds (e.g., Maeda and Badillo, 1966; Raju et al., 1981). These examples of coupling and the mechanisms behind them have been further investigated extensively in the past few decades. Vertical propagation of atmospheric waves has been the general line of thought to explain the meteorological effects in the ionosphere. In particular the knowledge about the propagation of tides, gravity and planetary waves which have mainly relied on modeling and observational studies have been very important. The next paragraph mentions some of these studies which have contributed to our understanding of the atmospheric waves in the ionosphere.

Tides have been measured in the ionospheric E-region through incoherent scatter radar measurements (e.g., Monro et al., 1976; Hocke, 1996) and in the F-region through ionosonde measurements (e.g., Canziani, 1994). Tides are also known to play an important role in the formation of sporadic-E layer in the ionosphere (e.g., Haldoupis et al., 2004) and introducing significant variability in the f_0F2 (critical frequency of the maximum electron density in the ionosphere) (e.g., Fesen, 1997). Modeling studies by Fesen (1997) have reported significant variability due to tides in the F2-region

during both day and night time. Gravity waves have been identified in the rocket density profiles in the lower ionosphere (e.g., Mechtly and Smith, 1970), in echoes of the sporadic-E layer (e.g., Kazimirovsky et al., 2003) and through radar and ionosonde measurements in the F-region (e.g., Oliver et al., 1997). Unlike tides and gravity waves, planetary waves cannot propagate directly to F-region heights but their signatures have been observed in all the ionospheric regions. Planetary waves are only capable of directly penetrating up to about 110 km (e.g., Vincent, 1990) but their effects at higher altitudes have been explained through indirect propagation methods such as the planetary wave modulation of tides (e.g., Pancheva et al., 2002; Pancheva et al., 1994) and gravity waves (e.g., Meyer, 1999). Typical planetary wave periods of 2, 5, 10 and 16 days have been observed in mesospheric winds through radars in a number of studies. Planetary waves play an important role in the sporadic-E layer formation (e.g., Pancheva et al., 2003) and they also modulate the E-region dynamo significantly as their oscillations are observed in geomagnetic field measurements on the ground (Parish et al., 1994; Kohsiek et al., 1995; Elhawary and Forbes, 2016). Our present state of knowledge which has relied on observational and modeling studies acknowledges the role of atmospheric waves in the lower atmosphere-ionosphere coupling. For a more detailed understanding of this topic the readers may refer to following reviews by:

- Kazimirovsky et al. (2003)
- Laštovička (2006)
- Laštovička (2009)
- Forbes (2007)
- Yiğit and Medvedev (2015)

In this thesis, however, the main focus of study is the case of stratosphere-ionosphere coupling during a phenomenon known as SSW which is initiated by an anomalous growth of planetary waves that propagate from the troposphere into the stratosphere. This chapter first provides a summary of the previous observational and modeling studies that have discussed the stratospheric - ionospheric coupling during SSW events, which is then followed by a short background of the phenomena studied in this thesis. Thereafter the scope and goals of this thesis is presented followed by its organization and author's contributions.

1.3 STRATOSPHERIC - IONOSPHERIC COUPLING DURING SSW EVENTS

SSW events are extreme meteorological events usually occurring during the Northern Hemisphere winters. During this event the polar vortex shows

a dramatic breakdown due to planetary wave amplification and breaking that leads to a sudden increase in the polar temperature and deceleration or reversal of the zonal mean zonal winds at stratospheric altitudes. The sudden increase in temperature is the reason for this phenomenon being coined as "Stratospheric Sudden Warming".

The knowledge about the vertical coupling between stratosphere and lower ionosphere at middle latitudes dates back to early 1960s. Numerous studies since then have focused on the correlation between the stratospheric temperature variations and lower ionosphere plasma density. Figure 1.4 taken from Shapley and Beynon (1965), provides an example of a superposed epoch analysis between the temperatures at 10 hPa over Berlin and radiowave absorption (plasma density) over Lindau/Harz during the SSWs. In this figure the stratospheric temperature and the plasma density are observed to be widely correlated with each other.

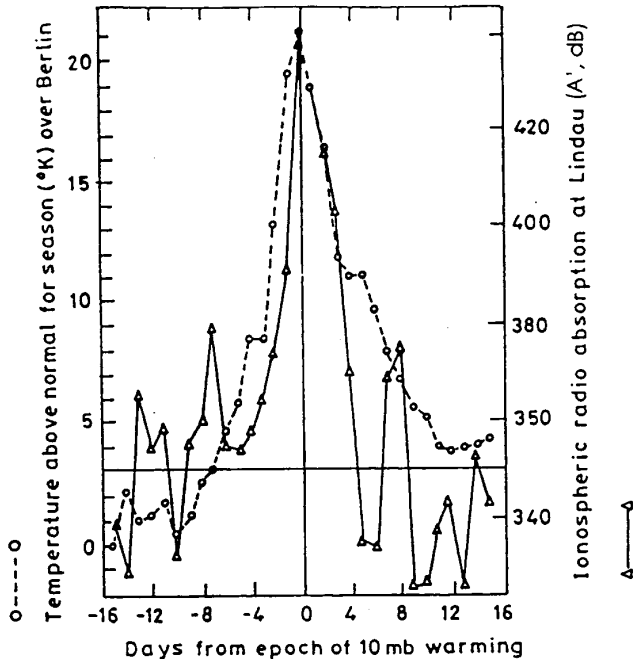

Figure 1.4: Superposed epoch analysis comparing 10 mb temperature over Berlin (Germany) and radiowave absorption over Lindau/Harz (Germany) (adapted from Shapley and Beynon (1965), Figure 1).

Although the coupling is always present to a certain degree but it becomes rather apparent during the SSWs (e.g., Chau et al., 2012). In recent times, research in this subject has received a sudden resurgence due to the following reasons correctly pointed out by Chau et al. (2012):

- Extensive atmospheric observations
- Unexpectedly low solar minimum conditions during the solar cycle 24

The availability of extensive data in the equatorial and low latitude ionosphere from ground- and satellite-based observations have led to the understanding of previously unknown connections with the stratosphere during SSWs. On the other hand, due to low solar minimum conditions forcing from the sun was substantially reduced which resulted in the effects due to lower atmospheric forcing being more pronounced in the ionosphere. Both these factors have been strongly responsible for the increased number of observational and modeling findings in the past few years. Based on these findings it is now known that the effects of SSW events are not just confined to the polar stratosphere, rather SSW related changes are seen across both hemispheres from the ground up to the thermosphere. A lot of our current knowledge in this field developed after the observations reported by:

- Goncharenko and Zhang (2008) - in which they identified the correlation between the polar stratospheric wind and temperature measurements and the ion temperature at mid-latitudes during the 2008 SSW event.
- Chau et al. (2009) - in which they showed the variations of vertical $E \times B$ plasma drifts correlating with the stratospheric wind and temperature during the 2008 SSW event.

Chau et al. (2009) noted a semidiurnal pattern in the equatorial plasma drifts velocity during the 2008 SSW event, where a large increase in the plasma drifts velocity was seen during the morning hours along with a decrease in the afternoon hours. This observation was also seen in the GPS (Global Positioning System) TEC (Total Electron Content) data during the 2009 SSW event (Goncharenko et al., 2010b), where a strong increase in TEC was seen in the morning hours in response to the large upward drift and a large decrease in TEC in the afternoon hours when the drift was downward. SSW related effects have been demonstrated in TEC (e.g., Goncharenko et al., 2010a; Goncharenko et al., 2010b), peak electron density (e.g., Pancheva and Mukhtarov, 2011) and geomagnetic observations (e.g., Fejer et al., 2010; Yamazaki et al., 2012b; Park et al., 2012).

The connection between the polar stratospheric variability during SSWs with the low latitude ionosphere is puzzling. It is generally believed that the ionospheric perturbations during SSWs take place through the modulation of atmospheric tides which impact the E-region dynamo (e.g., Chau et al., 2012). A number of studies have focused on the SSW related changes in the migrating solar tides (e.g., Fuller-Rowell et al., 2011), migrating lunar tide (e.g., Fejer et al., 2010) and non-migrating tides (e.g., Pedatella and Forbes, 2010). Simulation studies by Liu et al. (2010) have shown that the quasi-stationary planetary waves which remain confined to the high latitude stratosphere and mesosphere can affect the migrating and non-migrating solar tides globally. Some of the mechanisms that have been

proposed to explain the tidal changes during SSWs can be summarized as following:

- Migrating solar semidiurnal tide (SW2)
  - change in the ozone distribution due to SSW which effects the generation mechanism of SW2 (Goncharenko et al., 2012)
  - change in the tidal propagation conditions due to SSW (Jin et al., 2012)
  - tides-planetary wave interaction (Liu et al., 2010)
- Non migrating tides
  - non-linear planetary wave-tide interactions during SSWs (Liu et al., 2010)
- Migrating lunar semidiurnal tide (M2)
  - change in the tidal propagation conditions due to SSW (Forbes and Zhang, 2012)

In combination with observations, numerical studies have also contributed much to our understanding about the global view of tidal variability by reproducing the general ionospheric features during the SSWs (e.g., Fuller-Rowell et al., 2011; Jin et al., 2012; Pedatella et al., 2012). Changes in the solar tidal variability during the 2009 SSW event have been reported using the Whole Atmosphere Model (WAM) (Fuller-Rowell et al., 2010). The investigations of the lunar tidal influence on the ionospheric variability during SSWs have been reported by Pedatella et al. (2012) by using the Whole Atmosphere Climate Community Model - eXtended version (WACCM-X) in combination with an ionosphere-electrodynamics model. They found that the changes in the equatorial vertical plasma drift velocity were similar to observations when the lunar tide was included in the simulations and in the absence of lunar tide the ionospheric changes were minor. Pedatella and Liu (2013) also investigated the relative contributions of the different tides in the MLT (mesosphere-lower thermosphere) that produces the observed ionospheric perturbations during SSWs. They concluded that the semidiurnal solar (SW2) and lunar (M2) tides and the non-migrating solar tide with zonal wave number 1 (SW1) are significantly responsible for driving the ionospheric variability in response to SSWs. They also found out that the contribution of M2 tide is dependent on the phase of the moon relative to the timing of SSW.

The ionospheric perturbations due to SSWs are complex and may be driven by a combination of the above mentioned mechanisms that lead to tidal changes (Pedatella and Liu, 2013). Observations and modeling efforts have been integral towards our understanding of the mechanisms behind this coupling that nonetheless still remains a topic under investigation.

1.4 BACKGROUND

The previous sections presented a short summary on the variability of the ionosphere due to lower atmospheric forcing in general and due to SSWs in particular. In this thesis, the broad goal is to study the effects of stratosphere-ionosphere coupling during SSWs on an intense equatorial ionospheric current flow known as the equatorial electrojet. For this purpose, in this section, a brief background of the physical processes involved in this coupling are first mentioned. The coupling is understood to be through atmospheric waves and in particular through tides. During SSW, large changes are seen in atmospheric tides and particularly in the amplitude of lunar tides that shows large enhancement in the MLT and at ionospheric heights.

In this section a concise description about the SSW, the equatorial electrojet and the lunar tide are presented. The purpose of this section is to briefly, albeit sufficiently describe the observed phenomena in order to facilitate a better understanding about the results and goals achieved in this thesis.

1.4.1 *The Stratospheric Sudden Warming*

Stratospheric sudden warming (SSW) is an extreme meteorological event that usually takes place in the northern wintertime polar stratosphere. During this event the westerly winds in the polar vortex is seen to slow down or even reverse their direction within a few days. This is also accompanied by a sudden rise in stratospheric temperature by several tens of degrees. SSW was first discovered by Scherhag (1952) when he observed a sudden increase in the 10 mbar temperature during a radiosonde experiment over Berlin on January 30, 1952. An example of the changes in the stratospheric mean zonal wind and temperature during an SSW event can be seen in Figure 1.5 taken from Goncharenko et al. (2010a), which includes the observation of stratospheric conditions at 10 hPa during the major SSW that took place in the winter of 2008-2009. The stratospheric data from the National Center for Environmental Predictions (NCEP) is used to illustrate conditions at 10 hPa ($\approx$ 32km) in this figure. Data for the winter of 2008-2009 are shown with solid circles, and multi-year means (averaged from 1978 to 2008) are shown with solid lines. During the stratospheric sudden warming event of 2009, stratospheric temperatures at 90°N sharply increased by more than 70 K, while the zonal mean zonal wind at 60°N reversed from westerly (wintertime) to easterly (summertime). The peak warming at the 10 hPa level is reached on 23-24 January 2009 with temperature in the 60°N-90°N latitude band increasing by 30 K. The circulation is dominated by a planetary wave 2, which exceeds the long-term mean level by a factor of almost 3, while the activity of planetary wave 1 remains

relatively low. The extremely low solar and geomagnetic activity, indicated by the F10.7 and Kp indexes shows that ionospheric effects are related to the stratospheric warming event.

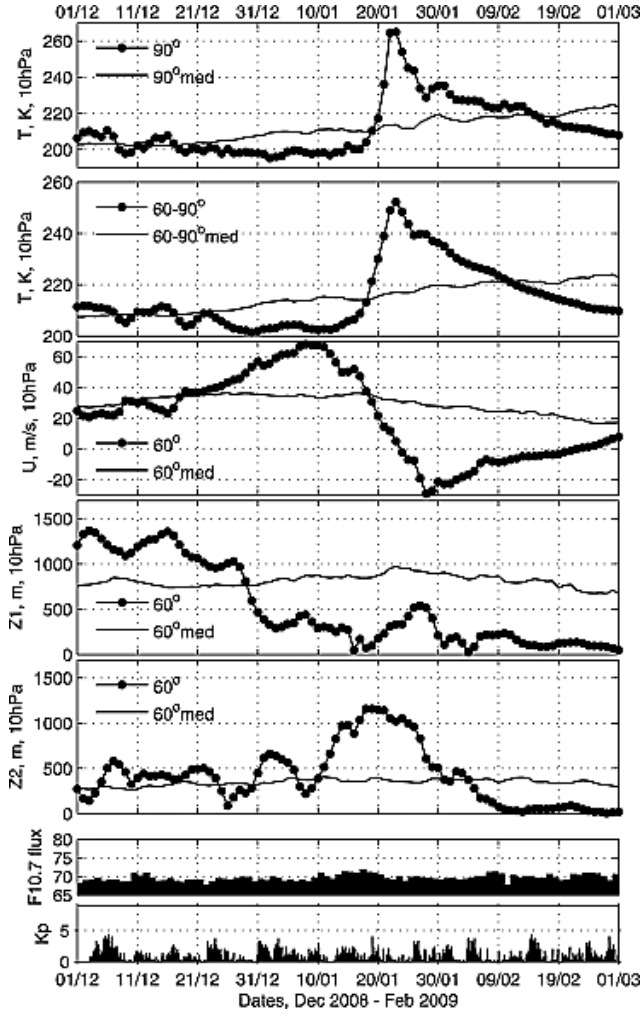

Figure 1.5: Summary of stratospheric and geomagnetic conditions for the winter of 2008–2009. (top to bottom) Stratospheric temperature at 90°N and 10 hPa ($\approx$ 32km), zonal mean stratospheric temperature at 60°N–90°N, zonal mean zonal wind at 60°N, planetary wave 1 activity at 60°N and 10 hPa, planetary wave 2 activity at 60°N and 10 hPa, F10.7 index, and Kp index. Lines indicate 30 year means of stratospheric parameters, and solid circles indicate data for the winter of 2008–2009 (from Goncharenko et al. (2010a), Figure 1, reprinted with kind permission from publisher John Wiley & Sons Ltd.).

The wintertime stratospheric polar circulation is characterized by strong westerly winds that constitute the polar vortex. Because there is an approximate geostrophic balance between the horizontal pressure gradient and Coriolis acceleration, the wind flows parallel to isobars. This mean circulation is occasionally disrupted by planetary waves that propagate from the troposphere and dissipate their energy and momentum in the

stratosphere (e.g., Andrews et al., 1987). Breaking of these waves causes poleward meridional circulation in the extratropical stratosphere, with upward motion in the tropics and downward motion in polar latitudes (e.g., Holton et al., 1995). The downward motion results in adiabatic heating as the air parcels get compressed with increasing pressure and this leads to a warming in the polar stratosphere. Matsuno (1971) originally proposed this mechanism of SSW by suggesting the extreme case of the wave-mean flow interaction which has been widely accepted. Through the amplification of planetary waves in the troposphere his numerical model was successful in reproducing many features of an SSW.

The World Meteorological Organization (WMO) classifies SSWs (e.g., Andrews et al., 1987) into two broad categories namely

- minor warming events
- major warming events

According to the WMO definition, an SSW is classified as major if a complete reversal of the zonal mean zonal wind is seen at 60°N & 10 hPa pressure level. If there is only a reversal of meridional temperature gradient poleward of 60°N & 10 hPa and an absence of the reversal of mean zonal wind then an SSW is usually classified as a minor warming event.

SSWs can be further classified into vortex displacement and vortex splitting events (e.g., Charlton and Polvani, 2007). Vortex displacement type SSWs are associated with large amplitudes of longitudinal wave number 1 planetary waves whereas vortex splitting SSWs are typically caused by amplification of wave number 2 planetary waves. Figure 1.6 presents a composite of geopotential height at 10hPa corresponding to a vortex displacement (left) type SSW during January 2012 and a vortex splitting (right) type SSW during January 2013. These two types of vortex breakups are associated with large amplitudes of planetary wave number 1 and 2, respectively.

1.4.2 *The Equatorial Electrojet*

The equatorial electrojet (EEJ) is a narrow ribbon of intense current flowing during the daytime above the dip equator in the E-region of the ionosphere. It is confined to a latitudinal extent of $\pm 3^\circ$ on either side of the dip equator. The EEJ was discovered when the geomagnetic variations at the Huancayo observatory in Peru were found to be unusually large in comparison to those at other latitudes away from the equator and it has since been extensively studied (e.g., Bartels and Johnston, 1940; Chapman, 1948). Figure 1.7 from Onwumechilli (1967) shows the variation of daily range of horizontal component (H) of the Earth's magnetic field with latitude. The

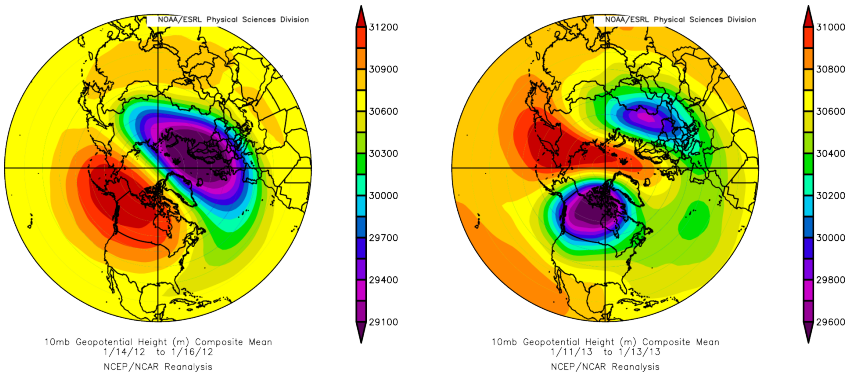

Figure 1.6: Composite of Geopotential height at 10 hPa corresponding to (left) a vortex displacement type SSW during January 2012 and (b) a vortex splitting type SSW during January 2013. The plots are downloaded from the website of PSD-ESRL, NOAA.

large magnitude of the daily range of H at the dip equator is due to the EEJ. The presence of an overhead current over the dip equator was suggested by Egedal (1947) as the reason for these abnormal variations and this phenomenon was later termed the "equatorial electrojet" by Chapman (1951). The major features of EEJ has been investigated extensively from ground observations (e.g., Forbes, 1981), from sounding rockets (e.g., Onwumechilli, 1998 and references therein) and from low-Earth orbiting satellites (e.g., Cain and Sweeney, 1973; Jadhav et al., 2002; Lühr et al., 2004). The locally excited diurnal tide in the thermosphere is considered to be the prime driver of ionospheric wind dynamo currents and it accounts for about half of the EEJ current (Yamazaki et al., 2014). In addition to in situ generated tides, the other half of the EEJ current flow is accounted by the upward propagating tides of lower atmospheric origin (Yamazaki et al., 2014).

The unique geometry of the magnetic field at the dip equator along with the relatively low conductivity (in comparison to the E-region) at the lower and upper boundaries are the factors largely responsible for the existence of equatorial electrojet. The phenomenon of EEJ can be explained through a schematic plot as shown in Figure 1.8. At low latitudes, the wind-dynamo mechanism sets up an eastward polarization electric field (E_1 in Fig. 1.8) due to accumulation of charges at dawn and dusk terminators. Due to anisotropic conductivity in the ionosphere, the eastward polarization electric field drives an eastward flowing Pedersen current ($\sigma_P E_1$) and a downward flowing Hall current ($\sigma_H E_1$) that is perpendicular to both the direction of electric and magnetic fields. The flow of the vertical Hall current is inhibited at the boundaries due to regions of lower conductivity leads to a creation of a vertical polarization field (E_2 in Fig. 1.8) to negate the accumulation of charges (Baker and Martyn, 1953). This vertical polarization field not only drives an upward Pedersen current ($\sigma_P E_2$) that

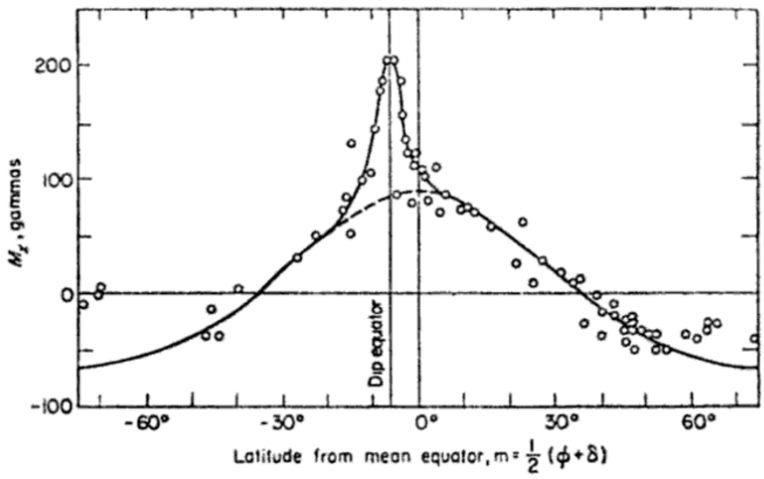

Figure 1.7: Variation of the daily range of horizontal component of magnetic field with latitude on international quiet days between September and October, 1958. Figure taken from Onwumechilli (1967).

balances the downward Hall current ($\sigma_H E_1$), but also an eastward Hall current ($\sigma_H E_2$) in the direction of the original electric field thus reinforcing it. The balance of vertical currents gives the relation,

$$\sigma_H E_1 = \sigma_P E_2 \tag{1.6}$$

and the net eastward current can be written as,

$$\sigma_P E_1 + \sigma_H E_2 = \left(\sigma_P + \frac{\sigma_H^2}{\sigma_P}\right) E_1. \tag{1.7}$$

The effective conductivity in the eastward direction $\sigma_P + \frac{\sigma_H^2}{\sigma_P}$ is called the Cowling conductivity. The physics of this process was already in place much before the actual discovery of this phenomenon. Cowling (1932) theoretically discovered that when a Hall current flowing normal to the boundaries is restricted then the effective conductivity parallel to the boundaries becomes greater than the Pedersen conductivity. This physical mechanism has been used to explain the phenomenon of the equatorial electrojet.

1.4.3 *The Lunar Tide*

1.4.3.1 *The Atmospheric Lunar Tide*

The lunar influence on the tides in the ocean has been known much before the modern scientific age. Pytheas of Marseilles (around 320 B.C) is credited to have been the first to recognize the relation between coastal tides and lunar transit times during his extensive voyages. The occurrence of the high tide and moon's crossing across the meridian became an accepted

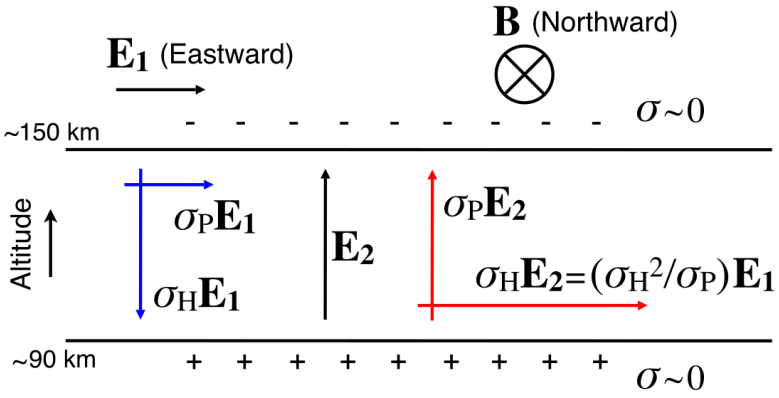

Figure 1.8: A schematic illustrating the Cowling effect in the equatorial electrojet. From Yamazaki et al. (2011).

idea much before the issue of second high tide was resolved by Newton (1687). Atmospheric tides, though they existed, were not observed until the invention of barometer by Torricelli in 1643. Newton recognized that tidal forces must affect the atmosphere in a similar way as the oceans but he thought that the atmospheric tides would be difficult to detect due to their smaller amplitudes. In the 19th century, Laplace attempted to detect the lunar tide through barometric observations in Paris but his attempts were unsuccessful. It was Sabine (1847) who first detected the atmospheric lunar tide from tropical pressure data. The first detection of lunar tide outside the tropics was demonstrated by Chapman (1919) when he succeeded in determining the semi-diurnal lunar tide from the Greenwich barometer data. The mathematical theory of lunar tide in the atmosphere and the historical descriptions have been elucidated in great detail in Chapman and Lindzen (1970).

The atmospheric lunar tides are primarily caused by the gravitational attraction of the moon on the lower and denser regions of Earth's atmosphere. Other sources of lunar tides include tidally induced movement of solid Earth and oceans (e.g., Hollingsworth, 1971; Vial and Forbes, 1994). Atmospheric lunar tides propagate vertically upward and are capable of penetrating up to the thermosphere. The tidal amplitude grows exponentially with height and reaches its maximum at approximately 120 km before dissipating (Vial and Forbes, 1994). The atmospheric lunar tides are dominated by the semi-diurnal (12.42 h) component.

Observational studies on the analysis of the atmospheric lunar tide for many years were based on the ground pressure data due to the requirements of long data records. At the surface, the amplitude of lunar semidiurnal tide in barometric pressure is almost $\frac{1}{20}$th of the solar semidiurnal tide (Chapman and Westfold, 1956). Above it, tidal analysis from ground up to 10 hPa rely on data from radiosonde stations. From 30 to 60 km the

vertical structure of lunar tides have been obtained from meteorological rocket soundings. In the MLT region radar observations have generated data sets which have greatly advanced our knowledge about the lunar tidal characteristics. Through radar measurements, the seasonal and annual variation of lunar tides have been determined (e.g., Stening et al., 1987; Stening and Vincent, 1989; Sandford et al., 2006) at heights between 80 and 105 km. In recent times global structure of the lunar semidiurnal tide has been obtained by Paulino et al. (2013) by using the continuous temperature measurements from the SABER (Sounding of the Atmosphere Using Broadband Emission Radiometry) instrument on board the TIMED (Thermosphere Ionosphere Mesosphere Energetics and Dynamics) satellite. Modeling studies by Vial and Forbes (1994) and Forbes (1982) have also been useful in examining various characteristics of the atmospheric lunar tides. Forbes (1982) used a numerical model to investigate the vertical characteristics of lunar tide from the surface to 400 km. Stening et al. (1997) used a lunar atmospheric tidal model similar to Forbes (1982) and investigated the effects of changes in atmospheric propagation conditions to the structure of lunar tides.

The study of atmospheric lunar tides is of particular interest because the forcing mechanism in general is precisely known and thus comparison between numerical simulations and observations provide a diagnostic tool to verify the atmospheric models. In future we may be able to attain a level where the state of the lunar tide in the mesosphere or lower thermosphere could make us deduce the lower atmospheric propagating conditions.

1.4.3.2 *The Geomagnetic Lunar Tide*

The daily geomagnetic field variation on the ground shows a dependence on the phase of the moon which is termed as the lunar daily variation and denoted by **L**. The cause of this variation lies in the ionospheric dynamo region which when driven by lunar tidal winds induce electric fields through dynamo mechanism that drives the ionospheric electric currents (e.g., Tarpley, 1970).

The first attempt to recognize **L** in geomagnetic field variation was undertaken by Kreil of Prague in 1839 but his efforts were not successful until 1850. Geomagnetic lunar variation was recognized by Van Bemmelen (1912) as a worldwide phenomenon based on his applications of spherical harmonic analysis on the geomagnetic data. Early efforts on this subject also include the work by Chapman (1919), in which detailed studies of geomagnetic lunar variations at individual magnetic stations was reported. Through the use of ground magnetic recordings Chapman and Bartels (1940) derived the equivalent external (overhead) lunar current system. Later, Matsushita and Maeda (1965) were the first to determine the

equivalent external (overhead) and internal (induced within the earth) current systems responsible for lunar daily variations.

The main component in **L**, derived from ground based magnetometers is the semidiurnal lunar variation with a period of 12.42 hours. As mentioned earlier, lunar tides are excited near the surface of the Earth mainly due to the gravitational attraction of the moon and the tidal movements of oceans and land mass. These waves can propagate vertically upward into the ionospheric dynamo region where they drive the current system through the dynamo mechanism. In the dynamo region the semidiurnal component of the lunar tide in the wind reaches an amplitude of up to 10 - 15 m/s (Zhang and Forbes, 2013). This amplitude is at least 3 times smaller than the amplitude of solar semidiurnal tide in the winds at dynamo region heights. The magnitude of the geomagnetic lunar (**L**) variation is estimated to be approximately $\frac{1}{10}$th of the geomagnetic solar quiet (**Sq**) variation (Yamazaki et al., 2011). The global behavior of **L** on the ground can reasonably be well explained by the existence of a current system in the ionosphere which is driven by the atmospheric lunar tides (Maeda and Fujiwara, 1967).

It is also important to mention here that the characteristics of **L** near the equatorial electrojet is quite different from those which are observed at other latitudes. Near the magnetic equator, **L**, is amplified to the extent that on occasions it is comparable or greater than the **Sq** variation. In the next section the anomalous behavior of **L** in EEJ is discussed.

1.4.3.3 *Lunar tide in the equatorial electrojet*

The lunar tidal modulation of the equatorial electrojet intensity has been known for a long time (e.g., Bartels and Johnston, 1940; Rastogi and Trivedi, 1970). A large amount of our knowledge about **L** in the electrojet has been gained through magnetic observations at Huancayo, Peru. The high intensity of the electrojet over Peru due to the local configuration of the geomagnetic field (Sugiura and Cain, 1966; Sugiura and Poros, 1969) leads to anomalously large values of **L** in the horizontal component of magnetic field observations (H) (e.g., Bartels and Johnston, 1940; Forbush and Casaverde, 1961). The lunar daily variation in the equatorial electrojet also displays certain anomalous features that differentiates its behavior from the lunar variations elsewhere. A specific example is the maximum amplitude of **L** in the electrojet which is recorded during December solstice (e.g., Chapman and Rao, 1965, Rastogi and Trivedi, 1970). At other latitudes, the maximum in **L** is recorded during local summer. Bartels and Johnston (1940) pointed out the existence of 'big-L days' at Huancayo in January during which the **L** in H becomes conspicuously large and even comparable to solar daily variations. In recent literature the 'big-L days' have been linked with the occurrence of SSWs (Fejer et al., 2010; Yamazaki,

2014). Studies have shown that an amplification of the lunar tidal effects in the ionosphere is associated with the changed tidal propagation conditions during SSWs (Stening et al., 1997; Forbes and Zhang, 2012). The effect of the SSWs on the lunar tidal amplification in the equatorial electrojet is discussed in greater detail in Chapters 2 and 3 of this thesis.

1.4.4 *SSW impacts on the equatorial electrojet*

In this section the impacts of stratospheric sudden warming on the equatorial electrojet is discussed. Stening et al. (1996) first showed an association between the occurrence of counter-electrojet (reversed equatorial electrojet) and SSW events. Their results were confirmed by Vineeth et al. (2009) when they also found the increased occurrences of counter-electrojets (CEJs) with a quasi 16-day periodicity during SSW events. A probable explanation for this stratosphere-low ionosphere connection was made by Sridharan et al. (2009) and they suggested that the enhanced semi-diurnal tidal amplitudes during SSWs influence the day-to-day variability of CEJ events. The onset of CEJ events during SSWs was found to occur near the new moon and full moon phases by (Fejer et al., 2010) and they also pointed out the semi-diurnal perturbations in the EEJ during SSWs that moved to later hours in succeeding days signified the enhancement of lunar effects in the EEJ.

Figure 1.9 taken from Fejer et al. (2010), shows the semi-diurnal perturbation in the EEJ at the Pacific, Indian and Peruvian sectors during the 2002-2003 SSW event. In this period, new moon days (solid circles) occurred on December 4th and January 2nd, and full moon days (open circles) occurred on December 19 and January 18. After the late December warming onset, the electrojet intensities (ΔH) first weakened for about 2 days in all the sectors and then, around new moon, suddenly developed multi-day perturbation patterns with largely enhanced morning eastward and afternoon westward currents that systematically shifted to later local times. Strong morning counter-electrojets were seen around the first and last quarters (January 10 and 25). The morning and afternoon current perturbations occurred first and were strongest in the American sector and developed last and were weakest (particularly in the afternoon) in the Pacific sector. Similar, but weaker, current perturbations developed near full moon after the second warming, when the high-latitude wind perturbations were even larger. These perturbation events are about 14 days apart, as expected for the lunar semimonthly tide.

Ground-based results were further confirmed from satellite measurements by Park et al. (2012) when they found a one-to-one correspondence between lunar modulation of EEJ intensity (from CHAMP magnetic recordings) and SSWs between 2001-2009. Figure 1.10 taken from Park et al. (2012), demonstrates the lunar tidal enhancements of the EEJ during De-

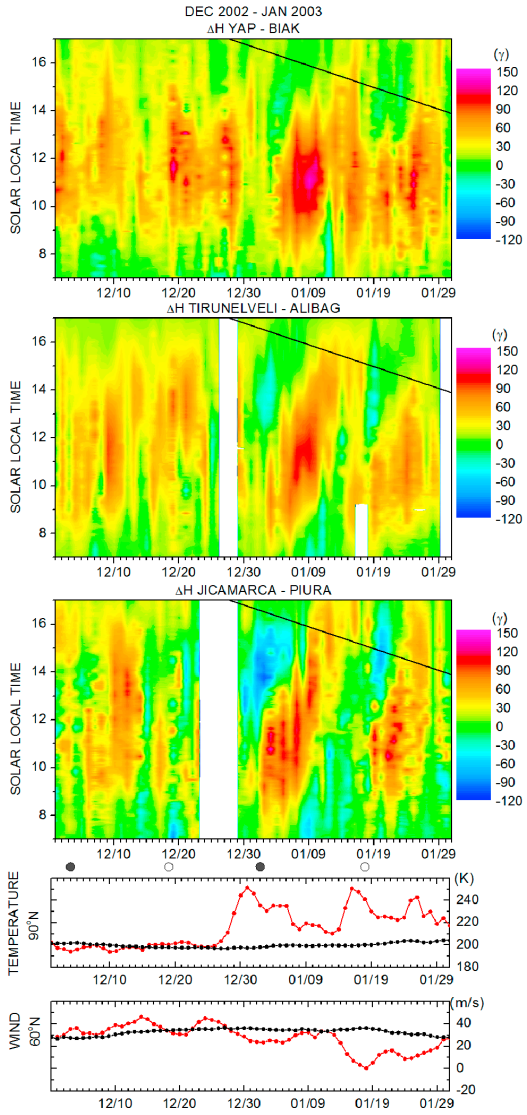

Figure 1.9: Equatorial horizontal magnetic field deflections in three longitudinal sectors and high-latitude zonally averaged stratospheric temperatures and zonal winds during December 2002 and January 2003. The days of new and full moons are indicated by open and solid circles, respectively (from Fejer et al. (2010), Figure 4, reprinted with kind permission from publisher John Wiley & Sons Ltd.).

cember 2001 to August 2009. The 13 day oscillations (third panel of Figure 1.10) correspond to lunar semidiurnal periods from the frame of the CHAMP satellite. From their results, the enhancement of 13 day oscillations of the EEJ strength in each midwinter with SSW are observed suggesting a one-to-one correspondence between the lunar tidal enhancements and SSW occurrence. Yamazaki et al. (2012b) later showed the correlation between amplification of geomagnetic lunar tides in EEJ and the occurrences of SSWs using the magnetic recordings at Addis Ababa between 1958-2007. They also found out a correlation between lunar tidal amplifica-

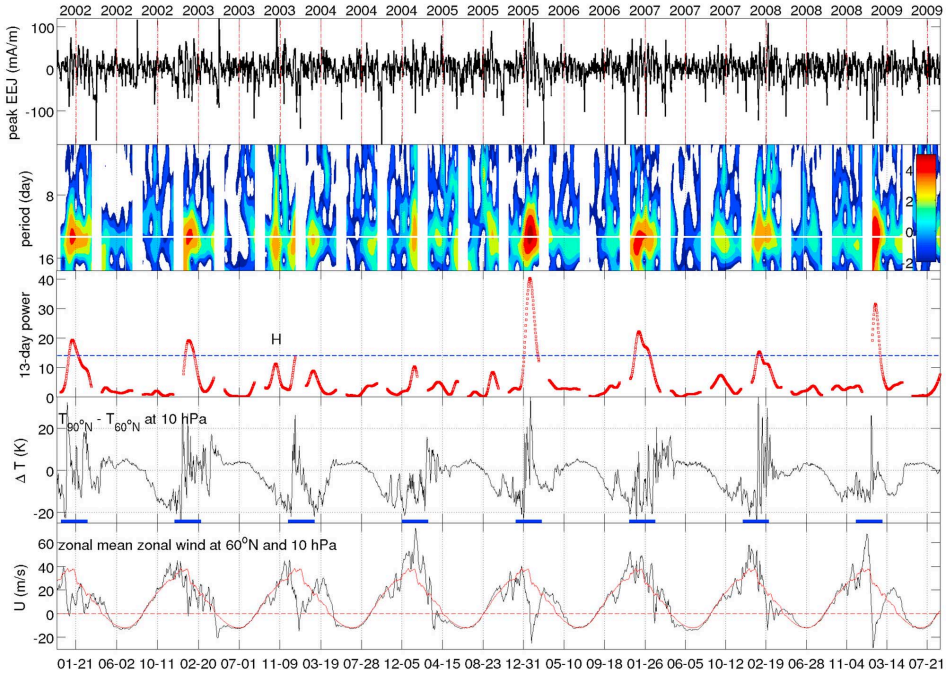

Figure 1.10: SSW observations from December 2001 to August 2009. From top to bottom the panels show detrended daily averages of normalized EEJ strength, the wavelet power spectrum, wave power at the 13 day period, stratospheric temperature difference, and zonal wind. Red vertical lines correspond to noon LT of the CHAMP orbit. The white horizontal line in the second panel represents the 13 day period, and the blue horizontal line in the third panel is intended to guide the eye (from Park et al. (2012), Figure 3, reprinted with kind permission from publisher John Wiley & Sons Ltd.).

tion and the occurrence of SSW events but their results showed instances when there was no lunar amplification despite of an SSW event.

Most of the these observational results have been well supported by modeling studies. Amplification of solar and lunar tides at dynamo region heights has been deduced during SSWs from model results (e.g., Pedatella et al., 2012; Pedatella and Liu, 2013). Lunar tidal amplification has been explained by Forbes and Zhang (2012) through the shifting of a resonance peak of the atmosphere to semidiurnal lunar periods. Tidal changes have been mainly attributed to changed propagation conditions during SSWs which then could also affect the generation of electric fields and currents in the ionosphere. The impacts of SSW on the equatorial electrojet has been specifically explored in this thesis through ground- and space-based magnetic field observations. The next three chapters in this thesis present results of published papers, each discussing a detailed analysis of the lunar tidal modulation of the EEJ during SSWs.

1.5 SCOPE AND OBJECTIVES OF THE THESIS

The day-to-day variability of the ionosphere due to lower atmospheric processes has so far been an outstanding issue that needs to be addressed. The stratosphere-ionosphere coupling during SSWs provide an opportunity to better understand the processes behind the lower atmospheric forcing of the ionosphere and to improve the capabilities that may lead to ionospheric weather forecasting in the future. In this thesis, the SSW induced variability in the strongest low latitude ionospheric current, known as the equatorial electrojet, is particularly studied in detail. One particular reason for studying the SSW impacts in the EEJ is the availability of several decades of observational data. Ground-based magnetic observations underneath the EEJ date back to early 1920s at the Huancayo observatory in Peru. This extended dataset has been used to analyze the response of the equatorial electrojet to all the listed major and minor SSWs since they were first detected in 1952.

The SSW impacts on the EEJ result in the enhancement of lunar tidal amplitudes, and it has been studied using ground- and satellite-based measurements (e.g., Fejer et al., 2010; Yamazaki et al., 2012b; Park et al., 2012; Sathishkumar and Sridharan, 2013). Quantitative estimation of global lunar tidal enhancements in the EEJ during SSWs using the CHAMP satellite measurements has been carried out by Park et al. (2012). Lunar tides in the EEJ have also been quantitatively derived during SSWs using the ground-based measurements in the Indian (Sathishkumar and Sridharan, 2013) and African (Yamazaki et al., 2012b) sectors. In the Peruvian sector despite the availability of Huancayo observatory data, no such studies have been carried out. As the number of observatories near the magnetic dip equator that have continuous magnetic field recording capabilities are very limited it becomes important to study the SSW impacts in the EEJ by making use of the data from the Huancayo observatory.

The central theme in this work is the long-term investigation of the lunar tide in the equatorial electrojet during SSWs mainly by using the ground magnetometer recordings at Huancayo (Chapters 2-4). Additionally, the EEJ data from the CHAMP satellite, SABER temperature measurements and ground magnetometer recordings at Tirunelveli, India have also been used for comparison studies in Chapter 4. The polar stratospheric diagnostics for SSWs have been achieved by making use of the NCEP/NCAR (Chapter 2)and MERRA (Chapters 3 & 4) reanalysis data sets at different pressure levels.

The general pattern of analysis in this work involves the estimation of the lunar tidal amplitude in EEJ during SSWs from magnetic recordings followed by a comparison with the polar stratospheric wind and temperature measurements corresponding to the SSW events. The stratospheric diagnostics for identifying SSWs in the literature have generally relied on

the wind and temperature measurements poleward of 60°N and 10 hPa (≈ 31 kms) pressure level. The state of polar vortex can also be measured by another criteria proposed by Zhang and Forbes (2014) which quantifies the concept of Polar Vortex Weakening (PVW) and has been described in detail in Chapter 3. This criteria has been used in Chapters 3 and 4 for establishing a relation between the enhancement of lunar tides in the EEJ and the occurrence of the SSW.

In addition to using the magnetic recordings at Huancayo, in Chapter 4, the EEJ data from CHAMP and the magnetic recordings at Tirunelveli have also been utilized to investigate the longitudinal differences in the lunar tidal modulation of the EEJ in the Peruvian and Indian sectors during two major SSWs (2006 and 2009) of the past decade. It is found that the lunar tidal enhancements in the EEJ during SSWs are not globally similar suggesting that the local variabilities also play an important role and should be necessarily considered for an improved understanding of the mechanisms behind the stratosphere-ionosphere coupling.

Although, the scope of this study is limited to ground- and space-based magnetic measurements, it is expected that the results from this work would be particularly helpful in understanding the temporal variations of lunar tides in EEJ during SSWs. The following part of this section summarizes the objectives that have been considered in this thesis:

- The magnetic recordings at the Huancayo observatory started much earlier in time when the first SSW event was not yet detected. The SSW events have been shown to impact the ionospheric current systems through the modulation of lunar tides. One primary goal that has been pursued in this thesis is the possibility of identifying historical SSWs (pre-1952) from magnetic field recordings at Huancayo. The EEJ intensity at Huancayo can be derived as early as 1922 which is not feasible at any other magnetic observatory under the dip equator. In Chapter 2, a simple but an intuitive approach is developed which utilizes this data set to identify historical SSWs from magnetic records.

- The polar stratospheric wind and temperature diagnostics for the SSW events are abundantly available in the literature. It is therefore a difficult task to recognize a particular definition of SSW which provides the best representation of middle atmosphere dynamics that can be associated with lunar tidal enhancements in the MLT and in the E-region of the ionosphere. The second objective of this study deals with identifying one such definition of an SSW that could be used to compare the correlation in timing and intensities between the stratospheric conditions and ionospheric response during the SSWs. In Chapter 3, the definition of Polar Vortex Weakening (PVW) is dis-

cussed and its timing and amplitude have been compared with the lunar tidal enhancements in the EEJ.

- The availability of data from magnetic observatories near the dip equator across different longitudes also present an opportunity to investigate the longitudinal variation of the lunar tidal effects in the EEJ during SSWs. The third objective carried out in this thesis is to identify the longitudinal variabilities in the lunar tidal enhancements in EEJ during SSW events and to explore the mechanisms that could explain the difference in the lunar tidal response in different longitudinal sectors. In Chapter 4, the lunar related effects in the EEJ during major SSWs in 2006 and 2009 have been studied from ground and satellite observations in the Peruvian and Indian sectors.

1.6 ORGANIZATION OF THE THESIS

This thesis is structured in the form of a publication-based cumulative thesis and is comprised of three published articles. The first chapter introduces the relevant background information and the scope of this thesis. The next three chapters comprise of the published papers and the last chapter presents the summary from this work and further possible research opportunities. The methods of analysis that have been used in this work are described accordingly in individual chapters. The following subsections present a brief overview of the three manuscripts that is then followed by the individual contributions of the authors.

1.6.1 *Chapter 2: Relation between stratospheric sudden warming and the lunar effect on the equatorial electrojet based on Huancayo recordings*

This chapter investigates the relationship between the lunar tidal modulation of the equatorial electrojet (EEJ) and the stratospheric sudden warming (SSW) based on the magnetic field recordings at Huancayo observatory in Peru. A new method (Sec. 2.4) based on the phase of the semi-monthly lunar tide is proposed for determining the modulation of the EEJ during SSWs due to lunar effects. This is followed by a superposed epoch analysis (Sec. 2.6.2) of the semi-monthly lunar tide and lower stratospheric parameters to showcase a relationship between them.

1.6.2 *Chapter 3: On the relationship between weakening of the northern polar vortex and the lunar tidal amplification in the equatorial electrojet*

In this chapter magnetic field recordings at Huancayo between 1997 and 2013 are again employed to determine the lunar tidal modulation in the equatorial electrojet (Sec. 3.4.1). Thereafter, the concept of polar vortex

weakening (PVW) (Sec. 3.4.2) is utilized to demonstrate that the timing and magnitude of both the PVW and the lunar tidal enhancements in the EEJ (Sec. 3.5) show a correlation with each other. It is found that the timing of lunar tidal peaks and PVW correlate better than their respective magnitudes.

1.6.3 *Chapter 4: Longitude dependent lunar tidal modulation of the equatorial electrojet during stratospheric sudden warmings*

In this chapter the longitudinal dependence of the lunar tidal modulation of the EEJ during 2006 and 2009 major SSWs is analyzed using the ground-based magnetic field recordings (Sec. 4.4.1) at Huancayo, Peru and Tirunelveli, India and CHAMP derived EEJ current densities (Sec. 4.4.2). The lunar tidal modulation of EEJ was found to be significantly stronger at Huancayo than over at Tirunelveli during both these SSW events from ground and space measurements (Sec. 4.5). The lunar tidal amplitude also showed similar enhancements in the Peruvian sector during the two major SSWs, but the enhancements in the Indian sector were notably different during these SSW events. It is suggested that the local variabilities such as ionospheric conductivity, the magnetic field strength and changing atmospheric conditions from year to year could be the cause behind the observed longitudinal variations.

Contributions

The author of this thesis carried out the research and wrote the published articles. Along with Prof. Dr. Claudia Stolle and Prof. Dr. Hermann Lühr, the author developed the ideas and theories which led to the final versions of these articles. As co-authors, Dr. Stolle and Dr. Lühr provided significant suggestions and instructions during the course of submission and revision of the articles. Dr. Jaeheung Park and Dr. Jürgen Matzka also provided critical comments and valuable scientific inputs in the articles that form Chapters 2 and 3, respectively, in this thesis.

Part II

PUBLICATION-BASED CHAPTERS

2

RELATION BETWEEN STRATOSPHERIC SUDDEN WARMING AND THE LUNAR EFFECT ON THE EQUATORIAL ELECTROJET BASED ON HUANCAYO RECORDINGS

Tarique A. Siddiqui[1,2], Hermann Lühr,[1] Claudia Stolle[1,2] and Jaeheung Park[1,*]

[1]GFZ German Research Centre for Geosciences, Potsdam, Germany
[2]Institute of Earth and Environmental Science, University of Potsdam, Germany
*Present address: Solar and Space Weather Research Group, Korea Astronomy and Space Science Institute (KASI), Daejeon, Republic of Korea

Manuscript published as:
Siddiqui, T. A., H. Lühr, C. Stolle, and J. Park (2015). "Relation between stratospheric sudden warming and the lunar effect on the equatorial electrojet based on Huancayo recordings." In: Annales Geophysicae 33.2, pp. 235-243. doi: 10.5194/angeo-33-235-2015.

2.1 ABSTRACT

It has been known for many decades that the lunar tidal influence in the equatorial electrojet (EEJ) is noticeably enhanced during northern hemisphere winters. Recent literature has discussed the role of stratospheric sudden warming (SSW) events behind the enhancement of lunar tides and their findings suggest a positive correlation between the lunar tidal amplitude and lower stratospheric parameters (zonal mean air temperature and zonal mean zonal wind) during SSW events. The positive correlation raises the question whether an inverse approach could also be developed which makes it possible to deduce the occurrence of SSW events before their direct observations (before 1952) from the amplitude of the lunar tides. This study presents an analysis technique based on the phase of the semi-monthly lunar tide to determine the lunar tidal modulation of the equatorial electrojet (EEJ). A statistical approach using the superposed epoch analysis is also carried out to formulate a relation between the EEJ tidal amplitude and lower stratospheric parameters. Using these results, we have estimated a threshold value for the tidal wave power that could be used to identify years with SSW events from magnetic field observations.

2.2 INTRODUCTION

The equatorial electrojet (EEJ) is a narrow band of intense electric current flowing in the east-west direction above the magnetic dip equator in the daytime E-region of the ionosphere. The electrojet is a Hall current which is driven by the large vertical electric field set up at the dip equator (Stening, 1995). The influence of the lunar tides on the Equatorial Electrojet (EEJ) has been known for a long time. Bartels and Johnston (1940) carried out the initial study of the lunar influence on the EEJ and they reported the existence of 'big L' days between the months November to March at Huancayo in Peru. During these days they observed that the lunar daily variations in the horizontal component of the magnetic field get considerably enhanced compared to normal days. This similar enhancement was then reported at other equatorial observatories (e.g., Kodaikanal (Egedal, 1956), Ibadan (Onwumechilli, 1960), Addis Ababa (Gouin, 1960). Rastogi and Trivedi (1970) discussed the seasonal variation of lunar tides within the equatorial electrojet at several equatorial observatories. Lühr et al. (2012) presented a comprehensive overview of lunar tides in the EEJ using the data from the CHAMP satellite. All of these studies confirmed the enhanced tidal amplitudes around the December solstice.

It has been proposed in recent years that this noticeably enhanced lunar tidal effect in the equatorial electrojet during northern winters coincide with stratospheric sudden warming (SSW) events. The phenomenon of SSW was first observed by Scherhag (1952) and since then it has been studied quite extensively. An SSW is a large scale meteorological event characterized by the weakening of the westerly winds in the northern stratosphere and a breakdown of the polar vortex which leads to a sudden rise in the polar stratospheric temperature by several tens of degrees (e.g., Andrews et al., 1987). Matsuno (1971) proposed the non-linear interaction of the vertically propagating planetary waves with the zonal mean flow as the key mechanism for generating SSWs. The effects of SSW are not only restricted to the stratosphere but also extend into the ionosphere. Therefore, SSW is sometimes regarded as one of the most important large scale meteorological phenomena (e.g., Chau et al., 2012).

Recent literature has debated whether SSW events facilitate the lunar tidal propagation which in turn leads to enhanced tidal amplitudes around the December solstice (e.g., Fejer et al., 2010; Fejer et al., 2011; Stening, 2011; Park et al., 2012; Yamazaki et al., 2012a; Yamazaki et al., 2012b). Stening (2011) pointed out that the relation between the large lunar tide in EEJ and SSW events could be coincidental, while Park et al. (2012) confirmed a one-to-one correspondence between the lunitidal enhancement at ionospheric heights and the occurrence of SSW events between 2001-2009. Likewise, Yamazaki et al. (2012b) investigated the correlation between the amplitude of the geomagnetic lunar tide at Addis Ababa and lower stratospheric

parameters and confirmed the occurrence correspondence between SSWs and the enhancement of the geomagnetic lunar tide for the majority of years between 1958-2007. However, their report certains counter examples during January 1983 and January 1985 where the occurrence correspondence breaks down.

The purpose of this paper is an attempt to deduce the occurrence of SSWs for the times before their direct observations (before 1952). For achieving this goal we make use of magnetic field recordings of the Huancayo observatory, which is located under the magnetic equator. The observatory started recordings in 1922.

In the following sections we first describe the various data sets used in this study in Section 2.3. In Section 2.4 we introduce our approach for determining the strength of the lunar tidal modulation of the equatorial electrojet. In Section 2.5 results are presented. We start with the years past 1952 and make direct comparison with stratospheric observations of the SSWs. Afterwards we also show EEJ lunar modulations from time before SSW observations. Section 2.6 provides a discussion of our results in comparison to related studies. Furthermore, we provide a statistical assessment of the relation between SSW parameters and lunar tidal amplitude and make predictions of SSW events derived from lunar tides in magnetic data. Results are summarized in Section 2.7.

2.3 DATASET

The choice of the observatories is based on the fact that we want to monitor the variation of the equatorial electrojet as far back into the past as possible. In addition, we require that one of the observatories lies within the electrojet zone and the other lies outside of it. The purpose of this approach is that a major part of magnetospheric variation at an equatorial observatory can be removed by considering variations at a non-equatorial observatory (e.g., Manoj et al., 2006). Thus the observatories Huancayo, HUA, (-12.05°N, 284.67°E) and San Juan, SJG, (18.11°N, 293.85°E) constitute one such pair. The latitudinal difference between the Huancayo - San Juan pair is 30.16° while the longitudinal difference between the stations is 9.18°. San Juan serves as a reference station to the equatorial station at Huancayo for eliminating the effects of large scale magnetospheric fields. The San Juan magnetic observatory has a continuous data record of hourly means of the horizontal component of magnetic field since 1926. On the other hand, the hourly means recorded at the Huancayo observatory are available from 1922 onwards; however, there are some lengthy durations of missing data for the periods 1962-1963, 1970-1978, 1981-1984 and 1991-1996. Here we use the data available between the years 1926 to 2009 for the Huancayo and the San Juan observatories to determine the lunar tides.

We employ the hourly means of the geomagnetic horizontal field component from these two magnetic observatories in our study. The data were downloaded via the website of the World Data Centre (WDC) for Geomagnetism, Edinburgh.

To consider the effects of solar activity on the EEJ strength we use the solar flux values $F_{10.7}$ in sfu $(10^{-22} W m^{-2} Hz^{-1})$ which are available since 1947 on the website of the Dominion Radio Astrophysical Observatory in Penticton, British Columbia, Canada. For earlier years we use the sunspot numbers which are available since 1818 and can be downloaded from the website of WDC-SILSO, Royal Observatory of Belgium, Brussels.

For identifying the SSW events, daily mean values of the zonal mean temperature at 60°N and 90°N at the 10 hPa level and daily means of the zonal mean zonal wind at 60°N and at 10 hPa level were obtained from the reanalysis data of the National Centers for Environmental Prediction/-National Center for Atmospheric Research (NCEP/NCAR) (Kalnay et al., 1996) for the years 1948 to 2010.

2.4 METHOD OF ANALYSIS

The total magnetic field variation at the dip equator includes the contributions from the EEJ, magnetospheric and Sq current systems and it is proportional to $(j_H + j_P)$ where j_H and j_P are the Hall and Pedersen currents, respectively. In this paper, we follow the assumption that the magnetic signature of the electrojet on ground, H_{EEJ}, is proportional to j_H. For the horizontal magnetic field component, H, we can write

$$H = H_{MF} + H_{MP} + H_{Sq} + H_{EEJ} \tag{2.1}$$

where H_{MF} is the main field, H_{MP} the field of magnetospheric currents (e.g., ring current), H_{Sq} the field of large-scale ionospheric currents and H_{EEJ} the magnetic effect of the electrojet. To calculate the intensity of the magnetic field that is only due to the effect of the electrojet, the first three terms on the right hand side have to be removed. An estimate for the main field, H_{MF}, is obtained from the quiet night-time values. For both stations we first calculate,

$$\Delta H = H - H_{MF} \tag{2.2}$$

For the isolation of the electrojet effect we assume that large-scale fields of magnetospheric currents are the same at both observatories (e.g., Stolle et al., 2008). The equatorial electrojet strength is estimated from an observatory pair by evaluating the difference of the horizontal intensities ΔH, at the two locations as,

$$H_{EEJ} = \Delta H_{HUA} - \Delta H_{SJG} \tag{2.3}$$

The strength of the EEJ currents shows a linear relationship with the solar activity (Alken and Maus, 2007). Stronger EEJ currents are recorded during periods of solar maximum and vice-versa. In order to take into account also the resulting day-to-day variability caused by EUV radiation, the effects of solar activity on the EEJ are normalized with the help of $F_{10.7P}$ where $F_{10.7P} = \frac{F_{10.7}+F_{10.7A}}{2}$ (Richards et al., 1994). $F_{10.7}$ is the observed value of solar radio emission at 10.7 cm for each day and $F_{10.7A}$ is the 81-day centered mean of $F_{10.7}$. As the $F_{10.7}$ readings are available only since 1947, we make use of the recordings of the sunspot numbers for normalization before 1947.

For the correction of the solar flux dependence we apply the relation deduced by Alken and Maus (2007) for their EEJM model. They propose the linear relation

$$J = 4.458 \times 10^{-5}(A/m)\, E + 0.040(A/m) \tag{2.4}$$

where J is the height-integrated peak current density of the EEJ in A/m and E is the EUVAC (Extreme UltraViolet flux model for Aeronomic Calculations) value, which is practically identical with our $F_{10.7P}$ readings. It was shown by Manoj et al. (2006) that the EEJ peak current density estimated from the CHAMP satellite is highly correlated with the EEJ intensity derived from a ground observatory (H_{EEJ}). We normalized all our H_{EEJ} values to a solar flux value of $F_{10.7P} = 150$ sfu. However, since the solar flux index $F_{10.7}$ is available only since 1947, we had to use an alternative for normalizing the solar activity influence before 1947. Our EUVAC index E in equation (2.4) is in this case based on the sunspot number. Based on a correlation analysis using the data from the years 1960-2009 we could establish a linear relation between the $F_{10.7}$ and the sunspot number.

$$F_{10.7} = \frac{SunspotNumber + 62.58}{1.03} \tag{2.5}$$

The dominant variation of H_{EEJ} is the diurnal variation, but we are interested in the lunar tidal modulation of that signal. In order to suppress the daily wave, the data are sorted into bins of 1 day by 1 h in Local Time (LT) for two synodic months (59 days). The effect of solar tides is removed by subtracting the mean over the 59-day period for each local time hour from the bin averages. Figure 2.1 shows an example of this processing approach. The top frame shows the H_{EEJ} obtained from the Huancayo - San Juan pair before removing the dominant diurnal variation and the bottom frame shows the similar plot after removing the diurnal variation. The local time sector considered here is from 07:00 to 17:00 LT. Outside of this time interval the EEJ signal is considered to be weak. Each dataset for analysis starts with the day of the new moon phase and ends on the day before the new moon. A sliding window of 59 days advanced by one synodic month is applied for each subsequent dataset, as this overlap ensures improved

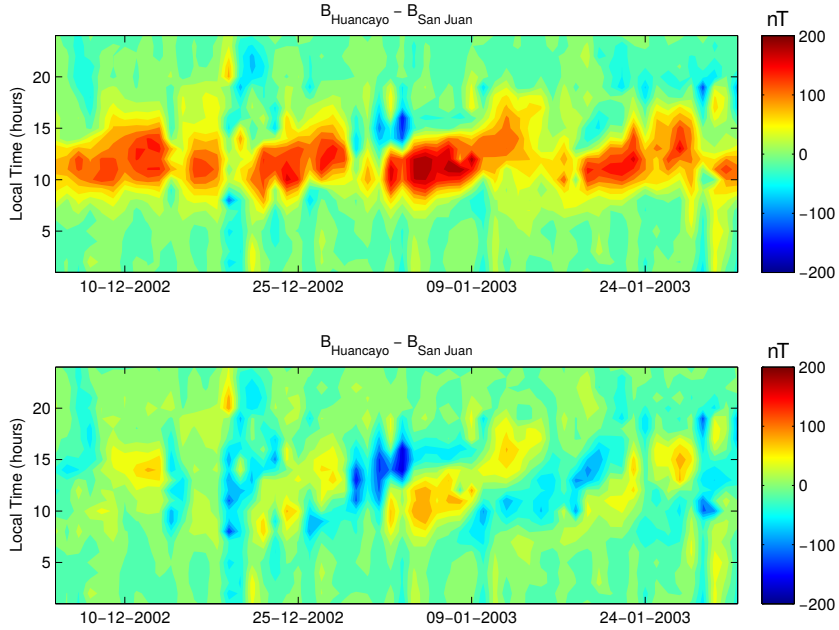

Figure 2.1: The top frame shows H_{EEJ} obtained from the Huancayo - San Juan pair during December 2002 - January 2003 before removing the solar tidal effects. The bottom frame shows the same plot after the removal of solar tidal effects.

amplitude resolution. We apply harmonic analysis for each local time hour over the period of two synodic months (59 days) for a quantitative investigation of the lunar signal. The frequency of interest is the fourth harmonic signal (semi-monthly wave) for which both the phase (ϕ_{obs}) and the amplitude (a) are determined for each local time hour. We use the relation described by Lühr et al. (2012) to predict the phase of the semi-monthly lunar tide as a function of the lunar age (d) and local time (LT). The lunar age is taken as the number of days, d, since new moon.

$$LT = 0.98(d - d_0) + 8.5\,h \tag{2.6}$$

where d_0 is calculated by converting the moon phase of 12 h in terms of lunar age. As the moon phase of 24 h corresponds to lunar age of 29.53 days, the moon phase of 12 h can be calculated to correspond to lunar age of 14.76 days.

The lunar tide is an astronomical phenomenon. Therefore its phase is well known. We take advantage of this *a posteriori* information for our analysis. The expected phase, ϕ_{pre}, of the lunar wave can be obtained by using the relation for each local time hour

$$\phi_{pre} = \frac{\pi}{6\,h}(LT - 12\,h) + \phi_0 \tag{2.7}$$

where ϕ_0 is the angle (in radians) corresponding to the common delay of 4.4 days from the new moon day until the tidal wave crest reaches 12 h

local time, as described by Park et al. (2012). The value of the phase (ϕ_{pre}) is used as the expected phase and compared with the value obtained from the harmonic analysis.

We define a parameter ϵ as

$$\epsilon = \phi_{obs} - \phi_{pre} \tag{2.8}$$

The cosine of the difference between the computed and the observed phase values is used as a weighting function and it has been determined experimentally.

$$a^{'} = a \cos\epsilon \quad \text{for } |\epsilon| < \frac{\pi}{2} \tag{2.9}$$

We use a filtering condition that if $|\epsilon| > \frac{\pi}{2}$, then the derived amplitude and the phase for that local time is not considered. A value lower than $\frac{\pi}{2}$ could also be chosen but then it would result in fewer wave amplitude values. The wave amplitude ($a^{'}$) obtained is then divided by the sum of weights.

We further normalize the amplitude for the expected diurnal variation of the ionospheric conductivity, C, as described by Lühr et al. (2008). Their assumption is based on the fact that the electron density of the E-layer varies proportional to the square root of the cosine of the solar zenith angle. The diurnal variation of the ionospheric conductivity does not only influence the Sq currents but also the amplitude of the lunar tidal signal, as has been shown by Lühr et al. (2012). Without the normalization, the values around noon would dominate the tidal results.

$$C = C_0 \sqrt{\cos\left\{\frac{\pi}{12\,h}(LT - t_0)\right\}} \tag{2.10}$$

where C_0 is the value of the peak conductivity and t_0 is the local time of the peak conductivity. A suitable value for t_0 has been found to be 12:30 LT. For our purpose we chose C_0 to be equal to 1.

In the determination of the mean amplitude, A, over the two synodal months the lunar phase propagation from hour to hour is taken into account. The semi-monthly lunar tidal amplitude, A, is obtained by comparing the coefficients in equation (2.11) where ω is the angular frequency given by ($\frac{2\pi}{59}\,day^{-1}$), t, denotes time in days and ϕ_{mean}, denotes the phase of the mean lunar tidal wave computed for 07:00 to 17:00 LT.

$$A\,\cos(4\,\omega\,t - \phi_{mean}) = \frac{1}{11}\sum_{LT=7}^{17}\frac{a^{'}(LT)}{C}\sum_{LT=7}^{17}\beta \tag{2.11}$$

where,

$$\beta = \cos(4\,\omega\,t - \phi_{obs}(LT) + \epsilon) \tag{2.12}$$

The amplitude A is given in nT. For every lunar month we compute one value.

2.5 OBSERVATION

It has been observed that the influence of the lunar tide on the EEJ intensity is generally quite small except during certain 'big L days' which were reported by Bartels and Johnston (1940). During these days the lunar tidal influence is much more prominent. Figure 2.2 shows two examples of the diurnal magnetic field variations underneath the EEJ from the Huancayo observatory. On the left side (top) we see a two months period from a non-SSW winter where the tidal effects are weak while the figure on the right (top) corresponds to the EEJ variation with a prominent lunar tidal modulation during an SSW winter. The dashed lines mark the expected lunar tidal wave propagation with local time from day to day, which fits very well with the observed tidal wave crests. We plot the difference between the stratospheric temperature at the North Pole (90°N) and the zonal mean temperature from 60°N, both at 10 hPa in the middle panels and the difference between the zonal mean zonal wind (U_{60}) at 60°N and 10 hPa from the climatological mean (U_C) in the bottom panels to explain the different response of the EEJ signal during the two periods.

It can be observed that on the left side the temperature difference between the two latitudes is quite constant but there is a fairly large variation on the right side. This variation in temperature difference is due to an stratospheric sudden warming event. Therefore it can be clearly seen that SSW events coincide with an amplification of the lunar tidal effect on the EEJ.

The definition of a major SSW event according to the World Meteorological Organization (WMO) involves the reversal of the latitudinal temperature gradient poleward of 60°N and the reversal of the zonal mean zonal wind at 60°N at 10 hPa. The criteria for a minor warming event is the increase in the stratospheric polar temperature by 25 K or more within a week and involves no reversal of the zonal mean zonal wind. However, here we follow the definition adopted by Yamazaki (2013) in which an SSW winter is identified if the zonal mean zonal wind at 60°N and 10 hPa shows a significant change from the climatology ($U_{60} - U_C$ <-20 m/s), and there is a significant reversal in the temperature gradient ($T_{90} - T_{60}$ >10 K) during December - February. The readers may refer to Yamazaki (2013) for more details on the definition. We determine the climatology (U_C) for the zonal mean zonal wind by calculating the mean value from 1948 to 2010 at each day of the year. We list the dates of all the SSW (peak warming) events obtained using this definition from 1952-2009 in Table 2.1.

We hereafter refer to the difference between the temperature at the North Pole (90°N) and the zonal mean temperature at 60°N, both at 10 hPa as the zonal mean temperature gradient.

In Figure 2.3, the top frame shows the wave power of the lunar tides obtained according to equation (2.11) from the Huancayo - San Juan pair,

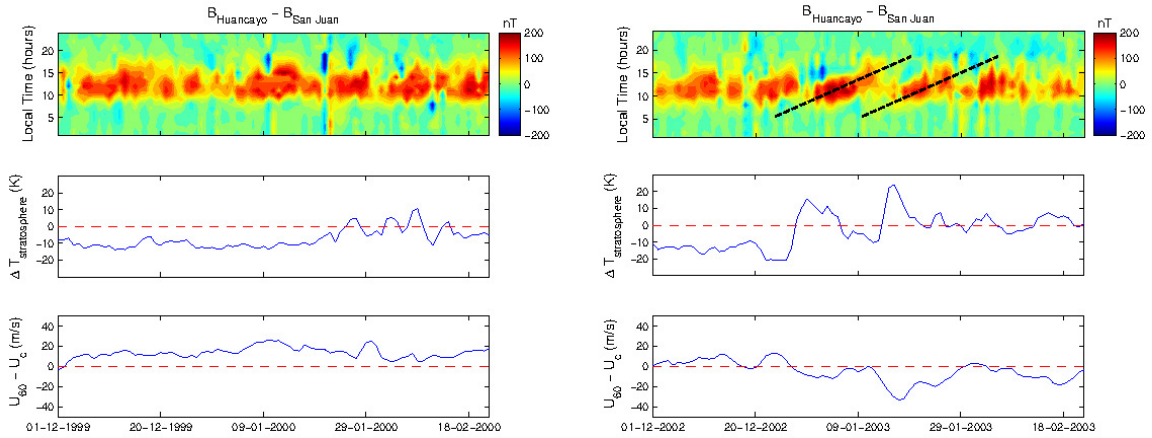

Figure 2.2: The top panels show the diurnal variation of the EEJ intensity (nT) as observed at Huancayo. The middle panels show the temperature difference in the stratosphere between the polar region and 60°N latitude at 10 hPa. The bottom panels show the deviation of the zonal mean zonal wind at 60°N and at 10 hPa from the climatological mean. The left figure (top) shows the EEJ variation on normal days with weak lunitidal effect while the figure on the right (top) corresponds to the EEJ variation during an SSW event. The lines in the top right panel mark the expected lunar tidal wave propagation in local time.

the middle frame shows the zonal mean temperature gradient for the period 1952-1962 and the bottom frame shows the difference between the zonal mean zonal wind (U_{60}) at 60°N and 10 hPa from the climatological mean (U_C). The red lines denote the days of SSW (peak warming) events. Though the SSW events of February 1952 and January 1960 show enhanced lunar tidal powers, we do not observe a one-to-one correspondence between the reversal of the temperature gradient and the enhancement of the lunar tidal power during this period. During November 1952 and December 1954, there is a significant deviation of U_{60} from U_C reaching close to -20 m/s but $T_{90} - T_{60}$ <10 K during this time. During March 1953, a significant increase in the temperature gradient can be observed but there is no prominent deviation in the zonal mean zonal wind from climatology. However, the lunar tidal enhancements can be seen during all these times. Similarly, this behaviour can also be seen during December 1953 and February 1962 when only one of the parameter satisfies the SSW criteria. However, during January 1958 no such enhancements are observed even though $U_{60} - U_C$ <-20 m/s. The lunar tides are also enhanced during March 1959 and 1961 when both the SSW criteria are satisfied. We also observe some counter-examples like during December 1955 where the lunar tidal power increases without any of the SSW criterion being satisfied. These examples suggest there are also other physical processes behind the enhancement of the lunar tides that are not discussed by this definition

Number	SSW Events (Peak Warming)
01	23 Feb 1952
02	03 Jan 1960
03	10 Dec 1965
04	07 Jan 1968
05	07 Dec 1968
06	29 Dec 1969
07	10 Jan 1971
08	30 Jan 1973
09	02 Jan 1974
10	15 Dec 1976
11	21 Dec 1978
12	27 Feb 1979
13	05 Feb 1981
14	28 Jan 1982
15	19 Jan 1987
16	10 Dec 1987
17	12 Feb 1989
18	27 Jan 1991
19	19 Jan 1992
20	02 Jan 1994
21	29 Jan 1995
22	27 Dec 1997
23	19 Dec 1998
24	20 Dec 2000
25	25 Dec 2001
26	17 Jan 2003
27	28 Dec 2003
28	23 Jan 2006
29	23 Feb 2008
30	23 Jan 2009

Table 2.1: SSW events between 1952-2009 identified using NCEP/NCAR reanalysis data. The definition used to identify SSW events is described in Section 2.4.

of SSW. Yamazaki et al. (2012b) also reported some cases where no such correspondence was observed. We suggest further clarifications in the def-

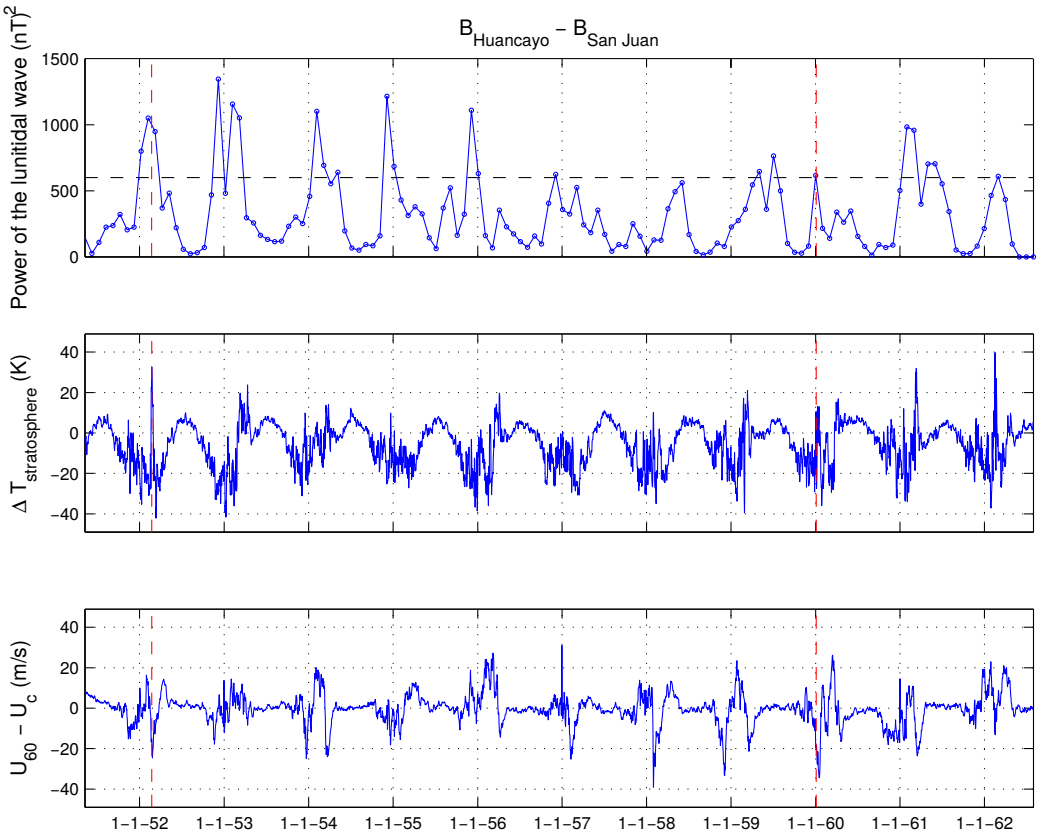

Figure 2.3: The top frame presents the wave power of the lunar tide derived from the Huancayo-San Juan pair for the years 1952-1962. The middle frame shows the zonal mean temperature gradient for the same period. The bottom frame shows the difference between the zonal mean zonal wind (U_{60}) at 60°N and 10 hPa from the climatological mean (U_C). The red lines mark the days of SSW (peak warming) events and the black dashed line in the top panel, denotes the threshold level calculated for classifying SSW and non-SSW years.

inition of an SSW event might improve the correlation between the lunar tidal enhancements and the lower stratospheric parameters.

The next set of continuous data records available for the Huancayo observatory and with much improved quality starts from 1997. In Figure 2.4 we show the same parameters as in Figure 2.3 for the period 1997-2009. A much clearer lunitidal signature is obtained for this duration. Periods of SSW events are much better confined and the ratio in signal power is improved between periods of SSW events and other times. All the SSW events between 1997-2009 except 2001 show enhanced lunar tidal powers.

Since, common datasets for observatories Huancayo and San Juan are available from 1926 onwards, we computed the lunar tidal wave power in the same way as before for these earlier years. Figures 2.5 and 2.6 show the lunar wave power for the years 1926-1938 and 1939-1951, respectively. We

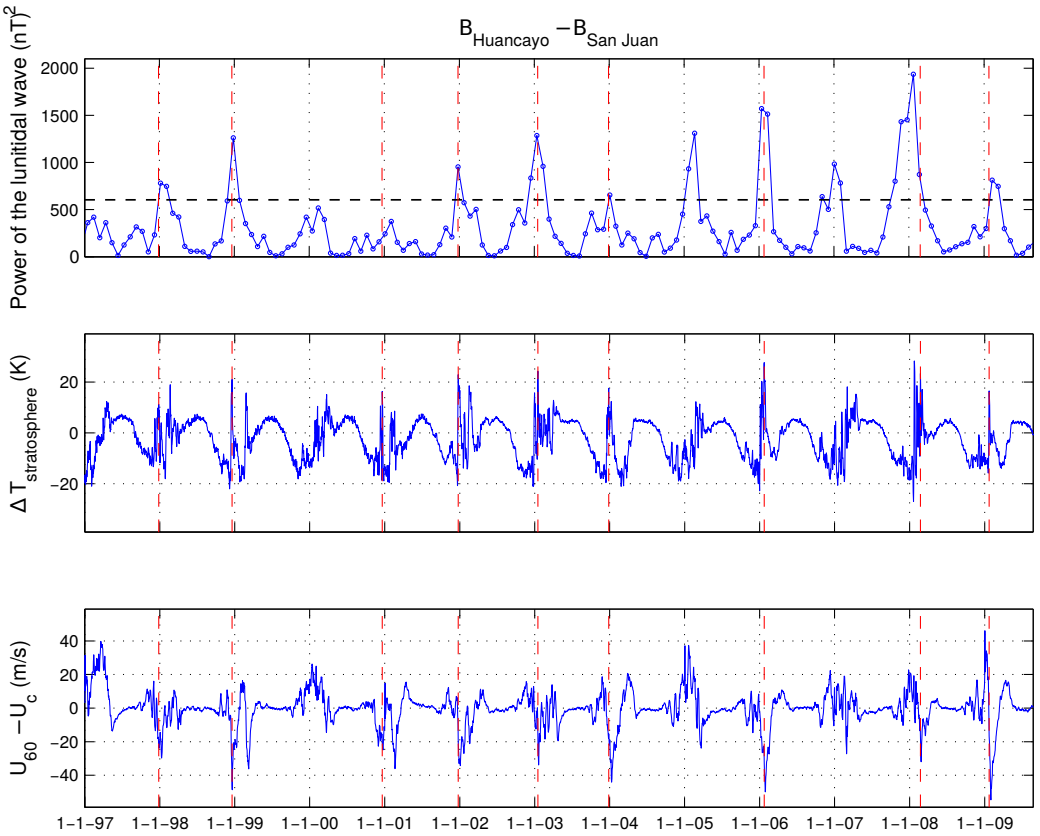

Figure 2.4: Same as in Figure 2.3 but for the period 1997-2009.

again find clear peaks around the beginning of the years and minimum values during the middle of the years. The annual variation is partly not so clear for the early years up to 1932. During that time span repeatedly data gaps are encountered that may have compromised the results. For the rest of the time, values consistent with our assumption are derived for the modulation of the EEJ amplitude. For these early years the zonal mean air temperature values from high latitudes are not available.

2.6 DISCUSSION

2.6.1 *Comparison with earlier studies*

Another study on the relation between lower stratospheric parameters (zonal mean air temperature and zonal mean zonal wind) and lunar tidal modulation of the electrojet was performed by Yamazaki et al. (2012b). They used EEJ recordings of the Addis Ababa observatory for the years 1958-2007. In general they can confirm with their independent dataset the close correlation between the enhancement of the Northern Polar stratospheric temperature and lunar tidal amplitude. They also identify years when the correlation breaks down, but these are a minority. They confirm

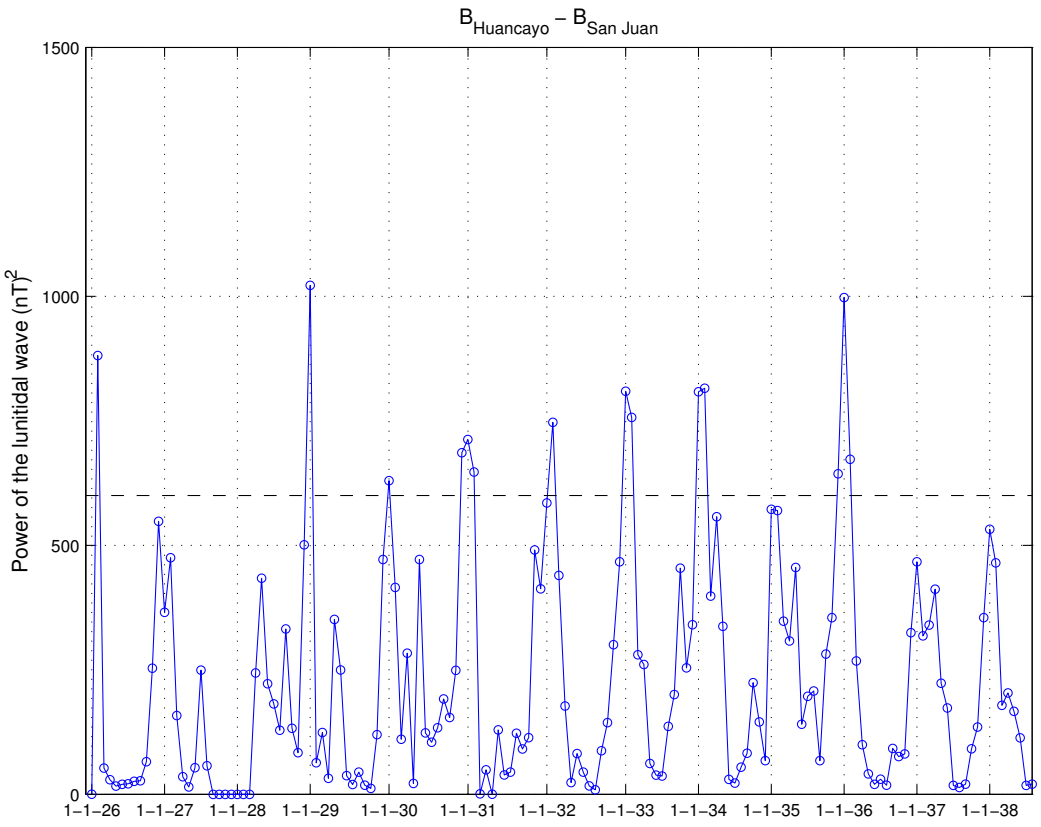

Figure 2.5: The figure presents the wave power of the lunar tide derived from the Huancayo - San Juan pair for the years 1926-1938. The black dashed line shows the threshold level for classifying SSW and non-SSW years.

the correspondence in approximately 70% of the SSW events between 1958-2007.

When deducing the occurrence of an SSW event from the EEJ tidal signature a clear criterion is needed. For example, Park et al. (2012) defined a threshold for the level of wave power of the lunar tide. In their publication they demonstrated a one-to-one correspondence between actual SSW events and large enough lunar tidal signals for the years 2001-2009. It would be desirable to also find a threshold value for the wave power we deduced for Huancayo. A possibility is to estimate the threshold from the average wave power of the years from 1997-2009 when the lunitidal signatures are very clear. For this period we obtain an average value of 800 nT^2. We define the threshold value to be 75% of the average value, A_{thr}= 600 nT^2. The black dashed lines in Figures 2.5 and 2.6 mark this threshold. According to this rather simple classification we predict from the early EEJ recordings several non-SSW years. It is found that the occurrence frequency of historic SSWs from ground magnetic recordings is around 6 events per decade. Since the frequency of major SSW events is also approximately 6 per decade (Charlton and Polvani, 2007), this ap-

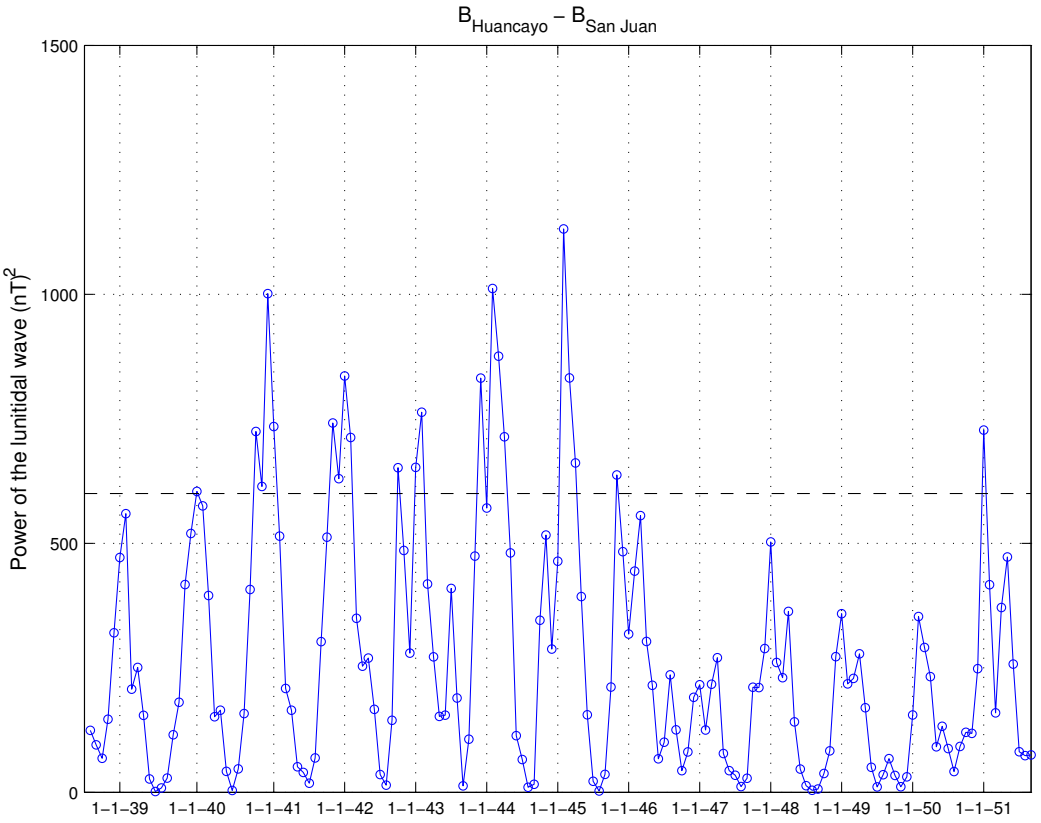

Figure 2.6: Same as in Figure 2.5 but for the period 1939-1951.

proach seems realistic. Even though there are uncertainties involved these are the first estimates of SSW events before the direct observations.

2.6.2 *A superposed epoch analysis*

For a more quantitative assessment of the timing between the enhanced lunar tide and the SSW event, we use the method of superposed epoch analysis (SEA). The SEA method is performed on the lunar tides estimated from the Huancayo - San Juan station pair for the period of the best data quality 1997-2009. It is then compared with the SEA results obtained from the zonal mean temperature gradient ($T_{90°N}$ - $T_{60°N}$ both at 10 hPa) and $U_{60} - U_C$ for the same time period. For our study, we define the starting day of an SSW event as the first maximum of the zonal mean temperature gradient during the northern winters. This date is taken as the key time for selecting an interval of 60 days before and 120 days after the starting day for performing the superposition. From Figure 2.4 it can be seen that thirteen events are available for the SEA according to our classification for the period 1997-2009. Since the wave power of the lunar tide is only sampled once per lunar cycle, we use linearly interpolated values.

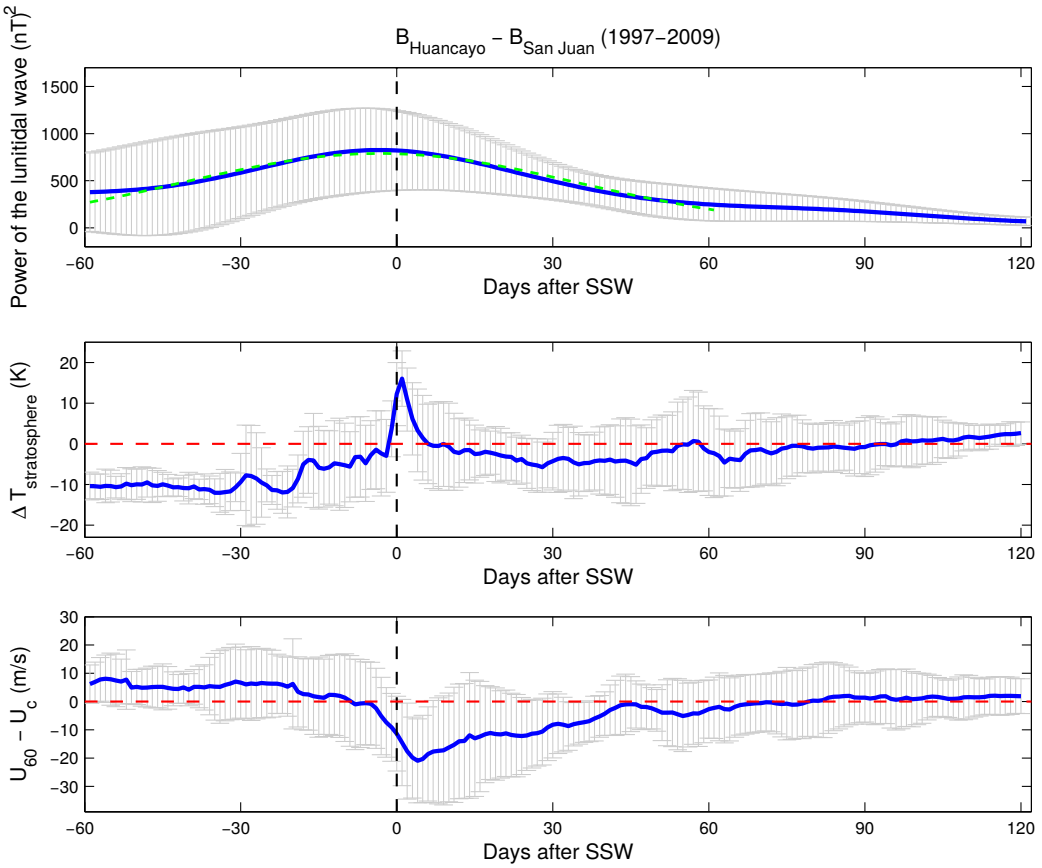

Figure 2.7: Results of the superposed epoch analysis: Composite of the semi-monthly lunitidal wave power (top), zonal mean temperature gradient (middle) and $U_{60} - U_C$ (bottom) for the years 1997-2009. The vertical dashed lines indicate the starting day of SSW events. The error bar represents the standard deviation in all the three panels. The dotted green curve in the top frame shows the Gaussian curve fitted for 60 days each on the either side of starting date of SSW events.

Figure 2.7 shows the result of superposed epoch analysis. The top panel contains the composite of lunitidal wave power with a maximum around the starting day of SSW events. The second and the third panels show the composite of the zonal mean temperature gradient and $U_{60} - U_C$. As expected the composite of the temperature gradient shows a sharp peak at about 1 day after the key time and a width of 5 days around the start of the SSW events. It can also be seen that the composite of the $U_{60} - U_C$ reaches the value of -20 m/s, which we used to define an SSW event. We observe there is not much variability between the zonal mean zonal wind and the climatology before the start of SSW events. After about a month average wind velocity reaches the normal climatological levels.

Our analysis confirms a close relation between the increase in stratospheric temperature difference and enhanced lunitidal signal. For quantifying our SEA result we fitted a Gaussian normal distribution to the

wave power curve (see green dashed line in Figure 2.7). The fitting results are listed in Table 2.2. Since an SSW event starts independently from the moon phase this approach seems justified. From the fit to the composite wave power curve we obtain the peak of the Gaussian curve ($A = 789\ nT^2$) about 4.3 days before the SSW start date and with a standard deviation of $\sigma = 38$ days. The fairly large width of the distribution is partly due to the random difference between the SSW start and lunar phase, but primarily due to our long analysis interval of 59 days.

Amplitude $(nT)^2$	σ (days)	μ (days before SSW)
800	38	4.3

Table 2.2: Gaussian curve parameters.

It is assumed that the lunar tidal wave originates from the lower atmosphere and propagates upward. According to Forbes and Zhang (2012) a certain atmospheric resonance peak shifts right onto the quasi-semidiurnal period (12.42 h) of the moon phase. This strongly supports an efficient upward propagation of the tidal wave. From the results of our superposed analysis we may conclude that the sudden change in stratospheric temperature at the North Pole immediately triggers the condition that is shifting the resonance peak. Further investigations including model simulations are probably needed for fully explaining the observed relation.

2.7 CONCLUSIONS

We have used the magnetic field data of the Huancayo observatory to determine the modulation of the equatorial electrojet (EEJ) by the lunar tide. The size of tidal amplitude is compared with the occurrence of SSW events. Major points of our study are:

1. A new analysis technique is used focusing on the harmonic signal that is strictly in phase with the expected tidal wave. This helps efficiently to suppress the influence of solar activity dependent EEJ fluctuations and day-to-day variabilities.

2. As expected, large lunar tidal amplitudes are observed during northern winter months. As far as we can suggest from our data analysis, peak amplitudes occur generally around times of SSW events.

3. We have investigated the relation between tidal amplitude and SSW event by means of a superposed epoch analysis. From this approach a clear relation between these two quantities arises. When the reference day for the analysis is defined by the first peak in high latitude stratospheric temperature difference then the mean tidal amplitude peaks on average 4 days earlier. Individual years however, exhibit tidal peaks depending on the lunar phase within a month before or after the stratospheric warming peak, which we can't explain at the moment.

4. We also consider periods before the time of direct SSW observations (before 1952). Huancayo data from 1926 onwards are analyzed. The annual variation pattern emerges after 1932. We have estimated a threshold value for the tidal wave power that may help to identify years with SSW events from magnetic field observations. Our results propose an average of approximately six SSW events per decade also before 1952.

2.8 ACKNOWLEDGEMENTS

The results presented in this paper rely on the data collected at San Juan and Huancayo. We thank U.S. Geological Survey and Instituto Geofisico del Peru, for supporting its operation and INTERMAGNET for promoting high standards of magnetic observatory practice. We are also grateful to NOAA/OAR/ESRL PSD, Boulder, Colorado, for providing NCEP-NCAR reanalysis data. The solar activity index F10.7 is provided by Herzberg Institute of Astrophysics. The sunspot number data is provided by WDC-SILSO, Royal Observatory of Belgium, Brussels.

3

ON THE RELATIONSHIP BETWEEN WEAKENING OF THE NORTHERN POLAR VORTEX AND THE LUNAR TIDAL AMPLIFICATION IN THE EQUATORIAL ELECTROJET

Tarique A. Siddiqui[1,2], Claudia Stolle[1,2], Hermann Lühr[1] and Jürgen Matzka[1]

[1]GFZ German Research Centre for Geosciences, Potsdam, Germany
[2]Institute of Earth and Environmental Science, University of Potsdam, Germany

Manuscript published as:
Siddiqui, T. A., C. Stolle, H. Lühr, and J. Matzka (2015). "On the relationship between weakening of the northern polar vortex and the lunar tidal amplification in the equatorial electrojet." In: Journal of Geophysical Research: Space Physics 120.11, pp. 10006-10019. doi:10.1002/2015JA021683.

3.1 ABSTRACT

Enhanced lunar tidal effects in the equatorial electrojet (EEJ) during northern winters in the form of 'big L' days have been known for a long time. Recent studies suggest that the changes in the tidal propagation conditions due to stratospheric sudden warmings (SSW) could be responsible for this phenomenon. In this work we have used the *H* component of the magnetic field recorded at Huancayo from 1997-2013 to study the relation between the timing and magnitude of the semi-monthly lunar tide in the EEJ and the stratospheric polar vortex weakening (PVW). We prefer a definition of PVW by taking into account the atmospheric conditions from December to February for each winter. Our results indicate that the semi-monthly lunar tide in the EEJ gets enhanced during northern winters when a significant PVW occurs and its peak timing and magnitude is correlated with the timing and intensity of PVW. The timing of lunar tidal peaks and PVW correlate better than their respective magnitudes. Our results suggest that the initiation of the lunar tidal enhancement in most of the cases is closely related to a PVW event. Furthermore, we discuss events where the semi-monthly lunar tidal enhancements are not well timed with respect to PVW. We also suggest that the amount of tropospheric forcing into the stratosphere plays a major role in the enhancement of the lunar tides in the EEJ.

3.2 INTRODUCTION

Lunar tidal enhancement in the equatorial electrojet (EEJ) in relation to stratospheric sudden warming (SSW) events have been studied extensively in recent years (e.g., Stening, 2011; Park et al., 2012; Lühr et al., 2012; Yamazaki et al., 2012b; Yamazaki, 2013; Siddiqui et al., 2015b). Large lunar effects in the EEJ between November and March were first reported by Bartels and Johnston (1940) but the mechanism behind these observations were not fully understood. Recent publications have tried to explain this phenomenon through the enhanced planetary wave (PW) activity which is assumed to be responsible for causing SSW (Matsuno, 1971). Forbes and Zhang (2012) explained the amplified lunar tidal winds in the ionospheric dynamo region during an SSW through the changes in the zonal mean zonal wind and temperature of the middle atmosphere which shifts the atmospheric (Pekeris) resonance peak onto the lunar period (12.42 h). Subsequently, the amplification of the semi-monthly lunar tide in the EEJ during SSW winters were reported by Yamazaki (2013) to be almost three times larger compared to the non-SSW winters.

SSWs have been studied quite extensively since they were first observed by Scherhag (1952). SSWs are characterized by the weakening of the westerly winds in the northern stratosphere and a breakdown of the polar vortex which leads to a sudden rise in the polar stratospheric temperature by several tens of degrees (e.g., Andrews et al., 1987) and are usually classified into major and minor warming events. According to the World Meteorological Organization (WMO) definition, an SSW is identified as a major warming event if there is a reversal of the latitudinal temperature gradient poleward of 60°N and the reversal of the zonal mean zonal wind at 60°N/10 hPa and as a minor warming if there is an increase in the stratospheric temperature by 25 K or more within a week without the reversal of the zonal mean zonal wind. Moreover, different authors have also used modified versions of the WMO definition and other diagnostic variables to identify SSWs. For e.g., Charlton and Polvani (2007) used solely the wind reversal criterion to detect major SSWs. Martineau and Son (2013) identified SSWs based on the NAM (Northern Annular Mode) index at 10 hPa. Empirical orthogonal functions (EOFs) of gridded pressure-level data of geopotential height anomalies or zonal wind anomalies have been employed by Baldwin and Dunkerton (2001) and Limpasuvan et al. (2004), respectively to identify SSWs. The availability of numerous diagnostics has created a situation where there are at the moment many different ways to detect SSWs but there is an ambiguity in choosing the most suitable one. For more extensive information on the various SSW definitions that have been used in the literature, the readers may refer to Butler et al. (2015).

Recently, Zhang and Forbes (2014) defined the concept of Polar Vortex Weakening (PVW) by using measurements of the mean zonal wind (U)

at 70°N/48 km altitude and the zonal mean temperature (T) at 90°N/40 km, which showed good correlation between the timing and magnitude of PVWs and the M_2 lunar tide at 110 km altitude. The lunar tide was determined from the temperature measurements made by the SABER (Sounding of the Atmosphere using Broadband Emission Radiometry) instrument on board the TIMED (Thermosphere Ionosphere Mesosphere Energetic Dynamics) satellite between ±50° latitude. Chau et al. (2015) used this definition of PVW to demonstrate the correlation between the timing of PVW and enhancement of lunar tides in the upper mesosphere, lower thermosphere (MLT) by using wind data from mid and high latitude stations. However, they reported some observations where the correlation failed when the M_2 enhancement occurred much earlier than the defined PVW days for those years.

In this paper we use a PVW definition similar to the one put forward by Zhang and Forbes (2014) to demonstrate a correlation between the timing and peak magnitude of PVW and the semi-monthly lunar tidal modulation of the equatorial electrojet (EEJ) as estimated from the Huancayo magnetic observatory for the years 1997-2013. We also report two observations where the correlation breaks down and the semi-monthly lunar tide in the EEJ enhances much earlier than the PVW day in these cases.

The structure of this paper is as follows. Section 3.3 describes the various data sets used in this study. In Section 3.4, we introduce our approach for determining the strength of the lunar tidal modulation of the equatorial electrojet. In Section 3.5, we present our observations followed by discussion in Section 3.6. The conclusions from this work is presented at the end.

3.3 DATASET

Recordings of hourly means of the horizontal component, H of the geomagnetic field at Huancayo, HUA, (−12.05°N, 284.67°E; mag lat: −0.6°) and San Juan, SJG, (18.11°N, 293.85°E; mag lat: 28.31°) are available for the period 1997-2013 and from 1997-2011 for Fuquene, FUQ, (5.47°N, 286.26°E; mag lat: 18.12°) at the World Data Centre (WDC) for Geomagnetism, Edinburgh. Our study is limited to the above mentioned time intervals since the FUQ data is presently not available after 2011 and HUA data is missing at the WDC for the years 1970-1996.

To consider the dependence of the EEJ strength on solar activity we use the solar flux values $F_{10.7}$ in sfu ($10^{-22} W m^{-2} Hz^{-1}$) which are available at the GSFC/SPDF OMNIWeb interface at http://omniweb.gsfc.nasa.gov. To remove the ring current effect, the Dst index (availabe at the WDC for Geomagnetism, Kyoto) has been used for the period 1997-2013.

For quantitatively defining the weakening of the northern polar vortex we use the MERRA (Modern-Era Retrospective Analysis for Research and Application) data.

3.4 METHODS OF ANALYSIS

3.4.1 *Lunar tide identification in magnetic ground station records*

The lunar semi-diurnal component (M_2) dominates the lunar tidal effects in magnetic records. The M_2 tide shows a semi-monthly variation (14.77 days) at a fixed local time. The lunar tidal modulation of the equatorial electrojet related to stratospheric sudden warming has been estimated using the horizontal component of the geomagnetic field, H, e.g., at Huancayo (Siddiqui et al., 2015b) and Addis Ababa (Yamazaki et al., 2012b) in recent literature.

Both these studies employed different procedures to remove the effects of large scale magnetospheric currents in H. While the former study used a reference observatory at some distance away from the dip equator to remove these effects (e.g., Manoj et al., 2006), the latter one subtracted the Dst index from H.

The two studies also differed regarding the definition of the EEJ strength. The method used by Siddiqui et al. (2015b) eliminates some contributions of the Sq currents from the recordings of the equatorial observatory while calculating the EEJ strength whereas in the method used by Yamazaki et al. (2012b) the Sq contributions are retained.

To estimate the EEJ strength using a reference station, we first subtract the quiet night-time values from the recorded H data for both the equatorial and the reference station to remove the effects of the main field.

$$\Delta H = H - H_{MF} \tag{3.1}$$

ΔH reflects the daily variation with respect to the local midnight baseline. H_{MF} is computed daily using the mean of the four nighttime values of H at 23:30, 00:30, 01:30 and 02:30 LT. Then, H_{EEJ} is estimated by computing the difference between the daily variations at the equatorial and the reference station.

$$H_{EEJ} = \Delta H_{EEJ} - \Delta H_{NonEEJ} \tag{3.2}$$

The underlying assumption behind the differencing is that the large-scale fields of magnetospheric currents are expected to be approximately equal at both observatories (e.g., Manoj et al., 2006). A part of the Sq contributions at the equatorial observatory is also removed by this method.

In the second approach the H_{EEJ} which is proportional to the EEJ strength is estimated by subtracting the disturbance index Dst from the recorded H

data at the equatorial observatory to account for the effects of the ring current. Then, H_{EEJ} is estimated after subtracting the quiet night-time value. The Sq contributions at the equatorial observatory are not removed in this method.

In this paper we attempt to compare the semi-monthly lunar tidal amplitudes estimated from the Huancayo data by using both these methods for the period 1997-2013. San Juan and Fuquene have been chosen as reference stations for Huancayo. Figure 3.1 shows the geomagnetic field variation due to the primary ionospheric (excluding induced) currents at the Earth's surface as derived from the CM4 model at 16 UT on 1st January 2000. The black dots mark the locations of the three observatories used in this study. CM4 (Comprehensive Model) is a model of the quiet time, near-Earth magnetic field which has been derived using the POGO, Magsat, Ørsted and CHAMP satellite data (Sabaka et al., 2004). The significant difference in latitudinal separation from the magnetic equator also provides a chance to look at the dependence of the lunar tidal amplitudes on the spatial distance between the equatorial and the reference stations.

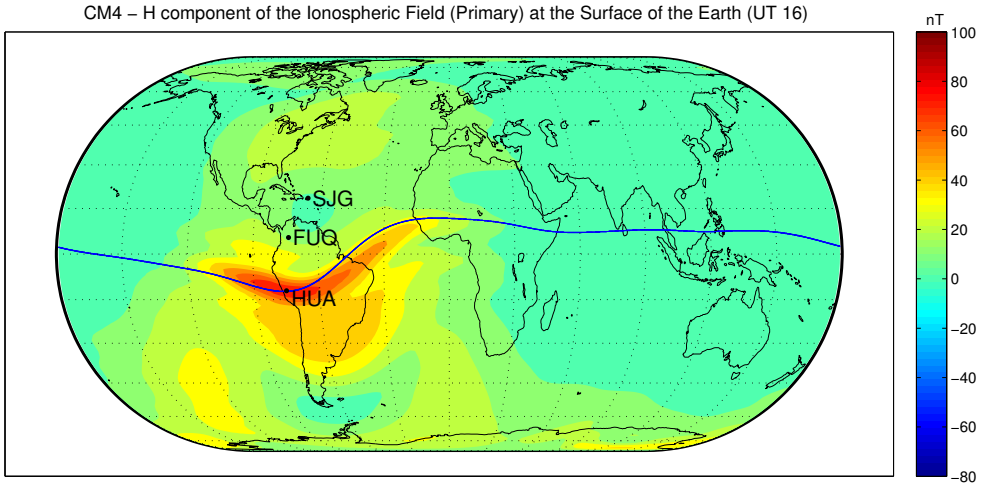

Figure 3.1: Geomagnetic field variations at the Earth's surface caused by ionospheric current as derived using the CM4 model at 16 UT on the first day of the year with $F_{10.7}$ = 100 s.f.u. The black dots mark the considered observatory locations. The blue line represents the dip equator latitude.

The EEJ has a strong dependence on the solar flux level due to varying ionospheric conductivity (e.g., Alken and Maus, 2007; Stolle et al., 2008; Yamazaki et al., 2010). To eliminate the effect of the varying conductivity, the EEJ strength is normalized to a solar flux level of 150 s.f.u. The data are then arranged into bins of 1 day by 1 h in local time (LT) over a period of two lunar months (59 days). For each day, a 59-day-centered sliding window is applied. The local time sector considered here is from

08:00 to 16:00 LT. Outside of this time interval the EEJ signal is considered to be weak. The daytime variation of the EEJ is dominated by the solar tidal effects. This dominant variation is estimated by calculating the means over a 59-day period for each local time hour. The calculated means are then subtracted from the data to remove the effect of the solar tides. We are interested in estimating the amplitude of the semi-monthly lunar wave (14.76 days) for each local time hour over the 59-day period. The frequency of interest is the fourth harmonic signal for which the amplitude and phase is determined for each local time hour. The amplitude obtained is then normalized for the expected diurnal variation of the ionospheric conductivity, C, as described by Lühr et al. (2008).

$$C = C_0 \sqrt{\cos\left\{\frac{\pi}{12\,h}(LT - t_0)\right\}} \tag{3.3}$$

where C_0 is the value of the peak conductivity and t_0 is the local time of the peak conductivity. A suitable value for t_0 has been found to be 12:30 LT. For our purpose we chose C_0 to be equal to 1.

The procedure for normalization is similar to the one explained in Siddiqui et al. (2015b). It has been shown by Lühr et al. (2012) that the diurnal variation of the ionospheric conductivity also affects the amplitude of the lunar tidal signal. Without the normalization, the values around noon would dominate the tidal results.

A reasonable estimate of the average semi-monthly lunar wave over 59 days was obtained by calculating the mean of the normalized amplitudes for all the considered local times. The mean semi-monthly lunar wave is thus computed for each 59-day window and is then tied to its central day. A sliding window of 59 days length advanced by 1 day is applied for each subsequent dataset.

3.4.2 *Quantifying SSW strength based on Polar Vortex Weakening*

Lately, various studies on the enhanced lunar response of the ionosphere during SSWs have used different diagnostics to identify an SSW event. Yamazaki (2013) used the NCEP/NCAR reanalysis data to recognize SSW events based on significant changes in the climatology of the stratosphere dynamics whereas Zhang and Forbes (2014) quantified the concept of polar vortex weakening (PVW) to characterize the strength of SSW events using the MERRA reanalysis data. Based on SABER V2.0 temperature measurements between $\pm 50^\circ$ latitude they demonstrated a correlation between the timing and peak amplitude of the M_2 at 110 km altitude and the polar vortex weakening. Chau et al. (2015) used this definition of PVW to demonstrate a correlation between the upper mesospheric lunar tides and PVW characteristics during SSW events. However, they have also reported inconsistencies for some years (see Figure 7, Chau et al., 2015) when the meso-

spheric lunar tides enhanced prior to the PVW day identified by Zhang and Forbes (2014).

They have used the daily time series of the zonal mean zonal wind (U) at 70°N and 48 km altitude and zonal mean temperature (T) at North Pole and 40 km altitude for the first 60 days of each year to describe the polar vortex weakening (see Figure 3.2, Zhang and Forbes, 2014). In our study we extend the time series for both parameters from 60 to 90 days by including the month of December. Figure 3.2 presents U (red curve) and T (black curve) as defined above from December onwards to February for the years 1998-2013. The dotted blue vertical lines denote the days of peak polar vortex weakening while the dotted black horizontal lines denote the zero value of mean zonal wind. The dotted vertical green line in each panel marks the day of peak lunar tidal enhancement estimated from the magnetometer data. The PVW events are identified according to the same criteria as used by Zhang and Forbes (2014) by locating the most significant and/or earliest pair of T and U extremes within these 90 days. Though, the PVW event of 2000 was not included in their analysis, we have included the event as it fulfills the criteria used for identifying PVWs. For the years 2005 and 2007, PVWs are not well defined. It is important to note that our results for the occurrence of PVW events are only different for the years 1998, 1999, 2001 and 2002 from the results of Zhang and Forbes (2014). During these periods the earliest T and U extremes were recorded during December. For the rest of the years between 1998-2013 we obtain the same PVW days as reported by them.

The strength of PVW is better represented by the peak magnitude of the reversed mean zonal wind than the zonal mean of the stratospheric temperature according to the results of Zhang and Forbes (2014). The magnitude of extreme values of the reversed mean zonal wind is taken as the measure of PVW strength and is denoted by PVW_mag. The magnitude and the occurrence date of PVWs for the years 1998-2013 are listed in Table 3.1.

3.5 OBSERVATION

Figure 3.3 shows the lunar tidal power obtained solely from Huancayo observations for the years 1997-2013. The red lines denote the peak PVW days as identified in Figure 3.2. The annual amplification of the lunar tidal power can be seen in all these years during the months of December-February with an amplitude of at least 600 nT^2. The peak amplification for a majority of the years occurs around the PVW day if a PVW has been identified. For the four largest events (2003, 2006, 2009, and 2013) with amplitudes of lunar wave power above 1500 (nT^2) we also identified PVW strengths above 50 ms^{-1} (See Table 3.1).

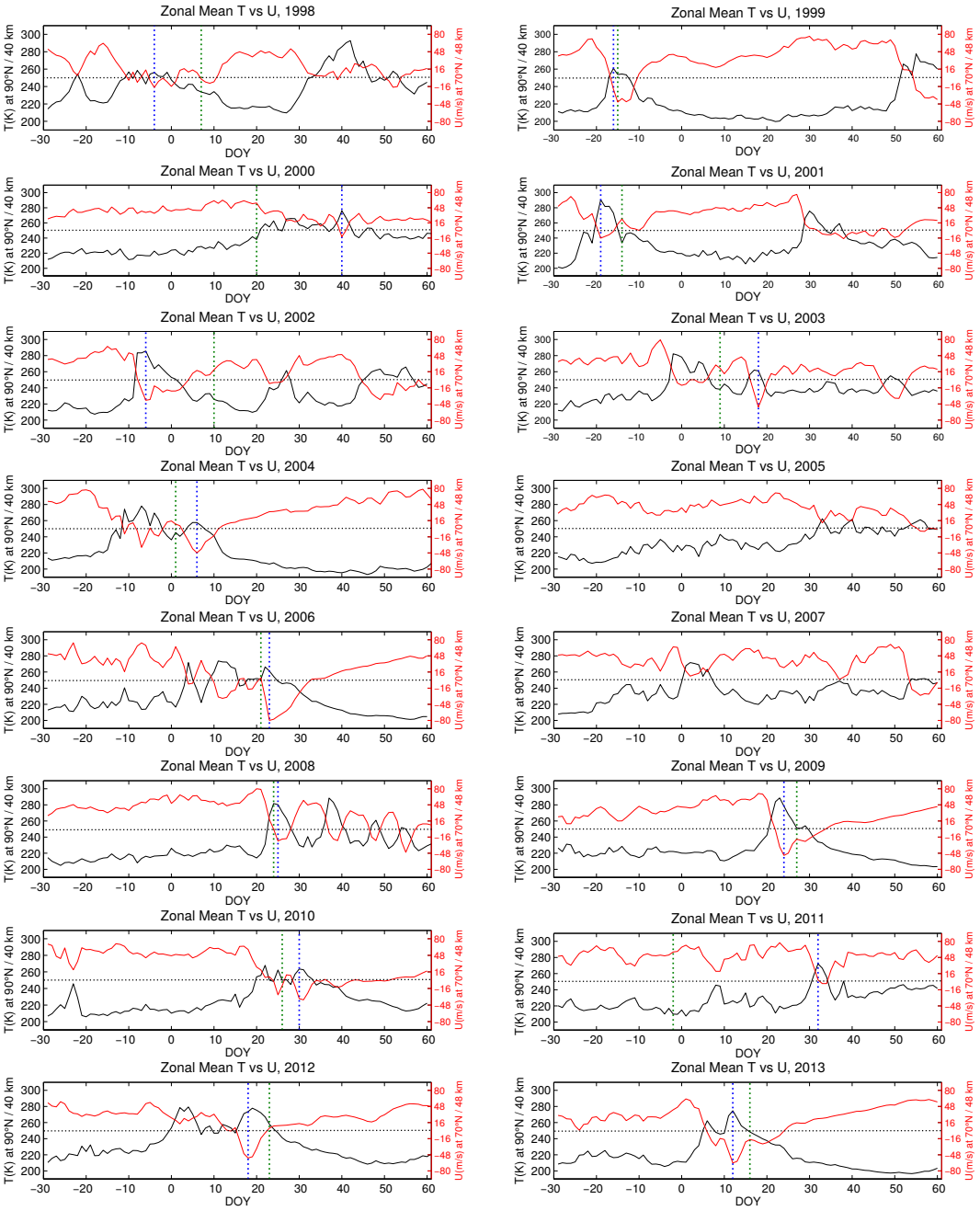

Figure 3.2: Daily time series of the mean zonal wind (U) at 70°N and 48 km altitude (red curve) and zonal mean temperature (T) at North Pole and 40 km (black curve) from December onwards to February for the years 1998-2013. The dotted vertical blue line in each panel marks the selected polar vortex weakening day. The dotted vertical green line in each panel marks the day of peak lunar tidal enhancement.

Date of PVWs	PVW strength (in ms^{-1})
26-12-1997	17.68
15-12-1998	44.57
08-02-2000	13.45
11-12-2000	16.12
24-12-2001	40.68
17-01-2003	54.21
05-01-2004	47.71
22-01-2006	79.78
24-01-2008	23.75
23-01-2009	52.42
29-01-2010	37.92
31-01-2011	3.78
17-01-2012	54.33
11-01-2013	64.31

Table 3.1: The date and strength of Polar Vortex Weakening (PVW) events derived from MERRA reanalysis data for the years 1998-2013. The strength of PVWs is represented by the magnitude of the westward zonal mean zonal wind at 70°N/48 km altitude.

The next large enhancement, in 2008, shows only a small amplitude of PVW with 23.75 ms^{-1}, however, it is influenced by multiple warming events at least up to the end of February. This suggests that the recurrence could be responsible for the large lunar wave amplitude seen in the semi-monthly lunar tide. Large M_2 temperature amplitudes during the years 2006, 2009 and 2013 were also reported by Zhang and Forbes (2014). We also find cases of lunar tidal enhancements without significant PVW in the years 2005 and 2007 exhibiting similar amplitudes as in the years 2001, 2002, 2011 and 2012 with significant PVW. This suggests there are other physical processes responsible for the lunar tidal enhancements in the EEJ that needs to be further investigated. Such counter-examples were earlier reported by Siddiqui et al. (2015b). We do not find a one-to-one correspondence between the timing of lunar tidal amplification and the PVW. The breakdown of a one-to-one correspondence between the lunar tidal enhancements and the warming events for certain years was also observed by Stening (2011) and Yamazaki et al. (2012b).

Figures 3.4 and 3.5 show the lunar tidal power obtained by using San Juan and Fuquene as reference stations, respectively. Similar amplifications during the major warming events are observed in both these plots. With Fuquene as the reference station the lunar tidal signature for the years

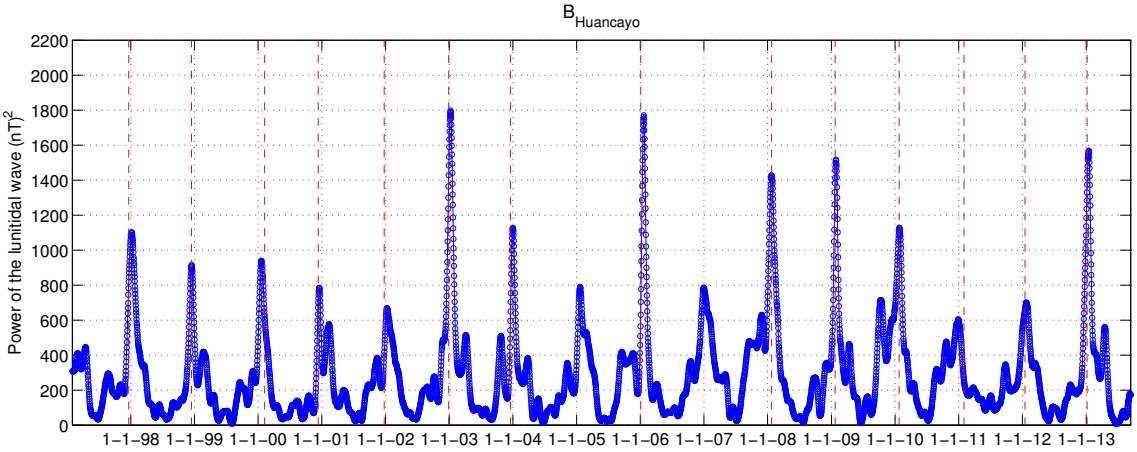

Figure 3.3: Daily EEJ lunar tidal wave power for the years 1997-2013. Results are obtained without a reference station to Huancayo. The red lines denote the PVW days derived from the reversed zonal wind (see text).

1997-2011 is slightly clearer compared to San Juan. It can be seen in the former case that the sidebands in general have lower amplitudes compared to the latter. Also, in case of the 2001 event the lunar enhancement correlates better with the PVW when Fuquene is the reference station for Huancayo. This could be due to the larger latitudinal and longitudinal separation between Huancayo and San Juan compared to Huancayo and Fuquene.

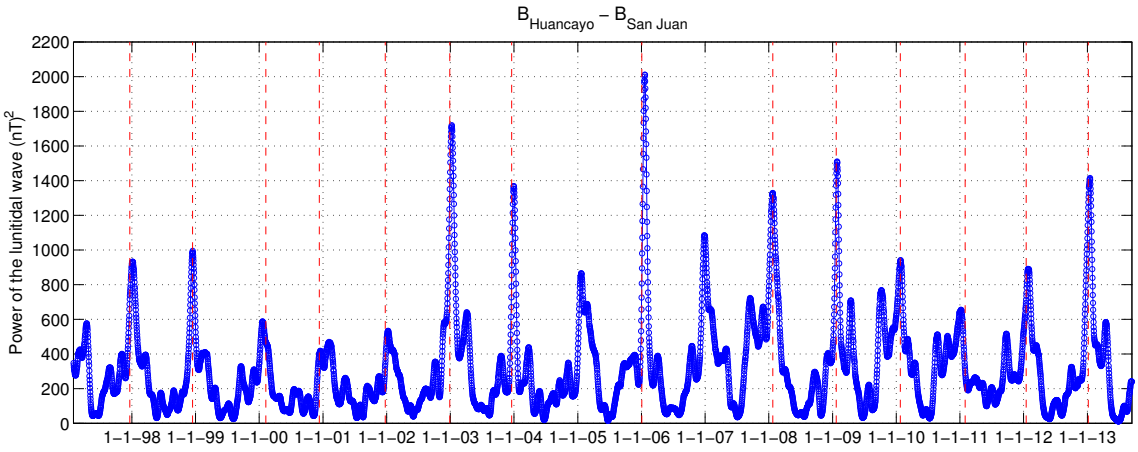

Figure 3.4: Same as Figure 3.3, but with San Juan as the reference station for Huancayo.

The contributions from the Sq current system are better eliminated when calculating the EEJ strength with respect to Fuquene as reference station than San Juan, since the latter lies close to the Sq focus with the values of H component recordings being close to zero. However, the overall lunar tidal pattern obtained from the Huancayo-Fuquene pair, Huancayo-San Juan pair and solely from Huancayo, suggest that the semi-monthly lunar

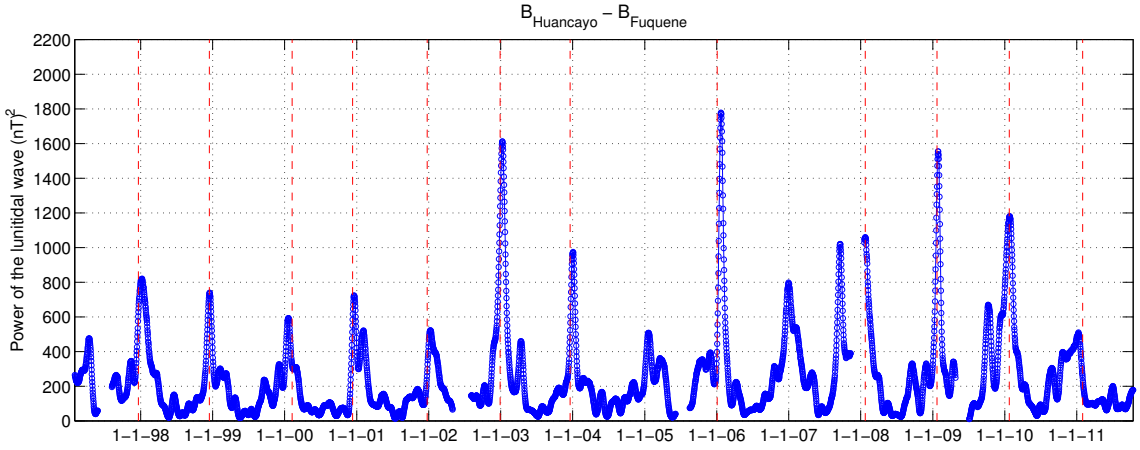

Figure 3.5: Same as Figure 3.3, but with Fuquene as the reference station for Huancayo.

tidal amplitude in the EEJ are dominant over the lunar tidal amplitude in the Sq currents. The *H* component data from Fuquene are presently only available till 2011. Moreover, occasional gaps in Figure 3.5 result due to the data gaps at the Fuquene station.

3.6 DISCUSSION

In order to quantify our observations we now present the correlations between the timing and amplitude of PVW and the semi-monthly lunar tide in the EEJ. Figure 3.6 presents the scatter plot between the occurrence day of PVWs and the semi-monthly lunar tidal peaks during 1998-2013 for Huancayo. The points depicted with the square symbol correspond to the years when the lunar tidal maximum occurred significantly earlier than the defined PVW day for that year. The solid red line depicts the linear least squares fit to the events. The lunar tidal amplification occurs much earlier than the defined PVW day for the 2000 and 2011 events. The mismatch between the occurrence of the PVW and the M_2 lunar tide derived from MLT winds, was also reported by Chau et al. (2015) in case of the 2011 event. These are the only two years remaining for which the revised definition of PVW (by including December) could not improve the temporal relation between the PVW and the lunar tidal enhancement in the magnetic data. The slope of the linear fit is 0.79. It is slightly lower than 0.92, as obtained by Chau et al. (2015) when they estimated the lunar tide in the upper mesospheric winds from a mid-latitude station while Zhang and Forbes (2014) reported a unity slope. They showed with the SABER temperature measurements at 110 km altitude that it took 2.8 days for the M_2 tide to respond to PVW. It can be seen in Figure 3.6 that the difference between the occurrence of lunar tidal peaks and PVWs in January is less

than 3 days in 6 out of 9 cases. For the 2003 and 2004 events the lunar peaks occurred even earlier than the identified PVW days. These events record multiple reversals of the zonal wind prior to the identified PVW days which might have triggered the early enhancement of the lunar tides. Delayed response of lunar peaks to PVWs can be found for the December events of 1998 and 2002. From the linear regression between the occurrence of the PVW event and the peak of the semi-monthly lunar tidal amplitude we derive an equation,

$$M_2\_peak\_timing = 0.79\, PVW\_timing + 4.6\,(days) \tag{3.4}$$

where, $M_2\_peak\_timing$ is the day of peak semi-monthly lunar tidal amplitude and PVW_timing is the identified PVW day. The slope of less than 1 is caused by the delayed response of the tidal enhancement (10-20 days) for PVWs occurring in December. It should be checked which processes cause these delays. When ignoring the December events in Figures 3.6-3.8 a unity slope (not shown here) as reported by Zhang and Forbes (2014), is justified.

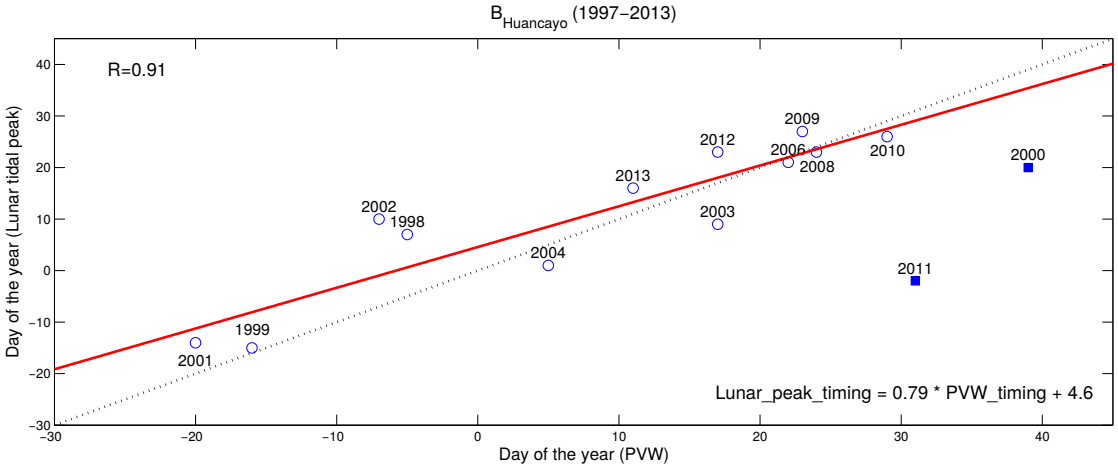

Figure 3.6: The figure presents a scatterplot between the occurrence days of PVW and EEJ semi-monthly lunar tidal peak during 1997-2013 for Huancayo. The filled squares correspond to the years when the lunar tidal maximum occurred much earlier than the selected PVW day for that year. The solid red line depicts the linear least squares fit to the events. The equation for the fit and the correlation coefficient are listed in the panel. The dotted black line represents the one-to-one correspondence.

The value of the correlation coefficient obtained compares excellently with the values reported by Zhang and Forbes (2014) and Chau et al. (2015), even though they derived the lunar tidal enhancements from completely different quantities. Our results thus support their observations and further demonstrates that the response of the upper atmosphere to

PVW events compares well on a global scale, i.e. at low, mid and high latitudes. Analyses at these three latitudinal regimes have been performed with ground-based observations of MLT winds at mid and high latitudes (Chau et al., 2015) and with observations of the E-region dynamo between ±50° latitude (Zhang and Forbes, 2014). It is noteworthy that similar results have been achieved in these analyses with different parameters of the upper atmosphere and at different latitudes.

Figures 3.7 and 3.8 present the same scatterplots as Figure 3.6, but for cases when San Juan or Fuquene have been used as a reference station for Huancayo. The slopes and the correlation coefficients are similar to the results obtained from the single station method. The largest correlation coefficient of 0.92 is obtained when Fuquene is considered as the reference station for Huancayo. With San Juan as the reference station the correlation coefficient is 0.87 whereas it is 0.91 when the single station method is considered.

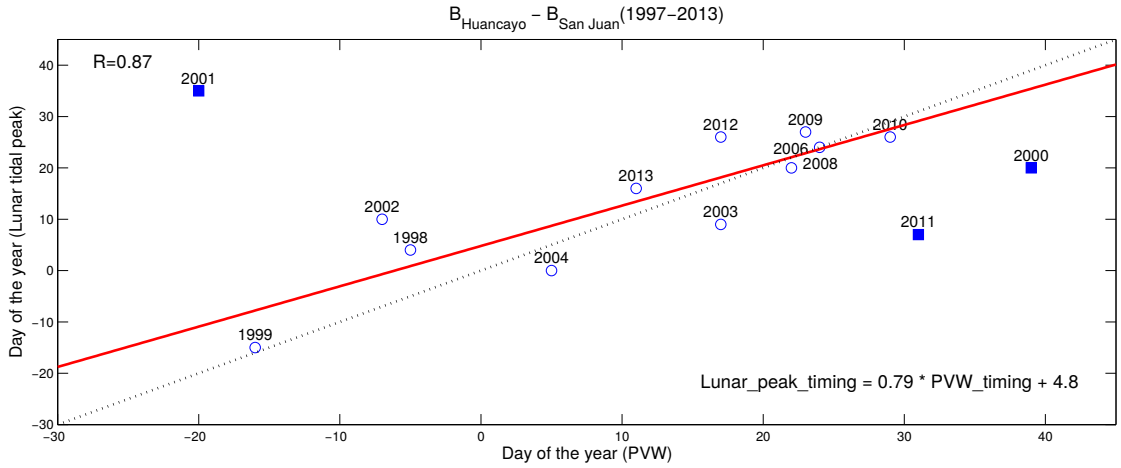

Figure 3.7: Same as Figure 3.6, but with San Juan as the reference station for Huancayo.

Figure 3.9 presents the scatterplot between the PVW strength and peak of the EEJ lunar tidal amplitude at Huancayo. The lunar tidal amplitude is considered in Figures 3.9-3.11 instead of the lunar tidal power in order to maintain consistency with the results of Chau et al. (2015) and Zhang and Forbes (2014). The solid red line depicts the linear least squares fit to the events. The dotted black horizontal and vertical lines mark a chosen threshold level for the lunar amplitude and PVW strength during major warmings. The 2000 and 2011 events are not included in the analysis due to the large difference between the occurrence time of PVW and the lunar tidal peak for these cases. In general larger lunar tidal amplitudes correlate with stronger PVW strength. During the four major SSW events (2003, 2006, 2009, 2013) the amplitude of the lunar tide is greater than 35 nT, and the PVW strength is greater than 50 ms^{-1}. In case of the 2012 event, a low

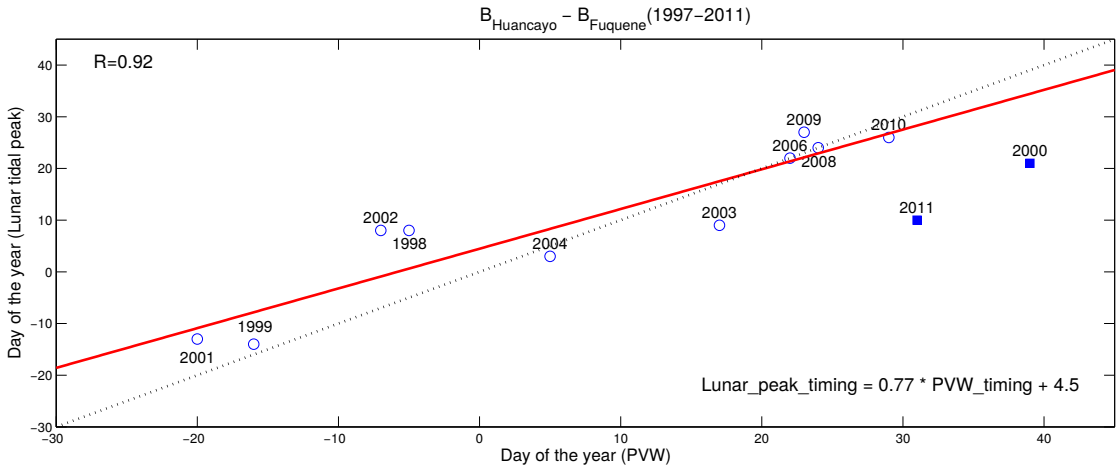

Figure 3.8: Same as Figure 3.6, but with Fuquene as the reference station for Huancayo.

amplitude of the lunar tide is obtained in spite of a similar value of PVW strength as during major warmings. However, our results are consistent with the observations of Zhang and Forbes (2014) and Chau et al. (2015) where they have also reported lower amplitude of the M_2 lunar tide for this particular event. This observation is discussed later in more detail in this section.

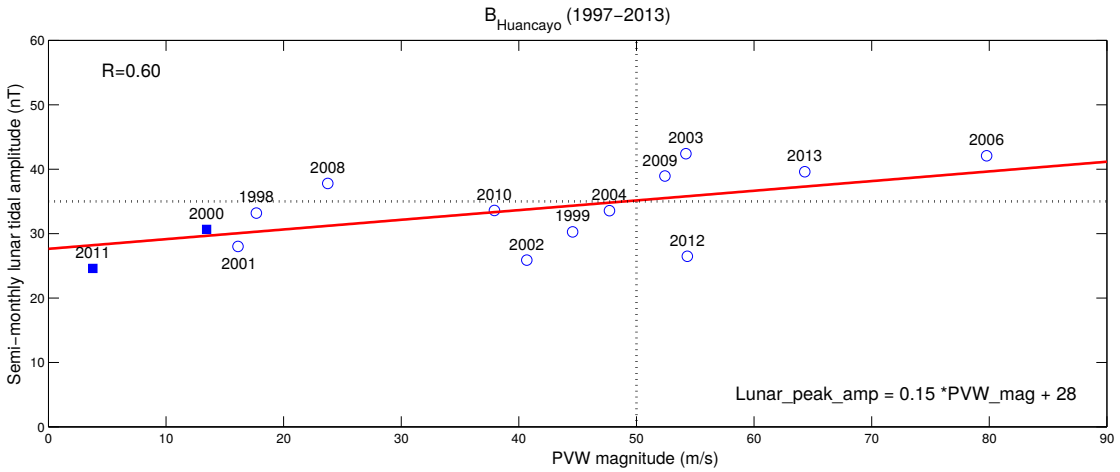

Figure 3.9: The figure presents a scatterplot between the strength of PVW and the peak amplitude of the semi-monthly lunar tidal peak during 1997-2013 for Huancayo. The filled squares correspond to the years when the lunar tidal maximum occurred much earlier than the selected PVW day for that year. The solid red line depicts the linear least squares fit to the events. The equation for the fit and the correlation coefficient are listed in the panel. The dotted black horizontal and vertical lines mark the threshold values for the lunar amplitude and PVW strength during major warmings.

Figures 3.10 and 3.11 present the scatterplot between the PVW strength and the lunar tidal amplitude when San Juan and Fuquene are used as the reference station for Huancayo. As seen from the earlier plot stronger PVW strength leads to larger lunar tidal amplitudes in these cases too. Slightly higher correlation is achieved between the PVW strength and the peak of the lunar tidal amplitude by using the reference station method in comparison to the single station method. The largest correlation coefficient of 0.75 is obtained when Fuquene is considered as the reference station for Huancayo and it is 0.71 in the case of San Juan. When the single station method is used the value of the correlation coefficient obtained is 0.60 and the lowest among the three cases. We expect a better separation of EEJ from Sq and magnetospheric fields when Fuquene is the reference station for Huancayo compared to San Juan.

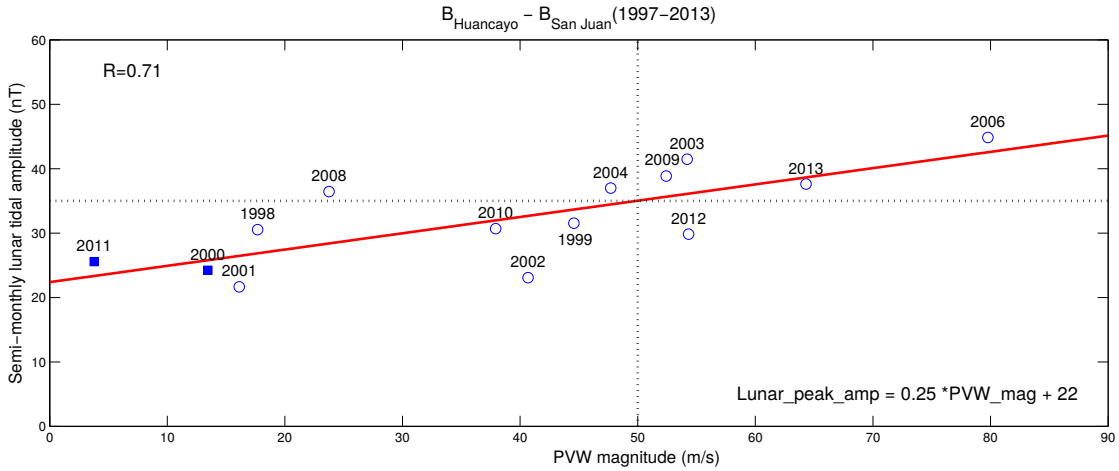

Figure 3.10: Same as Figure 3.9, but with San Juan as the reference station for Huancayo.

From the linear regression between the reversed zonal wind speed and the semi-monthly lunar tidal amplitude we derive the equation,

$$M_2\_peak\_amplitude = 0.25 \left(\frac{nT}{ms^{-1}}\right) PVW\_mag + 22\,(nT) \qquad (3.5)$$

where the peak magnitude of PVW, PVW_mag, is given in ms^{-1} and the peak amplitude of the semi-monthly lunar tide, $M_2\_peak\_amplitude$, is given in nT. From Figures 3.9 - 3.11 we see that the 2000 and 2011 events exhibit the smallest amplitudes. This may correspond to our findings that they appear as outliers for the timing in Figures 3.6 - 3.8.

The inconsistencies observed during the 2000, 2011 and the 2012 events could be better explained if the different external factors which influence the occurrence of the SSWs and the strength of the polar vortex such as the tropospheric wave activity, the 11 year sunspot cycle, the phase of the QBO (quasi-biennial oscillation) (e.g., Holton and Tan, 1980; Labitzke and

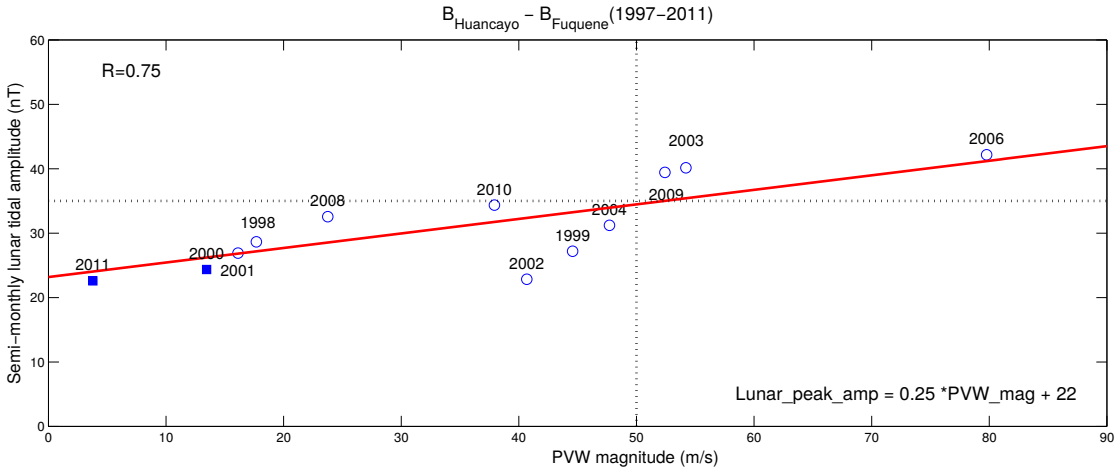

Figure 3.11: Same as Figure 3.9, but with Fuquene as the reference station for Huancayo.

Van Loon, 1988; Van Loon and Labitzke, 2000) and the phase of the El Niño-Southern Oscillation (ENSO) (e.g., Butler and Polvani, 2011) are also taken into account. The SSWs are more likely to occur under the solar minimum conditions during the east phase of the QBO and under solar maximum conditions during the west phase of the QBO (Labitzke, 2005). The SSWs also occur twice as frequently during the El Niño and La Niña winters as compared to ENSO-neutral winters although the probability of occurrence is almost equal during both El Niño and La Niña winters (Butler and Polvani, 2011). The 2003 SSW event, was characterized by the west phase of QBO under strong solar flux conditions together with the El Niño phase of the ENSO. Under these conditions the Brewer-Dobson circulation (BDC) is enhanced which leads to a weakened and warm polar vortex (e.g., Labitzke, 2005; Butler and Polvani, 2011). The 2006 SSW event was characterized by the east phase of the QBO during solar minima and with La Niña phase of the ENSO. These conditions also enhance the Brewer-Dobson circulation (BDC) which facilitates the occurrence of SSWs.

During the 2009 SSW event the conditions were favourable for an undisturbed and strong polar vortex (Labitzke and Kunze, 2009) because the event was characterized by a minima in solar cycle together with the west phase of the QBO. However, due to the large tropospheric forcing (estimated using the eddy heat flux value at 100 hPa) which was among the three strongest recorded since 1958 (Ayarzagüena et al., 2011), the stratospheric warming occurred. The eddy heat flux at 100 hPa averaged over 45°N - 75°N is regarded as a measure of the amount of wave activity entering the stratosphere (e.g., Waugh et al., 1999; Newman et al., 2001; Polvani and Waugh, 2004). Figure 3.12 presents the 45-day mean of the 45°N-75°N averaged eddy heat flux at 100 hPa denoted by red lines for the years

2008/2009 and 2009/2010 in the top panel and for the years 2011/2012 and 2012/2013 in the bottom panel. The bold black line in each panel denotes the climatological mean calculated over the period from 1978/1979-2012/2013. The enhanced eddy flux values during the 2009 SSW event can be clearly seen in Figure 3.12. The 2013 event was characterized by the east phase of the QBO under moderate solar flux conditions and the neutral phase of the ENSO. However, the 2013 SSW event also witnessed a strong tropospheric forcing albeit slightly lesser than the 2009 SSW event (Coy and Pawson, 2015) which may have led to the splitting of the polar vortex.

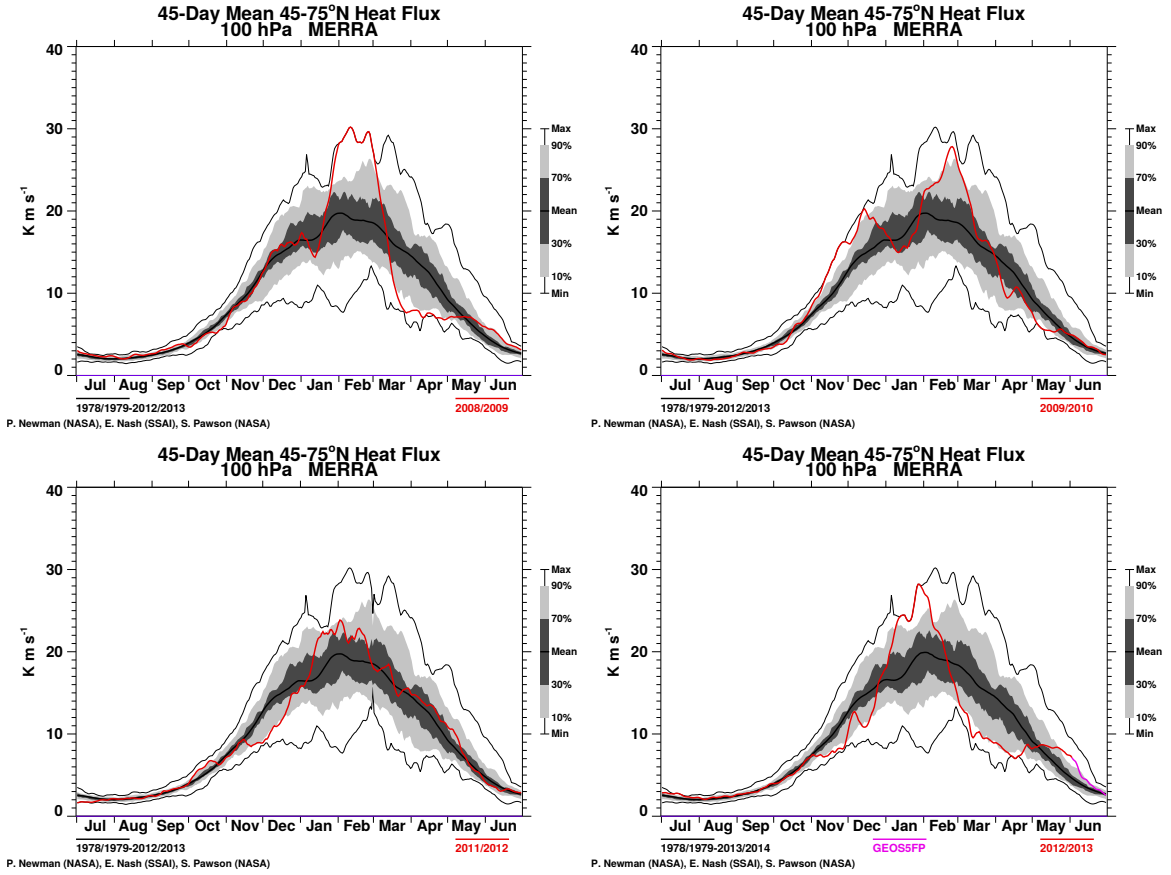

Figure 3.12: The 45-day mean of the 45°N-75°N averaged eddy heat flux at 100 hPa denoted by red lines for the years 2008/2009 and 2009/2010 in the top panels and for the years 2011/2012 and 2012/2013 in the bottom panels. The bold black line in each panel denotes the climatological mean of the eddy heat flux calculated over the period from 1978/1979-2012/2013. Figures downloaded from NASA GSFC.

The lower atmosphere and ionosphere coupling around SSWs is not directly related to the warming itself but to the Planetary Wave (PW) activity associated with it (Chau et al., 2012). In case of the 2012 SSW event, the lunar tidal enhancement was low in comparison to the magnitude of vortex weakening. During this event a weaker level of tropospheric forcing

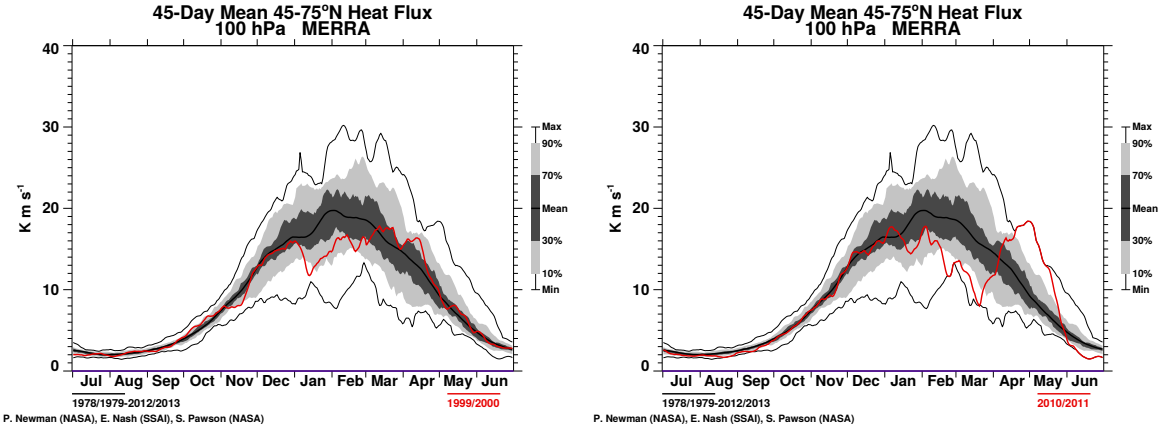

Figure 3.13: Same as Figure 3.12, but for the years 1999/2000 and 2010/2011 in the left and the right panel.

was witnessed (as seen in Figure 3.12 through the averaged eddy heat flux values) than the 2009 and the 2013 events even though the magnitude of PVWs were comparable. The 2012 SSW event was characterized by the east phase of QBO during solar minima with La Niña phase of the ENSO. Under these conditions a weak polar vortex is expected. The relatively lower level of tropospheric forcing combined with the weakened polar vortex could be the reasons for the low values of the semi-monthly lunar tide in the EEJ although the magnitude of PVW during the 2012 minor SSW event was large.

Figure 3.13 presents the 45-day mean of the 45°N-75°N averaged eddy heat flux at 100 hPa denoted by red lines for the years 1999/2000 (left panel) and 2010/2011 (right panel). The averaged eddy heat flux value at 100 hPa recorded during the 2000 and 2011 boreal winters were lower than the climatological mean (bold black lines) and the lunar tidal enhancement for these years do not seem to be related to the PVW. The existence of these cases suggest there are also other physical processes which are responsible for the lunar tidal enhancements that are not covered in our discussion.

Although the results obtained by Zhang and Forbes (2014) and Chau et al. (2015) were based on the lunar tidal measurements of different atmospheric quantities and heights, yet our observations are in general agreement with the ones reported by them. We suggest that the M_2 signatures identified in mesospheric winds by Chau et al. (2015) should be compared to the semi-monthly lunar signature in the EEJ caused by the E-region dynamo.

3.7 CONCLUSIONS

Using the *H* component data from Huancayo, San Juan and Fuquene we have compared

(a) the lunar tidal modulation of the EEJ for the years 1997-2013 based on two different approaches for the elimination of magnetospheric contribution and (b) the lunar tidal modulation of the EEJ estimated with and without the Sq contributions to the EEJ. The peak of the derived semi-monthly lunar tides are then compared with the timing and magnitude of the stratospheric polar vortex weakening (PVW). Major points of our study are as follows:

1. We determined correlation coefficients and linear regression functions when comparing timing or amplitude relations between PVW and peak lunar tidal amplitudes for the following cases: using Huancayo observatory data only, Huancayo data with a reference station located equatorward of the Sq focus (Fuquene), and with a reference station located close to the Sq focus (San Juan). These observations suggest that the variations of the EEJ in response to PVW events to a large degree determine the observed variations of the total current (EEJ + Sq), which is the sum of both the EEJ and Sq at the magnetic equator.

2. Our results show a good qualitative agreement with the observations of Zhang and Forbes (2014) and Chau et al. (2015). We obtain an improved correlation between the timings of PVW and lunar tidal peaks when the month of December is also included in the analysis. Similarly we find a direct relation between the peak amplitude of the semi-monthly lunar tide and the peak magnitude of the PVW.

3. The timing of the PVW events and the peak timing of the lunar tidal amplitude seem to be related closer to each other than the amplitudes of both quantities. This is demonstrated by higher correlation coefficients of about 0.9 between the two parameters for the timing and 0.75 for the amplitudes. Although many different parameters of the upper atmosphere system influence the amplitude of the EEJ lunar tidal modulation, the commencement of a lunar tidal enhancement in most cases is closely related to a PVW event.

4. The external factors affecting the state of the wintertime northern polar vortex such as the QBO, solar flux levels, ENSO and the tropospheric forcing levels have also been considered to explain the weak lunar tidal enhancements in the EEJ. However, other parameters that could not be covered in our work have to be considered in the future to explain all the observations consistently.

3.8 ACKNOWLEDGEMENTS

The results presented in this paper rely on the data collected at San Juan, Fuquene, and Huancayo. We thank the INTERMAGNET for promoting

high standards of magnetic observatory practice and the U.S. Geological Survey and the Instituto Geofisico del Peru for supporting geomagnetic observatory operations at San Juan and Huancayo, respectively. We thank the Instituto Geográfico Agustin Codazzi, Colombia, for supporting geomagnetic observatory operations at Fuquene. We employ the wind and the temperature data downloaded from MERRA (Modern Era Retrospective Analysis for Research and Applications). We are very thankful to WDC for Geomagnetism, Kyoto, for making available the Dst indices. The OMNI data for F10.7 were obtained from the GSFC/SPDF OMNIWeb interface. T.A.S. and C.S. thank the International Space Science Institute (ISSI) for organizing the team on "A three - dimensional ground-to-space understanding of sudden stratospheric warmings" and for sponsoring the team meetings on this research topic.

4

LONGITUDE DEPENDENT LUNAR TIDAL MODULATION OF THE EQUATORIAL ELECTROJET DURING STRATOSPHERIC SUDDEN WARMINGS

Tarique A. Siddiqui[1,2], Claudia Stolle[1,2] and Hermann Lühr[1]

[1]GFZ German Research Centre for Geosciences, Potsdam, Germany
[2]Institute of Earth and Environmental Science, University of Potsdam, Germany

Manuscript published as:
Siddiqui, T. A., C. Stolle, and H. Lühr (2017). "Longitude-dependent lunar tidal modulation of the equatorial electrojet during stratospheric sudden warmings." In: Journal of Geophysical Research: Space Physics 122.3, pp. 3760-3776. doi:10.1002/2016JA023609.

4.1 ABSTRACT

The effects of coupling between different layers of the atmosphere during Stratospheric Sudden Warming (SSW) events have been studied quite extensively in the past few years and in this context large lunitidal enhancements in the equatorial ionosphere have also been widely discussed. In this study we report about the longitudinal variabilities in lunitidal enhancement in the EEJ during SSWs through ground and space observations in the Peruvian and Indian sectors. We observe that the amplification of lunitidal oscillations in EEJ is significantly larger over the Peruvian sector in comparison to the Indian sector. We further compare the lunitidal oscillations in both the sectors during the 2005-2006 and 2008-2009 major SSW events and during a non-SSW winter of 2006-2007. It is found that the lunitidal amplitude in EEJ over the Peruvian sector showed similar enhancements during both the major SSWs but the enhancements were notably different in the Indian sector. Independent from SSW events, we have also performed a climatological analysis of the lunar modulation of the EEJ during December solstice over both the sectors by using 10 years of CHAMP magnetic measurements and found larger lunitidal amplitudes over the Peruvian sector confirming the results from ground-magnetometer observations. We have also analyzed the semi-diurnal lunar tidal amplitude in neutral temperature measurements from SABER at 110 km and found lesser longitudinal variability than the lunitidal amplitude in EEJ. Our results suggest that the longitudinal variabilities in lunitidal

modulation of the EEJ during SSWs could be related to electrodynamics in the E-region dynamo.

4.2 INTRODUCTION

Stratospheric Sudden Warmings (SSW) are large-scale meteorological events usually occurring in the winter hemisphere. The phenomenon of SSW was first observed by Scherhag (1952) and since then it has been studied extensively. SSWs are characterized by a weakening or sometimes even a reversal of the westerly winds in the northern stratosphere which leads to a sudden rise in polar stratospheric temperature by several tens of degrees (e.g., Andrews et al., 1987). The underlying mechanism behind SSWs is understood to be the non-linear interaction of the vertically propagating planetary waves with the zonal mean flow as proposed by Matsuno (1971). According to the World Meteorological Organization (WMO), SSWs can be classified into major and minor warming events based on the intensity of weakening of mean zonal wind at 60°N and 10hPa. An SSW is classified as a major warming if the zonal wind at 60°N and 10hPa shows a reversal from westerly to easterly. In case there is deceleration of the zonal wind but no reversal, then it is classified as a minor warming.

Although SSWs occur at polar stratospheric heights, their impact can be detected widely across higher altitudes. At high-latitudes, observational and modeling studies suggest that SSWs result in cooling of the mesosphere (e.g., Labitzke, 1972; Liu and Roble, 2002; Cho et al., 2004) and warming of the lower thermosphere (e.g., Funke et al., 2010). At middle-latitudes SSWs have been reported to be the cause behind alternating regions of warming and cooling in the ionosphere (Goncharenko and Zhang, 2008). At low-latitudes SSW related perturbations in the ionosphere have also been seen in different parameters such as vertical plasma drifts (e.g., Chau et al., 2009; Chau et al., 2010), the equatorial electrojet (e.g., Yamazaki et al., 2012b) and total electron content (Goncharenko et al., 2010a). The longitudinal variabilities in the ionosphere during the 2009 major SSW in $E \times B$ drifts have also been observed through model simulations (e.g., Fang et al., 2012). Their results showed that the longitudinal variability of the neutral winds and the strength of the geomagnetic field could be the reason behind the longitudinal variation of vertical drifts. At equatorial and low-latitudinal regions of the ionosphere, one characteristic signature which has been observed during SSWs is a clear semi-diurnal perturbation pattern which shifts in time at later days. This shifting pattern was suggested by Fejer et al. (2010) to be due to the enhancement of semi-diurnal lunar (M_2) tide during SSWs. They also observed these temporal perturbations in the equatorial electrojet in different longitudinal sectors. Usually, the perturbations were seen to occur at first in the American sector and lastly in the Pacific sector. The perturbations were also recorded

to be strongest in the American sector. However, a quantitative comparison between the lunitidal enhancements in different longitudinal sectors during SSWs was not presented. Large lunitidal amplitudes in the EEJ during SSWs have also been reported from ground-based and satellite observations (e.g., Park et al., 2012; Yamazaki et al., 2012b; Yamazaki, 2013; Siddiqui et al., 2015b). The readers may refer to a comprehensive review by Chau et al. (2012) for more details on impacts of SSW on the equatorial ionosphere.

The equatorial electrojet (EEJ) is a narrow band of an intense electric current confined to a latitude band of about $\pm 3^{\circ}$ and flowing above the magnetic dip equator in the daytime E-region of the ionosphere. Numerous studies have reported about the important characteristics of the EEJ based on the data from ground observatories and satellites (e.g., Doumouya et al., 1998; Rigoti et al., 1999; Jadhav et al., 2002; Lühr et al., 2004). The EEJ current system is primarily driven by the dynamo action of tidal winds in the E-region of the ionosphere. The atmospheric tides driven by solar heating constitute the dominant driver of this current system. In comparison, the effect of the gravitationally forced lunar tides are rather small. A comprehensive review on the EEJ can be found in Forbes (1981).

Lunitidal oscillations in horizontal component of magnetic field, H, at an equatorial station were first derived by Bartels (1936) at Huancayo, and the amplitudes were found to be significantly greater than at magnetic stations in higher latitudes. On certain days, the lunar influence in the EEJ was seen to become considerably large and even comparable to the solar effects. The existence of these 'big L' days was first reported by Bartels and Johnston (1940) from ground-based magnetic observations at Huancayo in Peru. Subsequently, large lunitidal amplitudes were also computed at equatorial stations in Kodaikanal, India (Rao and Sivaraman, 1958) and Ibadan, Nigeria (Onwumechilli and S., 1959). The electrojet was attributed by Forbush and Casaverde (1961) as the reason for large lunitidal variation at Huancayo. Rastogi (1963) also reported that the lunitidal oscillations in horizontal magnetic component, H, at stations close to the magnetic equator are greatly affected by the electrojet currents. Using a chain of magnetic observatories in Peru, he found that the semi-diurnal lunar variations in daily range of H during December solstice at Huancayo $(12.1^{\circ}S, 75.2^{\circ}W)$, which is located under the EEJ, was four times greater than at Talara $(4.6^{\circ}S, 81.3^{\circ}W)$, which is located outside the EEJ. Rastogi and Trivedi (1970) also demonstrated the longitudinal variation of semi-diurnal lunar tide (M_2) in EEJ. Using the horizontal magnetic intensity data at Huancayo $(12.1^{\circ}S, 75.2^{\circ}W)$, Addis Ababa $(9.0^{\circ}N, 38.7^{\circ}E)$, Trivandrum $(8.5^{\circ}N, 76.9^{\circ}E)$, Koror $(7.3^{\circ}N, 134.5^{\circ}E)$ and Jarvis $(0.4^{\circ}S, 160.0^{\circ}W)$, they compared the amplitude of M_2 at all these stations and found the M_2 amplitude during December solstice at Huancayo to be 8.7 nT compared to 4 nT in Trivandrum. Further, their results also showed an increase in the

M_2 amplitudes with an increase in the solar daily range of H. Hence, they concluded that the lunitidal oscillations in H show a strong longitudinal variability near the magnetic equator and it is related to the longitudinal variations of EEJ. This variability was not only observed in the EEJ but also in the mid-day values of critical frequency (f_0F_2). The lunar semi-diurnal variations in f_0F_2 also showed a maximum in the South American zone and a minimum over the Indian zone. Rastogi (1962a) suggested based on these observations that enhancement of the lunitidal variation over the dip equator in f_0F_2 is closely related to the equatorial electrojet. Stening et al. (2002) computed the amplitude and phases of lunitidal variations in H at many observatories in different latitudes and longitudes and determined the M_2 amplitude during December at Huancayo (Peru) and Trivandrum (India) to be 20.5 nT and 12.1 nT, respectively. They attributed the large lunitidal amplitude at Huancayo during December to higher Cowling conductivity over that region which results in the larger intensity of EEJ. However, Rastogi (1962b) have argued that the longitudinal variation of Cowling conductivity along the dip equator is too small to explain the difference in EEJ intensities and suggested a longitudinal variation in the tidal velocities to explain the larger lunitidal amplitude in EEJ over Peru as compared to over India.

This study follows the previous work by Siddiqui et al. (2015b) and Siddiqui et al. (2015a) in which they computed the lunitidal enhancements in EEJ at Huancayo during SSW and non-SSW winters and also showed a good correlation between the timing of lunitidal amplifications and the onset of stratospheric warmings. In this study we investigate the response of EEJ to SSW events in different longitudinal sectors. By quantitatively comparing the lunitidal enhancements in the Peruvian and Indian sectors using ground-based and satellite observations we suggest plausible causes for the observed longitudinal variabilities.

We describe the various data sets used in this study in Section 4.3. In Section 4.4 we introduce our approach for determining the strength of the lunar tidal modulation of the EEJ and in the neutral temperature measurements. In Section 4.5 we present our observations followed by discussion in Section 4.6. The conclusions from this work are presented in the final section.

4.3 DATASET

In this study we use multiple data sets to investigate the longitudinal variabilities of the lunitidal oscillations during SSWs. The details regarding the various sources of data considered in this study are elucidated in the following paragraphs.

To study the longitudinal characteristics of lunar tides in the EEJ, horizontal (H) component recordings from ground-based magnetometers in

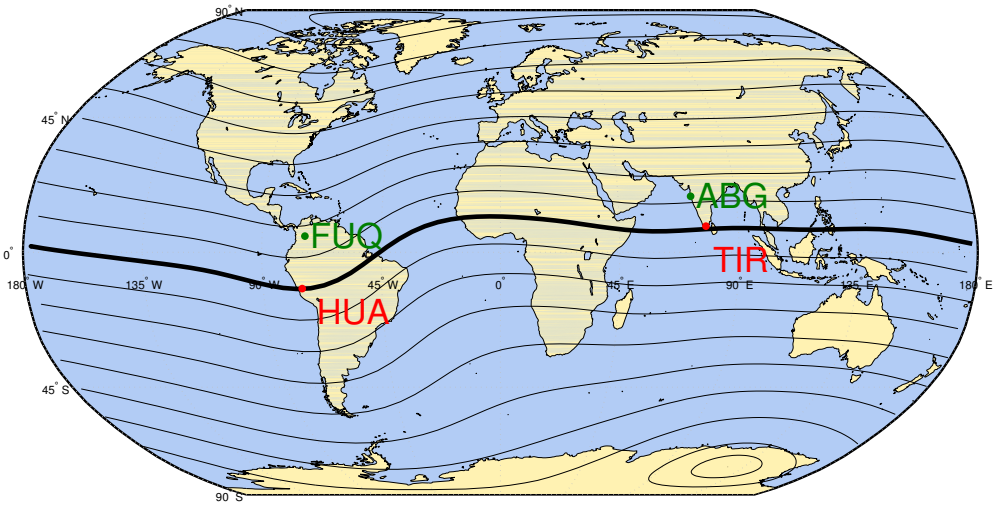

Figure 4.1: The locations of the observatories in the Peruvian and Indian sectors are presented in this plot. The black lines represent the quasi-dipole lines including the dip equator which is marked in bold black colour. The equatorial observatories are marked with red dots whereas the non-equatorial observatories are denoted with green dots.

the Indian and Peruvian sectors have been utilized. Hourly means of the geomagnetic *H* component at Huancayo, HUA, (-12.05°N, 284.67°E, 0.59° dip lat.), Fuquene, FUQ, (18.11°N, 293.85°E, 17.06° dip lat.), Tirunelveli, TIR, (8.7°N, 77.8°E, 0.59° dip lat.) and Alibag, ABG, (18.6°N, 72.9°E, 13.67° dip lat.) for the following periods were downloaded from the website of World Data Centre for Geomagnetism, Edinburgh:

(a) Dec 2005 - Feb 2006 , (b) Dec 2006 - Feb 2007 and (c) Dec 2008 - Feb 2009

Figure 4.1 shows the location of the observatories used in this study. The black lines represent the quasi-dipole lines including the dip equator which is plotted in bold black colour. The locations of equatorial observatories are marked with red dots while the location of non-equatorial observatories are represented with green dots.

The pair of magnetometers in both the sectors have been chosen such that one of the observatories is situated directly beneath the equatorial electrojet (HUA & TIR) and the other observatories (FUQ & ABG) lie outside the influence of EEJ. The purpose of using this approach is that a major part of solar quiet (S_q) daily magnetic variation at an equatorial observatory can be removed by using the S_q variation at a non-equatorial observatory (e.g., Manoj et al., 2006). The enhancement of lunitidal amplitudes in the EEJ has been compared in Siddiqui et al. (2015a) for both the cases when an equatorial station makes use of a reference station and when it

is used alone. The lunitidal enhancements seemed better correlated with stratospheric observations of SSW when a suitable reference station was considered. Here, Fuquene and Alibag serve as reference stations to the equatorial observatories at Huancayo and Tirunelveli, respectively.

For the purpose of direct comparison between ground and satellite observations, EEJ intensities derived from the CHAMP satellite measurements are also used in this study. The CHAMP satellite was launched into a circular, near-polar (inclination: 87.2°) orbit at 456 km altitude on 15 July 2000 and it provided highly precise gravity and magnetic field measurements over a 10-year period. It circled the Earth about 15.5 times per day and its orbital plane precessed through local time at a rate of 1 h per 11 days. It required 131 days to cover all local times, considering both ascending and descending orbital nodes. The electrojet current strength was deduced from magnetic field measurements on board CHAMP. The readers may refer to Lühr et al. (2004) for a more detailed description of the EEJ determination from CHAMP measurements.

The V2.0 temperature measurements from the Sounding of the Atmosphere using Broadband Emission Radiometry (SABER) instrument on the Thermosphere Ionosphere Mesosphere Energetics and Dynamics (TIMED) satellite are used to estimate lunar tidal amplitude in neutral temperature at an altitude of 110 km.

To consider the dependence of the EEJ strength on solar activity we apply the solar flux values $F_{10.7}$ in sfu ($10^{-22} W m^{-2} Hz^{-1}$) which are available at the GSFC/SPDF OMNIWeb interface. The weakening of the northern polar vortex is quantitatively deduced from the zonal-mean zonal wind (U) at 70°N and at 48 km altitude and from the temperature (T) at the North Pole and at 40 km altitude which were obtained from MERRA (Modern-Era Retrospective Analysis for Research and Application) data.

4.4 METHODS OF ANALYSIS

4.4.1 *Estimating lunar tidal amplitude in EEJ from ground magnetic records*

Regular daily variations with period and sub-periods of a solar day are found in ground magnetic records and are termed as geomagnetic solar (S) daily variations. Besides S there are also smaller periodic variations depending on lunar time called the geomagnetic lunar (L) daily variations. The amplitude of L is an order of magnitude smaller than S and its dominant component is the semi-diurnal variation (12.42 hours) which displays a semi-monthly variation (14.77 days) at a fixed local time. Normally, lunar modulation of the EEJ roughly amounts to about 15% of its intensity (e.g., Onwumechilli, 1963; Lühr et al., 2012) but during certain 'big L days' between November and February, lunar effects in the EEJ suddenly show

an increase by 4-5 times (Bartels and Johnston, 1940). One of the causes for these large lunitidal enhancements in the EEJ could be due to modified tidal propagation conditions during SSWs (Forbes and Zhang, 2012). In this study we first investigate the lunar modulation of EEJ during SSWs in the Peruvian and Indian longitudinal sectors by using the ground-based magnetic recordings in these regions.

We employ the method as explained in Siddiqui et al. (2015a) to deduce the semi-monthly lunar tidal amplitude from the H component of ground-based magnetic field recordings. Briefly, the electrojet strength is estimated by choosing a pair of stations such that one of the stations lies within the electrojet footprint and the other is located outside of it, thus acting as a reference station to the former. The nighttime values are used as a reasonable approximation for removing the effects of the Earth's core and crustal field. The nighttime values, H_{MF}, are first subtracted individually from the horizontal component recordings, H, of both the equatorial and the reference station. Here, H_{MF} represents the contributions of Earth's main field (MF) in the H component of ground-based magnetic field recordings.

$$\Delta H = H - H_{MF} \tag{4.1}$$

ΔH here reflects the daily variation with respect to the local midnight values. The electrojet strength, H_{EEJ}, is then estimated by computing the difference between the daily variations at the equatorial and the reference station.

$$H_{EEJ} = \Delta H_{EEJ} - \Delta H_{NonEEJ} \tag{4.2}$$

As mentioned in the earlier paragraphs, the stations chosen for the Peruvian sector are Huancayo and Fuquene and in case of the Indian sector the stations are Tirunelveli and Alibag. For both these station pairs, the EEJ derived strength is then normalized to a solar flux level of 150 s.f.u and the data are then arranged into bins of 1 day by 1 h in local time (LT) from 08:00 to 16:00 hr for an interval of 59 days. The dominant solar tidal variations are removed by subtracting the means over a 59-day period (two lunar months) for each local time hour. The amplitude of the semi-monthly lunar wave (14.77 days) is then obtained by Fast Fourier Transform (FFT) for each local time hour. The amplitude thus obtained is then normalized for the expected diurnal variation of the ionospheric conductivity, C, following Lühr et al. (2008).

$$C = C_0 \sqrt{\cos\left\{\frac{\pi}{12\,h}(LT - t_0)\right\}} \tag{4.3}$$

where $C_0 = 1$, indicates the peak conductivity and $t_0 = 12{:}30$ LT is the local time of the peak conductivity.

The semi-monthly lunar wave over 59 days is estimated from the mean of normalized amplitudes for each local time bin. A sliding window of

59 days length advanced by 1 day is applied to estimate the day by day lunitidal amplitude.

4.4.2 *Estimating lunar tidal amplitude from the CHAMP magnetometer measurements*

We further investigate the lunar modulation of EEJ during SSWs in the Peruvian and Indian longitudinal sectors by using the CHAMP magnetometer measurements. Since we are investigating the longitudinal variabilities in the lunar tide of the EEJ, we first sort the EEJ values derived from CHAMP, according to two longitudinal intervals each of 90 degrees width around the Peruvian and Indian sectors. The Peruvian sector is represented by the longitudes between $235^\circ - 325^\circ$E, while the longitudinal interval between $45^\circ - 135^\circ$E have been selected for the Indian sector. The EEJ dependence on solar activity is accounted by normalization using the statistical formula used by Park et al. (2012) (see their Equation 1)

$$EEJ' = \frac{EEJ}{\sqrt{\frac{F_{10.7P}}{150} \times |\cos\frac{\pi}{12}(LT - 12h)|}} \tag{4.4}$$

where EEJ and EEJ′ are the original and normalized EEJ peak current densities (Alken and Maus, 2007), respectively and $F_{10.7P} = \frac{F_{10.7}+F_{10.7A}}{2}$ where $F_{10.7}$ is the observed value of solar radio emission at 10.7 cm for each day and $F_{10.7A}$ is the 81-day averaged value of $F_{10.7}$ index.

Further, following Park et al. (2012), a similar approach for estimating the semi-diurnal lunar (M_2) tidal amplitude from the CHAMP EEJ data is applied in both these sectors. Instead of calculating zonally averaged EEJ′, which was used by them, we compute $\widetilde{EEJ'}$ which is averaged over each longitudinal sector. The averaged values are then detrended by using a 39-day 1-D median filter. Since the M_2 tide appears Doppler-shifted at a period of approximately 13 days in the moving frame of the CHAMP satellite (see Park et al., 2012), 3 cycles of the 13-day oscillation corresponds to the filter length of 39 days. The M_2 amplitude is then evaluated for a moving window of 39 days length using the FFT. The window is moved forward by one day and the same analysis is applied to subsequent days.

4.4.3 *Estimating lunar tidal amplitude from the SABER temperature measurements*

The SABER neutral temperature measurements within $\pm 5^\circ$ latitude around Huancayo and Tirunelveli and at 110 km altitude are also analyzed to study the longitudinal variability of the M_2 during SSWs. The longitudinal interval corresponding to the Peruvian and Indian sectors, have been

considered as above and the data are sorted for each day. For the estimation of M_2, we employ the method used by Forbes and Zhang (2012). The Doppler-shifted M_2 lunar tide in the frame of SABER instrument on board the TIMED satellite corresponds to 11.85 days (Forbes and Zhang, 2012). Using this fact, we start the procedure for the lunar tidal analysis by calculating residuals for each day by using a 12 day running-mean background temperature centered on that day. The residuals are then fitted within a 12 day moving window using the least-squares method to extract the semi-diurnal lunar signal. The window is subsequently moved forward by one day at a time to determine the evolution of the M_2 tide during SSWs.

In the above analyses, although we have used different window sizes based on the M_2 and semi-monthly lunar periods on the ground and on the two satellite frames, we do not expect a difference due to varying window lengths when comparing the lunitidal enhancements.

4.4.4 *Identification of Sudden Stratospheric Warming events using the concept of Polar Vortex Weakening*

The concept of using polar vortex weakening (PVW) for characterizing the strength of SSW events was introduced by Zhang and Forbes (2014). They used the daily time series of the zonal-mean zonal wind (U) at 70°N and 48 km altitude and temperature (T) at North Pole and 40 km altitude from the MERRA reanalysis dataset to describe the PVW. This same definition was then also used by Chau et al. (2015) and later by Siddiqui et al. (2015a) to demonstrate a correlation between the PVW characteristics and lunitidal enhancements in the upper mesosphere and in the EEJ, respectively.

In this study we also use the same definition of PVW to compare its timing with the lunitidal enhancements in the EEJ and in the SABER temperature measurements.

4.5 OBSERVATIONS AND RESULTS

4.5.1 *Lunar tidal modulation of the EEJ during SSW*

The top and middle panels in Figures 4.2, 4.3 and 4.4 present the diurnal magnetic field variations underneath the EEJ at the Huancayo and Tirunelveli observatories during December 2005 - February 2006, December 2008 - February 2009 and December 2006 - February 2007, respectively. Figures 4.2 and 4.3 include the SSW events of 2006 and 2009 while no SSW event (according to the WMO definition) was recorded during Dec 2006 - Feb 2007. The bottom panels in all three figures present the daily time series of the zonal-mean zonal wind, U (red curve) at 70°N and 48 km altitude and the temperature, T (black curve) at North Pole and 40 km al-

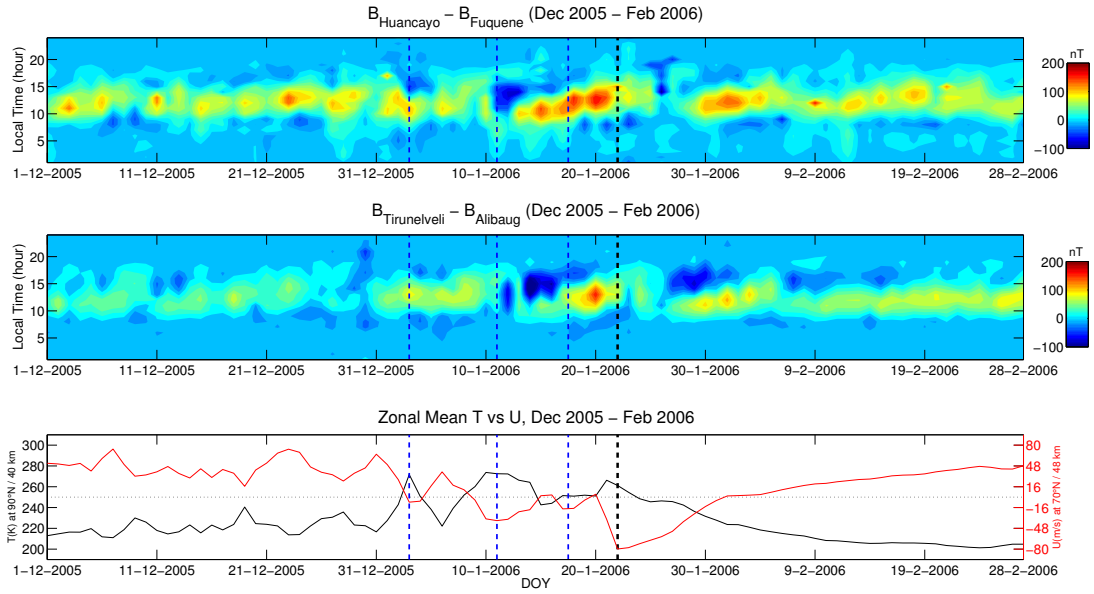

Figure 4.2: The top and middle panels present the daily variation of the EEJ at Huancayo, Peru and Tirunelveli, India during December 2005 - February 2006. The bottom panel presents the daily time series of the mean zonal wind (U) at 70°N and 48 km altitude (red curve) and temperature (T) at North Pole and 40 km (black curve) during the same period. The dashed black vertical line in each panel marks the peak polar vortex weakening (PVW) day. The dashed blue vertical lines denote the multiple episodes of warming prior to PVW during this time interval.

titude for the above mentioned periods. The dashed black vertical lines in Figures 4.2 and 4.3 mark the days of peak PVW. The dashed blue vertical lines in Figure 4.2 denote multiple warming events that occurred prior to the intense event (denoted by dashed black line).

The development of major SSW events in 2006 can be seen in Figure 4.2. During this period multiple episodes of major warming events are recorded. The zonal mean wind at 70°N and at an altitude of 48 km starts to decelerate around 31st December, reverses its direction and reaches a minimum on 3rd January. The temperature starts to increase along with deceleration of the winds and peaks on the same day when the minimum in winds are recorded. Later episodes of warming reached their peaks on 11th, 18th and 22nd January. The fourth warming event is the most prolonged during this period with the zonal winds reversing and reaching almost 80 m/s in the westward direction.

The second episode of warming is larger than the first one and starts around 11th January. During this period, the EEJ first weakens for a couple of days and then develops a semi-diurnal perturbation pattern with morning enhancement and afternoon weakening which shifts to later lo-

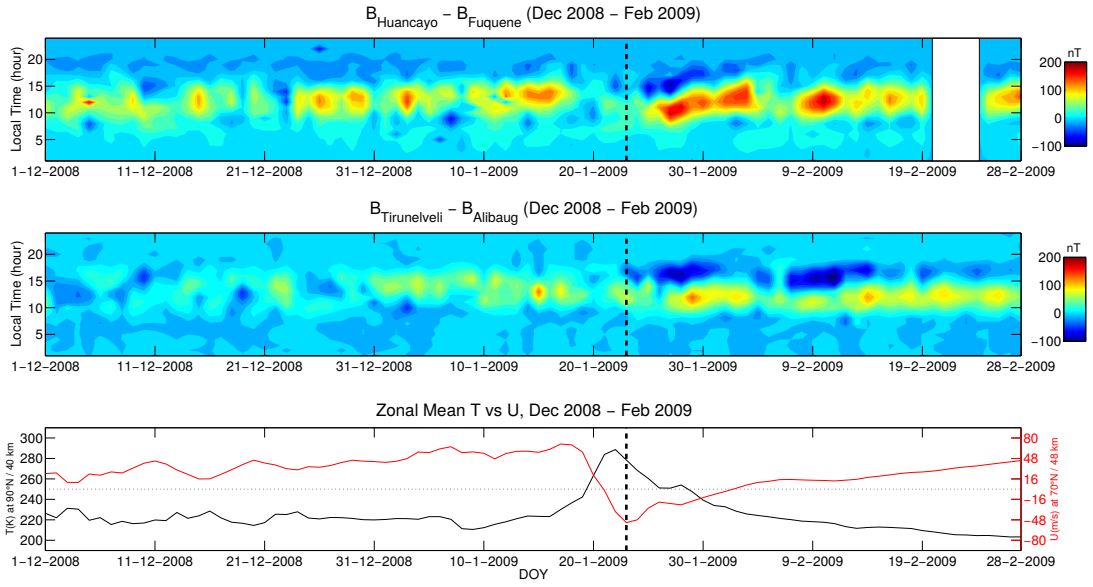

Figure 4.3: Same as Figure 4.2 but during the period December 2008 - February 2009.

cal times. The perturbation pattern is similar to the one described by Fejer et al. (2010) in case of the 2003 SSW event. A second perturbation pattern in EEJ starting around 28th January can also be seen in both these panels. As it has been reported earlier by Fejer et al. (2010), these perturbations are also seen first in the Peruvian sector and a few days later in the Indian sector. Another notable feature is the stronger perturbation patterns over the Peruvian sector than the Indian sector.

During the 2008-2009 winter, multiple warming events are not witnessed and can be seen in Figure 4.3. The zonal wind starts to decelerate around 18th January and reaches its minimum on 23rd while the temperature at the North Pole is also seen to peak during this period. The 2009 SSW event is one of the strongest and most prolonged SSW ever recorded in history (Manney et al., 2009). As seen earlier during the 2006 SSW event, in this case too, the EEJ intensity decreases at first and then after the peak warming around 26th January develops a similar semi-diurnal pattern with morning enhancements and afternoon weakening which shifts to later times at both longitudes. It can be further seen that the semi-diurnal pattern is much clearer and stronger in the Peruvian sector than in the Indian sector during this event.

Figure 4.4 presents the same plot as Figures 4.2 and 4.3 but during Dec 2006 - Feb 2007. According to WMO's definition of stratospheric warming, no SSW events are recorded during this period, however, we detect a minor episode of warming around 31st December. The temperature at the North Pole shows an enhancement and the zonal wind also shows a

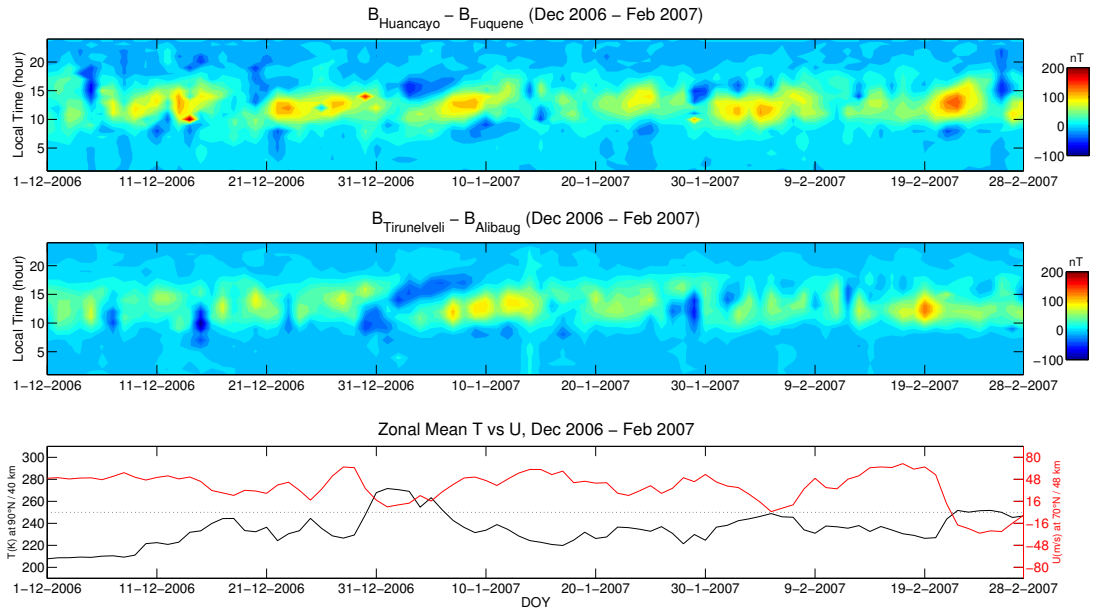

Figure 4.4: Same as Figure 4.2 but during the period December 2006 - February 2007.

deceleration, but it does not get reversed. A slightly weaker semi-diurnal pattern compared to the one in Figure 4.2 can be seen around 2nd January in the first two panels. The perturbation is much weaker as compared to major SSW events in Figures 4.2 and 4.3 in both the sectors. The difference in the perturbations of EEJ intensity during stronger and weaker zonal wind reversal conditions is evident in these three plots. The observed perturbations can be attributed to the amplification of lunitidal oscillations in the equatorial electrojet during SSWs (Fejer et al., 2010).

4.5.2 *Lunar tidal amplitudes in EEJ and neutral temperature measurements*

The three panels in Figures 4.5, 4.6 and 4.2 present the lunar tidal amplitudes that have been computed from the magnetometer recordings, peak EEJ intensity measurements from CHAMP and SABER temperature data, respectively, during the SSW winters of 2006 and 2009, and during the non-SSW winter of 2007. The dashed black vertical lines denote the day of strongest PVW in Figures 4.5 and 4.6 in all the three panels. The solid black and red lines in these figures denote the lunitidal amplitudes in the Peruvian and Indian sectors, respectively.

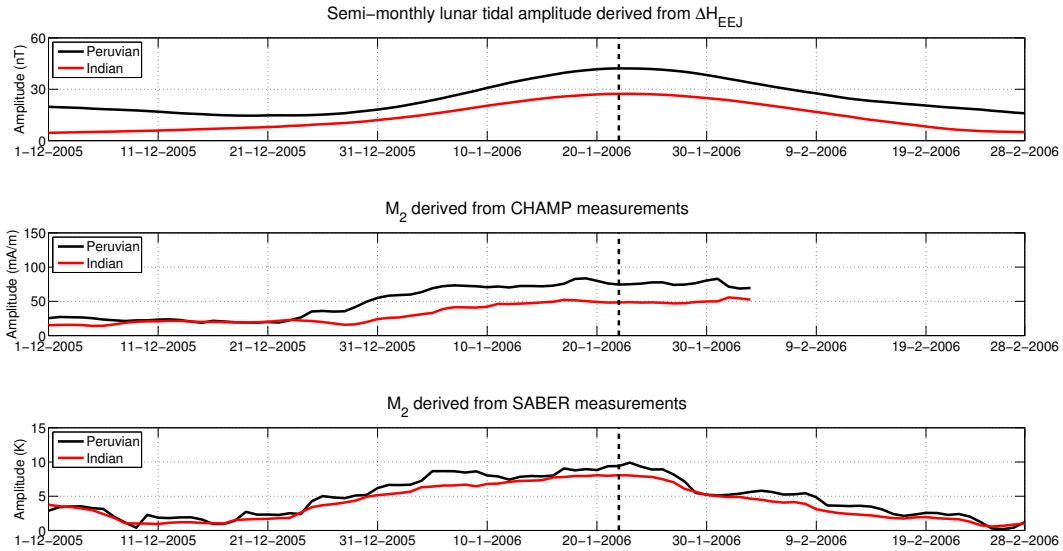

Figure 4.5: The top panel presents the semi-monthly lunar tidal amplitude in the EEJ derived from ground magnetometer recordings between December 2005 - February 2006. The black line denotes the lunitidal amplitude in the Peruvian sector and the red line denotes the same in the Indian sector. The middle panel presents the M_2 amplitude derived from CHAMP data during the same period and for the above two sectors. The lower panel presents the M_2 amplitude derived from SABER temperature measurements. The black vertical dashed line in all the panels denote the day of peak PVW.

4.5.2.1 *2006 SSW event*

The top panel in Figure 4.5 presents the semi-monthly lunar tidal amplitude derived from H_{EEJ} which is clearly larger at Huancayo (Peru) than at Tirunelveli (India) during the 2006 SSW winter. A strong enhancement in both the sectors starts towards the end of December followed by a peak in amplitude during the third week of January. The peak PVW also takes place during this time, and the close correlation between these two phenomena was demonstrated in Siddiqui et al. (2015a). In the Peruvian sector, the peak amplitude reaches a value of 42.2 nT and it occurs on 22nd January whereas in the Indian sector peak amplitude of 27.3 nT is achieved a day later on 23rd January. The ratio between peak amplitudes at Huancayo and Tirunelveli is 1.5. As the days of peak PVW are quite similar for both the 2006 and 2009 SSW, the percentage changes between the pre-warming and peak amplitudes are calculated relative to 1st January in both these cases. The relative changes in semi-monthly lunar tidal amplitude for both the Peruvian and Indian longitudes are similar, being 131% and 126%, respectively.

In the middle panel of this figure, the M_2 amplitude from CHAMP peak EEJ intensity data is presented. The local time coverage of the CHAMP satellite during the 2006 SSW event was favorable in the sense that CHAMP recorded the EEJ intensity during the daytime between 7 and 17 LT during Dec 2005 and January 2006. The enhancement in M_2 starts similarly towards the end of December as in the case of ground observations and then the maximum M_2 amplitude is recorded during the third week of January around the time of peak PVW in both sectors. Here, the lunitidal enhancement in the Peruvian sector is larger than in the Indian sector. The peak amplitudes however are recorded earlier than the day of PVW and this is due to decreasing LT in the satellite frame. The local time was 12 LT on 31st December 2005 and moved to 10 LT on the day of observed PVW maximum. The M_2 amplitudes on the day of peak PVW are 74.4 (mA/m) and 48.3 (mA/m) for the Peruvian and Indian sectors, respectively with the ratio again being 1.5. However, due to the varying LT in the satellite frame the relative percentage changes are difficult to compare and therefore are not shown. In both the ground-based and space measurements the lunitidal enhancements start at similar time and the level of enhancements are also similar in both sectors. Overall, the semi-monthly lunar tidal amplitude derived from magnetometer recordings and the M_2 amplitude derived from CHAMP satellite measurements show a good agreement with each other.

In the bottom panel the M_2 amplitude derived from SABER temperature measurements is shown for both the sectors. The M_2 amplitude starts increasing during the last week of December and it reaches the peak value of 9.4 K (Peruvian sector) and 8.1 K (Indian sector) on 23rd and 22nd January, respectively, with the ratio between peak M_2 enhancements being 1.1. Thereafter it shows a gradual decrease till the end of February in both the sectors. The M_2 enhancements in neutral temperature are similar in both the sectors unlike the lunitidal enhancements in EEJ. The day of peak M_2 amplification in neutral temperature measurements compares quite well with the respective lunitidal peaks in EEJ derived from ground observations. The peak lunitidal amplitudes from ground-magnetometer, CHAMP and SABER measurements are presented in Table 4.1 along with their respective delays in timing relative to the PVW.

4.5.2.2 *2009 SSW event*

The top panel in Figure 4.6 shows the semi-monthly lunar tidal amplitude computed from ground magnetometer recordings during the 2008-2009 SSW winter. The lunitidal amplitude in EEJ at Huancayo shows a similar enhancement as in the case of 2005-2006 SSW event and reaches its peak 4 days after the day of PVW, whereas the enhancement at Tirunelveli is much smaller and its peak appears 16 days later than the PVW day. The

Table 4.1: The peak semi-monthly lunitidal amplitude from ground-magnetometer recordings, M_2 amplitudes (on the day of PVW) from CHAMP data and peak M_2 amplitudes from SABER measurements in both the Indian and Peruvian sectors are presented here. The values are followed by their respective delays in timing (wherever applicable) with respect to the PVW day.

Year	Date of PVWs	Sector	Ground mag. (nT)	CHAMP (mA/m)	SABER (K)
2006	22nd Jan	Peruvian	42.2 (0 d)	74.4	9.4 (1 d)
		Indian	27.3 (1 d)	48.3	8.1 (0 d)
2007		Peruvian	28.3	47.3	6.1
		Indian	16.0	28.9	4.8
2009	23rd Jan	Peruvian	39.4 (4 d)		11.4 (5 d)
		Indian	16.5 (16 d)		9.9 (5 d)

peak amplitude at Huancayo during this event is 39.4 nT and it is 16.5 nT at Tirunelveli with their ratio being equal to 2.4. The relative changes in lunitidal amplitude for both the Peruvian and Indian longitudes being 125% and 108%, respectively.

The peak amplitude at Tirunelveli is attained during the post-warming phase when the wind direction started to change again from easterly to westerly and the temperature values started to reach pre-SSW levels. The 2006 and 2009 SSWs are both major warming events and the lunar tidal enhancement at Huancayo is similar during both these major SSWs, as peak values are alike and the timing of enhancements closely follows the PVW. However, the timing and amplitude in the Indian sector are different during both these SSWs. The shifting semi-diurnal perturbation in Figure 4.3 is clearly stronger in the Peruvian sector while in the Indian sector the perturbation more resembles a solar diurnal variation, which suggests a weaker lunar influence on the EEJ.

In the middle panel of Figure 4.6, the M_2 amplitude computed from CHAMP peak EEJ intensity data is presented. However, during December 2008 - January 2009, CHAMP crossed the magnetic equator during nighttime hours (LT) and the local daytime coverage of EEJ resumed only during the first week of February 2009. The lunitidal amplitude can therefore be estimated only during February - March 2009 for this SSW winter and a direct comparison between the top two panels is not possible likewise as in Figure 4.5. CHAMP precessed through 17 LT on 19th January 2009 and then moved to 16 LT on the day of observed PVW maximum. Here, the M_2 amplitude in February is probably in the declining phase after a plausible

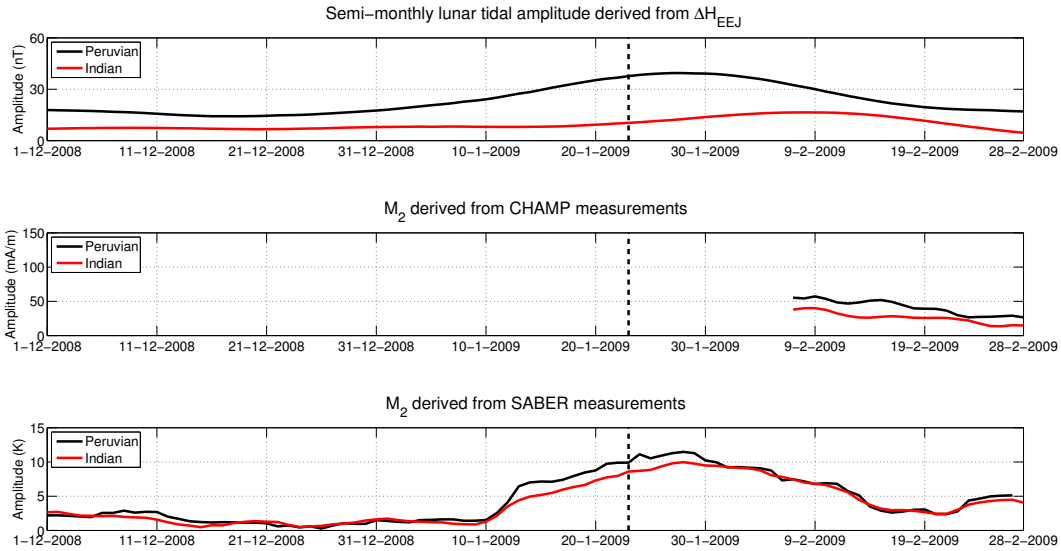

Figure 4.6: Same as in Figure 4.5 but only for the period December 2008 - February 2009.

enhancement during the SSW event. The amplitude is again consistently larger in the Peruvian sector than in the Indian sector.

The bottom panel of this figure presents the M_2 amplitude in SABER temperature data. In both the sectors, the enhancement in M_2 begins after 10th January and the peak amplitude is achieved on 28th Jan with values of 10 K and 9.7 K in the Peruvian and Indian sectors, respectively, with the ratio of peaks being 1.03. The timing of peak PVW is recorded on 23rd January for this SSW event. Post-SSW, the wind and temperature values start to reach their pre-SSW levels and the enhancement in M_2 amplitude also gradually subsides. The lunitidal amplification levels from SABER measurements are again similar in both the sectors and closely follow the semi-monthly lunitidal amplification at Huancayo.

4.5.2.3 *2006 - 2007 Northern winter*

In Figure 4.7, the lunitidal amplitudes from the three datasets are compared during the winter of 2006-2007 in which no major warming was recorded. In the top panel, unlike in the previous two figures, no sharp increase in the semi-monthly lunar tidal amplitude is observed. Although a gentler enhancement can be seen towards the end of December in the Peruvian sector and in the first ten days of January in the Indian sector, which could be either related to the seasonal enhancement of the lunar tide which happens during December solstice, or to the moderate enhancement of stratospheric temperatures around 31st December. Also, the amplitude

in the Peruvian sector is larger than in the Indian sector, as seen in the earlier two cases. The peak lunitidal amplitude at Huancayo is 28.3 nT on 31st December 2006 and 16 nT at Tirunelveli on 12th January and their ratio being equal to 1.7.

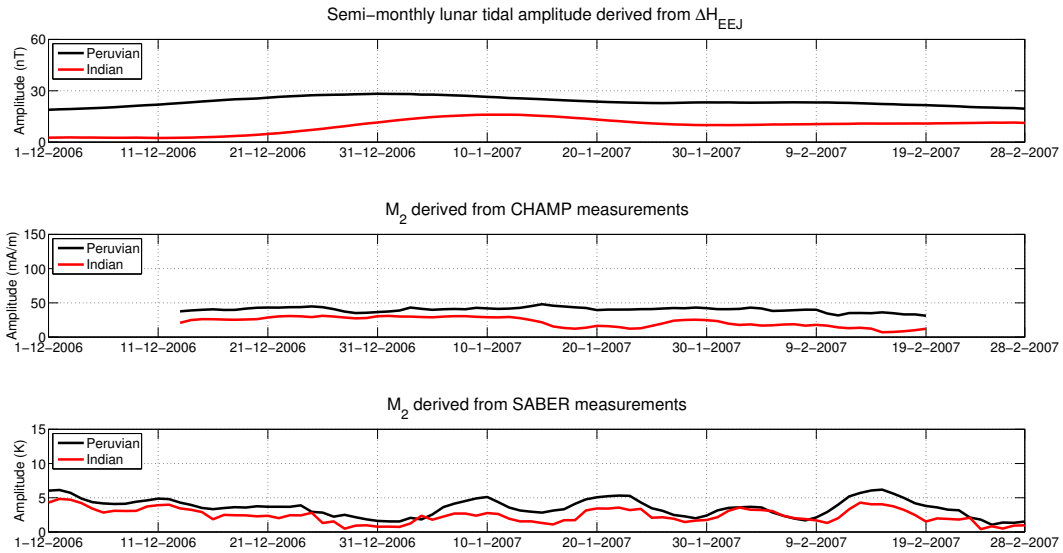

Figure 4.7: Same as in Figure 4.5 but only for the period December 2006 - February 2007.

In the middle and bottom panels, the M_2 amplitude from CHAMP and SABER measurements doesn't show a clear enhancement in both the sectors as during the SSW winters. The CHAMP satellite precessed from 15 to 7 LT during this period, making it suitable to derive M_2 amplitude for this interval. Although the M_2 amplitudes remain less than 50 mA/m during the entire period in both the sectors, larger values are again observed over the Peruvian sector in this case. The M_2 amplitudes in the neutral temperature show no major enhancements during this winter and the values remain less than 5 K over both the sectors during the entire time interval. A major difference in M_2 amplitudes is thus clearly visible between SSW and non-SSW winter periods. However, the M_2 amplitudes in neutral temperature measurements are similar over both the Peruvian and Indian sectors in all the three considered time intervals.

4.5.3 *Phase propagation of the semi-monthly lunar tide in EEJ*

The lunar tide is an astronomical phenomenon and therefore, its phase in general can be precisely determined. For example, Lühr et al. (2012) used 5 years of CHAMP data to investigate the phase propagation of the

semi-monthly lunar tide as a function of moon phase. They obtained a linear pattern of phase propagation with aging moon that is consistent with astronomical predictions (see Lühr et al., 2012, Figure 3). When fitting a regression line to the phase values of analysed lunitidal waves that were determined independently for each local time hour, they obtained the following formula for the linear fit which estimates the local time (LT) of the maximum of the semi-monthly wave for all moon phases (MP).

$$LT = 1.2(MP - 12h) + 8.5h \tag{4.5}$$

The above equation when written in terms of days from the new moon instead of moon phase, comes out to be (see Equation 6, Siddiqui et al., 2015b):

$$LT = 0.98(d - d_0) + 8.5h \tag{4.6}$$

where, d, is the number of days since new moon, LT, is the local time and d_0, on conversion from moon phase to days approximately equals 14.77 ($\approx \frac{12}{24} \times 29.53$) days.

As mentioned earlier the moon phase of 24 hours is approximately equivalent to 29.53 days whereas in our analysis we have used a window of $29.53 \times 2 \approx 59$ days. We tested the phase propagation of the semi-monthly lunar tide during the three periods of analysis to verify if the wave periods extracted through the method described in Section 4.4.1, can be attributed to lunar effects. In the following three subsections the phase propagation of the semi-monthly lunar tide in the EEJ at Huancayo and Tirunelveli has been determined from the H component of ground-based magnetic field recordings during the periods covering the SSW events of 2006 and 2009 and the 2006-2007 non SSW winter, respectively.

4.5.3.1 *2006 SSW event*

In Figure 4.8 the phase propagation of the semi-monthly lunar tide at the Peruvian and Indian sectors for a 59-day window starting from the day of a new moon during the 2005-2006 SSW event is presented. Here we have selected the window such that it starts and ends on the days of new moon and also covers the SSW period. The black dots and the red asterisks mark the phase propagation in the Peruvian and Indian sectors, respectively. The blue line is obtained by a linear regression fit made for the semi-monthly propagating phase in the Peruvian sector (black dots) and is similar to the one mentioned in Lühr et al. (2012) (see their Figure 3).

In cases of modified tidal propagation conditions such as during SSWs, the semi-monthly lunar phase could show slight changes but here despite the enhanced wave activity during the SSW period, the phase of the semi-monthly lunar tide resembles the expected pattern of phase propagation derived in Lühr et al. (2012) at both the Peruvian and Indian sectors. The

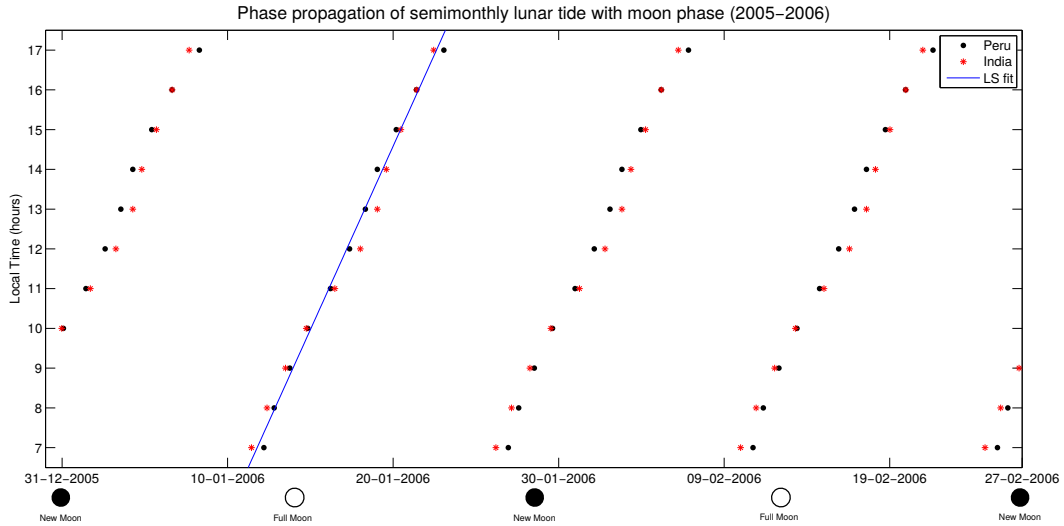

Figure 4.8: Phase propagation of the semi-monthly lunar tide in the EEJ determined from H component of ground-based magnetic field recordings is presented as a function of moon phase during the 2005 - 2006 SSW event. Dots mark for each local time hour the moon phase when the tidal wave crest is observed. The black dots and red asterisks represent the phase at Peruvian and Indian sectors, respectively. The blue line is obtained from least squares fitting to the propagating semi-monthly lunar phase in the Peruvian sector.

phase propagation of the semi-monthly lunar tide has been determined during the period when the SSW effects are strongest and here it is likely that the applied method robustly filters out the effects of other tides and waves which can impact the results.

Further, the equation of the regression line obtained by least squares fitting is,

$$LT = 0.94(d - d_0) + 8.9h \tag{4.7}$$

The regression parameters are also similar to the ones in Equation 4.6, which supports the fact that the amplitudes are largely related to lunar effects.

4.5.3.2 *2009 SSW event*

We also determine the phase propagation of the semi-monthly lunar tide during the 2008-2009 SSW event and is shown in Figure 4.9. The black dots and red asterisks mark the phase propagation in the Peruvian and Indian sectors, respectively, as seen earlier in Figure 4.8. The blue line is obtained by a linear regression fit made for the semi-monthly propagating phase in the Peruvian sector (black dots). The phase propagation follows the expected pattern to a large extent in the Peruvian sector but it deviates a small amount in the Indian sector during the noon hours before

returning again to the expected values during evening. It seems that the lunar tidal effects over the Peruvian sector are stronger during this SSW than over the Indian sector. As the 2009 SSW is one of the strongest SSW events recorded in recent history (e.g., Manney et al., 2009) and registered a strong amount of tropospheric forcing (e.g., Ayarzagüena et al., 2011), it is possible that the phase of the semi-monthly lunar tide gets slightly affected due to changed propagation conditions. However, since the semi-monthly lunar phase still follows the expected values closely it would not be unreasonable to believe that the results largely pertain to lunar effects.

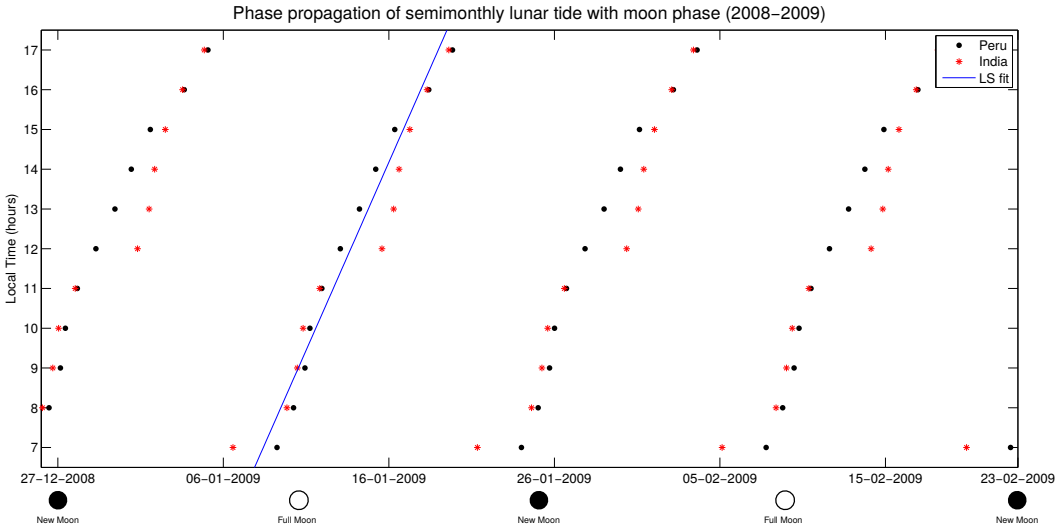

Figure 4.9: Same as Figure 4.8 except during 2008-2009 SSW winter.

The equation of the regression line obtained by least squares fitting is given by,

$$LT = 0.95(d - d_0) + 8.3h \tag{4.8}$$

Here Equation 4.8 again resembles the Equation 4.6 which was derived from climatological analysis, thus verifying our approach.

4.5.3.3 *2006-2007 Northern winter*

Figure 4.10 presents the phase propagation of the semi-monthly lunar tide at Peruvian and Indian sectors similar to Figure 4.8 except during the non-SSW winter of 2006-2007. A 59-day window is again selected starting from the day of new moon and the phase propagation of the semi-monthly lunar tide is determined as above. The pattern is again similar to the expected propagation in the Peruvian sector, whereas it diverges slightly in the morning hours in the Indian sector but returns back to the expected phase during later hours. The phase propagation in both the sectors closely resembles the climatology which leads us to believe that the

results are largely related to lunar tide. We also obtained the equation of the regression line by least squares fitting that is given by,

$$LT = 1.0(d - d_0) + 8.1h \tag{4.9}$$

and here also the regression parameters do not contradict the expected values from Equation 4.6.

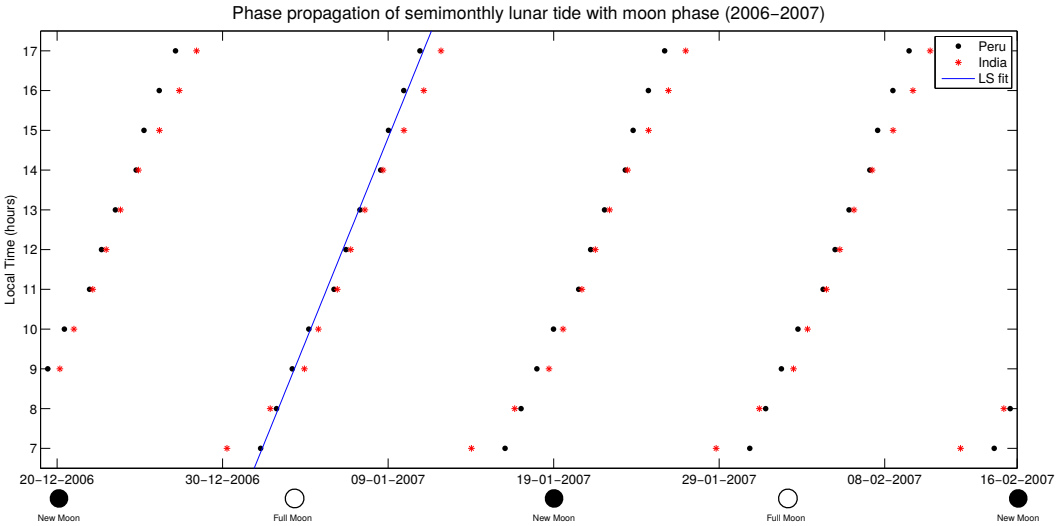

Figure 4.10: Same as Figure 4.8 except during 2006-2007 non-SSW winter.

4.5.4 *Climatological analysis of lunar tidal modulation of EEJ*

We carry out a statistical study using the CHAMP peak EEJ intensity measurements to compare the climatological lunitidal amplitudes in EEJ over the Peruvian and Indian sector during December solstice. In our analysis we use the entire peak EEJ measurements from 2000 - 2010 during December solstice (Dec - Feb). The procedure for sorting the data and further steps are explained as follows.

We consider the longitudinal intervals between 235°E - 325°E and 45°E - 135°E to represent the Peruvian and Indian sectors, respectively. The data are first sorted according to the longitudinal range of both the Peruvian and Indian sectors and then further sorted into bins of 2 h in moon phase and 1 h in local time (LT) for both the sectors. The local time interval here is again considered between 6 and 18 LT, as the EEJ signal outside of it is considered to be too weak. After sorting the data according to the moon phase and local time, there are on average 40 readings for each bin, from which a median value is calculated. Figure 4.11 shows the local time versus the moon phase distribution of the EEJ intensity obtained for both the Peruvian (top panel) and Indian (bottom panel) sectors. It is clear from the

figure that the EEJ intensity in the Peruvian sector is larger than in the Indian sector. However, we are interested in quantitatively investigating the lunar signal in the EEJ in both these plots and a quantitative comparison is shown in Figure 4.12.

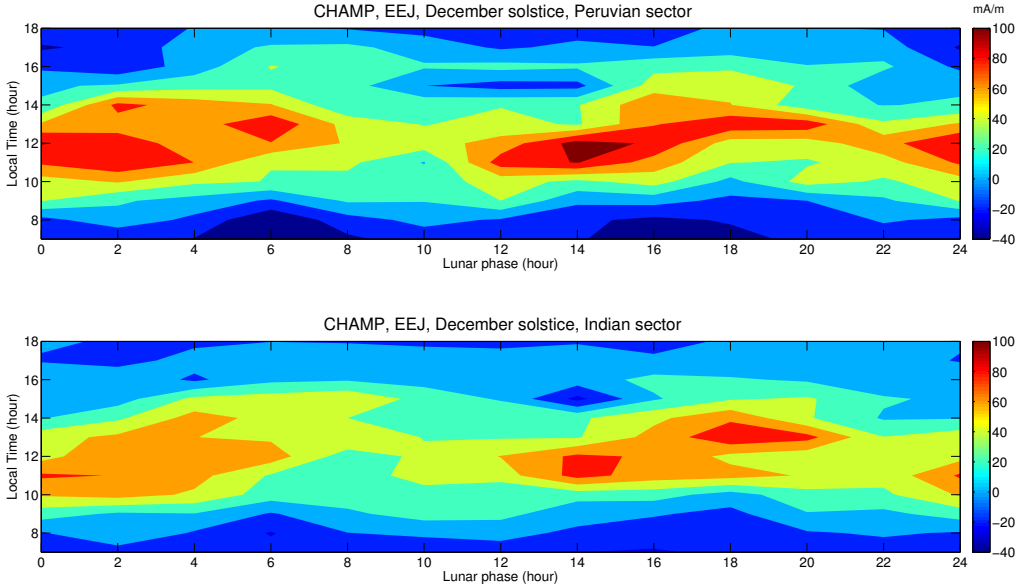

Figure 4.11: Local time variation of the electrojet lunar signal obtained using longitudinal averages of the EEJ peak current densities (mA/m) for the Peruvian and Indian sectors.

Since at a fixed local time, the lunar signal in the EEJ shows a semi-monthly oscillation, we estimate the amplitude of this tide for local times between 6 and 18 LT. The local time dependence of this amplitude can be seen in Figure 4.12 for both the Peruvian (solid black line) and Indian (solid red line) sectors. From Figure 4.12 we can deduce that the lunar tidal amplitude of the EEJ over the Peruvian sector is larger than over the Indian sector for all local times between 6 and 18 LT. The diurnal variation of the semi-monthly lunar tidal amplitude in both the sectors is also compared with the square root of cosine of the solar zenith angle which represents the electron density variation of a Chapman layer. The climatological lunitidal amplitudes in both the sectors are fitted with the function $\sqrt{A\cos(LT - t_0)}$ using the least-squares curve fitting method. The dashed black and the red lines represent the fitted curves in the Peruvian and Indian sectors, respectively. For the Peruvian sector the following values of A and t_0 were obtained; $A_{Peru} = 25.94$ (mA/m) and $t_0 = 12.01$ h and in case of the Indian sector the corresponding values were $A_{India} = 19.71$ (mA/m) and $t_0 = 12.00$ h. From the curve fitting results, the ratio of peak amplitudes, A_{Peru}/A_{India} equals 1.31 during the December solstice. These anal-

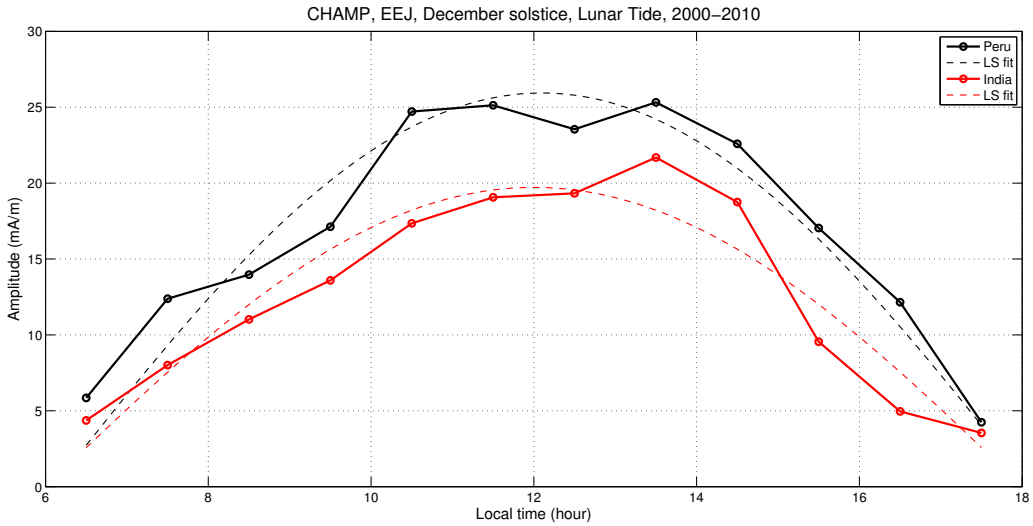

Figure 4.12: Comparison of the diurnal variation of the lunar tidal amplitude in the Peruvian (solid black line) and Indian (solid red line) sectors estimated using the CHAMP satellite data from 2000-2010 during December solstice. The dashed black and red lines represent the curves obtained after fitting (least-squares) the square root of cosine to the climatological amplitudes in the Peruvian and Indian sectors, respectively.

yses suggest that climatological lunitidal amplitudes in EEJ are larger over the Peruvian sector than over the Indian sector.

4.6 DISCUSSION

Our results clearly show the difference in lunitidal enhancements in EEJ and neutral temperature measurements during SSW and non-SSW periods in the Peruvian and Indian longitudinal sectors. Further, lunitidal enhancements in EEJ show a much greater longitudinal difference than in neutral measurements during SSWs.

Comparing our observations with the results obtained by Sathishkumar and Sridharan (2013) we find a good similarity. They estimated the M_2 amplitude in zonal wind at 90 km altitude at Tirunelveli for the 2009 SSW event and their results showed a peak in M_2 amplitude on the day of peak PVW. They also determined the M_2 amplitude in EEJ at Tirunelveli and found that its peak occurred approximately two weeks after the PVW, as seen in our results. Further they also found that the enhancement in solar semi-diurnal tide in EEJ was much larger than that in M_2 and concluded that the 2009 SSW event over Tirunelveli was mostly solar dominant. They performed the same analysis for the 2006 SSW event but in this case their results showed that the M_2 amplitude in EEJ dominated over the solar

semi-diurnal tidal amplitude. Although we have not determined the solar tidal amplitudes in our study, we can discern from Figures 4.2 and 4.3, that the lunar influence during the 2006 SSW was strong over both the Peruvian and the Indian sectors while during the 2009 SSW it was rather weak over the Indian sector. Based on this study we can state that while there can be a difference in lunar and solar tidal effects of the EEJ in different longitudinal sectors during the same SSW event, these effects can also be similar during another SSW event.

The connection between ionospheric variability and SSWs is generally accepted to be through the modulation of solar and lunar atmospheric tides (Chau et al., 2012; Pedatella et al., 2012; Pedatella and Liu, 2013). Simulation results by Pedatella and Liu (2013) suggest that the ionospheric variability during major SSWs is primarily caused due to the combined effects of the changes in migrating solar ($SW2$) and lunar semi-diurnal (M_2) tides. The changes in the M_2 tide occur due to changes in tidal propagation conditions during SSWs which shift the Pekeris resonance peak closer to the M_2 period (Forbes and Zhang, 2012). As the lunar tidal amplification is evident in SABER temperature measurements during the 2006 and 2009 SSW events, it may refer to the shift in Pekeris peak during both these events. While there is a clear correlation between the lunitidal enhancements in the EEJ and in SABER temperature measurements during the 2006 SSW event in both the sectors, there is a lack of correlation between them in the Indian sector during the 2009 SSW event. From our observations and the results of Sathishkumar and Sridharan (2013) we can suggest that the semi-diurnal enhancements during the 2009 SSW event over the Indian sector could be due to stronger modulation of EEJ by $SW2$ than by the M_2 tides. On the other hand we find that the semi-diurnal perturbations in EEJ over the Peruvian sector are strongly influenced by M_2 tides during both the 2006 and 2009 SSW events. It has also been suggested by Pedatella and Liu (2013) that planetary waves tend to damp the effects of $SW2$ tide in the Southern Hemisphere. There could also be a possibility that $SW2$ tidal effects at Huancayo are comparatively weaker than at Tirunelveli.

The M_2 amplitudes in neutral temperature measurements show lesser longitudinal variability during both the SSWs in the Peruvian and Indian sectors. Therefore the longitudinal variability in the lunitidal enhancements in EEJ should be related to the electrodynamics in the E-region dynamo. Maute et al. (2015) studied the longitudinal differences in $E \times B$ drift in the American and African sectors during the 2013 SSW event using the TIME-GCM simulations. The daytime vertical drift in the American sector showed an enhancement followed by progression of the daytime maximum from earlier to later local times but in the African sector the daytime maximum vertical drift showed no local time progression. Maute et al. (2015) found that the penetrating electric fields during moderate ge-

omagnetic activity could have partly caused the longitudinal difference in the daytime $E \times B$ in the two sectors. They conducted numerical experiments by shifting the neutral wind from the American sector to the African sector and vice-versa and found that the absence of semi-diurnal shift to later hours in the African sector can be created due to the combination of neutral wind and the geomagnetic main field configuration. The 2009 and 2013 SSW event were both major warming events and similar in terms of strength of the polar vortex weakening. The semi-diurnal perturbation in the EEJ in case of the 2009 SSW event is seen to be much stronger in the Peruvian/American sector but not so prominently in the Indian sector. This is similar to the observations of Maute et al. (2015) (see their Figure 5) where the semi-diurnal perturbation in $E \times B$ drift is weaker over the African Sector during the 2013 SSW event. We therefore suggest that the findings of Maute et al. (2015) also provide one explanation for the longitudinal differences in the diurnal variation of the EEJ at Huancayo (Peru) and Tirunelveli (India) during the 2009 SSW event.

4.7 CONCLUSIONS

In this study we have computed the lunitidal amplitude during major SSW events of 2006 and 2009 and during the non-SSW winter of 2007 using:

- the H component recordings from Peruvian and Indian magnetic observatories
- the peak EEJ intensity data from the CHAMP satellite
- the SABER temperature measurements

The evolution of derived tidal amplitudes from the three datasets are then compared during these periods in the Peruvian and Indian sectors. Major points of our study are as follows:

1. Our results show the difference in lunitidal enhancements in both the sectors during major SSWs and a non-SSW winter. It is observed that there is a significant lunitidal enhancement in all the three datasets during a major SSW event in comparison to a winter without an SSW.
2. Our results further show major longitudinal variabilities in lunitidal enhancements in EEJ in the Peruvian and Indian sectors. The semi-monthly lunar tidal amplitude in EEJ shows similar enhancements in the Peruvian and Indian sectors during the 2006 major SSW event but during the 2009 major SSW event lunar tidal enhancements in the Indian sector are much smaller and occur later with respect to the Peruvian sector.

3. The M_2 tidal amplitude derived from SABER temperature measurements are similar in both the sectors and show a strong amplification during the 2006 and 2009 SSWs. The M_2 tidal amplitude during SSWs closely follows the semi-monthly lunar tidal enhancements in the EEJ at Huancayo.

4. Our results suggest that the semi-monthly lunar tidal enhancements in the EEJ are not uniform across all longitudes and this could be either related to the local propagation conditions of the lunar tide or to the processes in the E-region dynamo. Although, the 2006 and 2009 SSW events were similar with respect to their PVW strengths but the lunitidal enhancements are quite different.

4.8 ACKNOWLEDGMENTS

The results presented in this paper rely on the data collected at Fuquene, Huancayo, Tirunelveli and Alibag. We thank Instituto Geográfico Agustin Codazzi, Colombia, Instituto Geofisico del Peru and Indian Institute of Geomagnetism for supporting geomagnetic observatory operations and INTERMAGNET for promoting high standards of magnetic observatory practice. We employ the wind and the temperature data downloaded from MERRA (Modern Era Retrospective Analysis for Research and Applications). The data for $F_{10.7}$ are obtained from the GSFC/SPDF OMNIWeb interface. T.A.S. and C.S. thank the International Space Science Institute (ISSI) for providing support to the International Team on "A three - dimensional ground-to-space understanding of sudden stratospheric warmings". The discussions during these meetings were helpful in this study. Jürgen Matzka assisted in analysing ground magnetometer data and global magnetic reference frames.

Part III

SUMMARY

5

SUMMARY AND FUTURE WORK

5.1 SUMMARY

The stratosphere-ionosphere coupling during SSWs provide an opportunity to better understand the processes behind the lower atmospheric forcing of the ionosphere and to improve capabilities that may, in future, lead to ionospheric weather forecasting. Recent modeling and observational studies present numerous evidences of lunar tidal enhancement in the ionosphere due to SSWs. It is believed that the change in the middle atmosphere due to SSW induced variabilities lead to the lunar tidal amplification in the MLT and in the ionosphere. In this thesis, the SSW induced variability in the EEJ has been studied in detail using the long-term ground-based magnetic observations at Huancayo, Peru that date as far back as 1922. The EEJ strength has been derived from these recordings and the investigation of the lunar tidal modulation of EEJ during SSWs has been carried out.

The results from this thesis aim to answer some of the existing questions regarding the lunar tidal modulation in the EEJ during SSWs. One such outstanding question is the existence of 'big-L' (lunar) days in the EEJ at Huancayo during northern winters. This observation has remained a big question for a long time and one of the causes that has been suggested is the enhancement of lunar modulation in the EEJ during SSWs. The results from Chapter 2 suggest that SSWs definitely lead to a major enhancement of lunar tides in the EEJ. Although a one-to-one correspondence between the occurrence of SSWs and the lunar tidal amplification in the EEJ is not witnessed but in most of the cases a significant correlation is obtained. For estimating the lunar tidal amplitude in EEJ, a new analysis approach is used that takes the phase of the lunar semi-monthly tide, which is known *a posteriori*, into account (Sec. 2.4). It is found that the method efficiently suppresses the influence of the solar activity dependent perturbations and day-to-day variabilities in the EEJ. By making use of a superposed epoch analysis technique (Sec. 2.6.2), the relationship between the lunar tidal enhancements in EEJ and occurrence of SSWs has been investigated and composite results showing a clear enhancement of the lunar tidal power corresponding to SSWs is obtained. From the composite analysis, a threshold value of lunar tidal power is estimated which physically represents a baseline for estimating SSWs, prior to their direct observations from magnetic field recordings. On identification of historic SSWs from magnetic data, it is found that an average of approximately six

SSW events per decade also took place from 1926-1952 and that does not differ from the occurring frequency of SSWs after 1952.

The SSWs have been usually identified in literature through numerous but not so identical definitions that normally take the temperature and wind conditions of the polar stratosphere into account. Section 3.4.2 of this thesis makes use of the concept of Polar Vortex Weakening (PVW), which has been used to quantify the state of the polar vortex during SSWs. The lunar tidal enhancement in the EEJ is then compared with the intensity and timing of peak PVW days to ascertain whether the lunar tidal enhancements in EEJ are dependent or independent of the polar stratospheric wind and temperature conditions (Sec. 3.6). The strong correlation between the timing of both the peak lunar tidal enhancements and peak PVW events suggest that the commencement of the lunar tidal enhancement in most cases is closely related to a PVW event. Although the correlation values between the amplitudes of peak EEJ lunar tidal modulation and PVW intensities is slightly weaker than their respective timings, it can be inferred that the lunar tidal amplitudes in EEJ in most of the cases show a direct relation with the intensity of polar stratospheric conditions. The correlation results are consistent with the findings of other studies conducted in the MLT (Chau et al., 2015) and at ionospheric heights (Zhang and Forbes, 2014).

The lunar tidal modulation of the EEJ during SSWs shows longitudinal variability with the effects being strongest in the American sector and weakest in the Pacific (e.g., Fejer et al., 2010). In this context, a quantitative study (Sec. 4.5) of the longitudinal differences in the lunar tidal enhancement of the EEJ has been performed using satellite and ground-based measurements in the Peruvian and Indian sectors during the two major SSWs (2006 and 2009) of the last decade and a non-SSW (2007) winter. It is found that the lunar tidal enhancements in EEJ in both the sectors show a significant difference during an SSW and a non-SSW winter. Additionally, it is found that major longitudinal variabilities in lunar tidal enhancements in EEJ exist between both the Peruvian and Indian sectors during the 2009 SSW event. It is important to note that the enhancements were similar in both the sectors during the 2006 SSW event. In contrast, lunar tidal analysis at 110 km from SABER temperature data reveals nominal longitudinal difference during both the SSW and non-SSW winters. The results suggest that the longitudinal variabilities in lunar tidal amplitude in EEJ could be related to electrodynamic processes in the E-region ionosphere.

In summary, the major findings from this work are as follows:

1. Historical SSWs, prior to their direct observations have been identified from ground-based magnetometer recordings at Huancayo. It is found an average of six SSW events per decade took place between 1926-1952. This frequency is seen to be equal to the occurrence fre-

quency of SSWs that have been identified after 1952 from meteorological observations.

2. High quantitative correlation has been found between the timing and amplitude of the polar stratospheric observations and the lunitidal enhancements in the EEJ during SSWs. Together with the observations of Chau et al. (2015) in which they showed similar results for the mid-latitude mesosphere, this result demonstrates that SSW events, as an example of strong vertical coupling phenomenon, impact the global atmosphere system at all latitudes and atmospheric layers.

3. This work discusses the differences in the Peruvian and Indian equatorial ionosphere in response to SSW events and shows that the Peruvian sector is more sensitive to lunitidal variations than the Indian sector. The longitudinal variabilities in these two sectors are also different for each of the SSW events. It is suggested that the local differences in conductivity, the magnetic field and year-to-year winter atmospheric conditions could be the cause of the observed longitudinal variations. Together with the previous studies by Yamazaki et al. (2012b) and Sathishkumar and Sridharan (2013) in which they looked at the lunar modulation in EEJ through ground magnetometer recordings at African and Indian sectors, respectively, this work largely contributes to the empirical understanding of the longitudinal variability of lunitidal oscillations at low latitudes.

5.2 FUTURE WORK

Stratospheric Sudden Warmings (SSWs) offer a great example of lower and middle atmospheric processes that can significantly produce variabilities in the upper atmosphere. SSW related disturbances in the ionosphere can generate a variability comparable to moderate geomagnetic storms largely through the changes in atmospheric tides. Modeling and observational results have shown that an amplification occurs largely in both lunar and solar semi-diurnal tides at dynamo-region heights in response to SSWs (e.g., Yamazaki et al., 2012b; Pedatella and Liu, 2013). These tidal changes during SSWs influence the electric field generation leading to significant changes in the ionospheric currents such as the equatorial electrojet (EEJ). The average tidal characteristics during SSWs have so far been solely obtained from simulations without being comprehensively compared with observations. The magnetic field data provides a likely observational source to deduce the average characteristics of these waves at different locations during major and minor warmings. A detailed comparison between the model results and observations is therefore required to elucidate the complex mechanism through which the stratosphere and ionosphere are coupled. Although, considerable progress has been made in understanding

the tidal changes in the ionosphere during SSWs, there are also a number of remaining questions that still need to be addressed. A few of them have been itemized as following:

- What are the differences in lunar and solar tidal characteristics during major and minor stratospheric warmings? Yamazaki (2013) have carried out a climatological study of lunar tidal amplification in EEJ during SSWs, but the solar tidal characteristics from ground observations have not been reported so far.

- What are the factors determining the relative contributions of lunar and solar tides to the observed SSW signatures in the EEJ? Pedatella and Liu (2013) have estimated the percentage contributions of solar and lunar tides responsible for the ionospheric variability during SSWs through simulation studies. These results can be validated from observations through a climatological study of solar and lunar tides in the EEJ.

- What are the reasons behind the longitudinal variability in the ionosphere during SSWs? This question should be explored through several decades of ground-based observations that show similar longitudinal differences in the EEJ response to SSWs. In parallel, whole atmosphere simulations, such as from WACCM-X are needed to understand the sources of the observed wave activity since a careful insight into the mechanisms behind the ionospheric perturbations during SSWs is needed to explain the longitudinal differences in the ionospheric variability.

Deciphering the role played by atmospheric tides in the coupling mechanism is an important step in development of prediction capabilities for the ionosphere and thermosphere. The broader impact of these research topics would also be a greater understanding of the ionospheric effects due to vertical coupling such as those initiated during stratospheric sudden warmings. These observations will be helpful in advancing the modeling of the whole atmosphere, which would then lead to an improvement in the tools that are urgently needed to explain the connections between global atmospheric and ionospheric variability.

Part IV

BIBLIOGRAPHY

BIBLIOGRAPHY

Alken, P. and S. Maus (2007). "Spatio-temporal characterization of the equatorial electrojet from CHAMP, Ørsted, and SAC-C satellite magnetic measurements." In: *Journal of Geophysical Research: Space Physics (1978–2012)* 112.A9. DOI: 10.1029/2007JA012524 (cit. on pp. 35, 53, 76).

Andrews, D. G., J. R. Holton, and C. B. Leovy (1987). *Middle atmosphere dynamics*. 40. Academic Press (cit. on pp. 9, 16, 32, 50, 70).

Ayarzagüena, B., U. Langematz, and E. Serrano (2011). "Tropospheric forcing of the stratosphere: A comparative study of the two different major stratospheric warmings in 2009 and 2010." In: *Journal of Geophysical Research: Atmospheres* 116.D18. D18114. ISSN: 2156-2202. DOI: 10.1029/2010JD015023 (cit. on pp. 64, 88).

Baker, W. G. and D. F. Martyn (1953). "Electric currents in the ionosphere. I. The conductivity." In: *Philosophical Transactions of the Royal Society of London A: Mathematical, Physical and Engineering Sciences* 246.913, pp. 281–294. DOI: 10.1098/rsta.1953.0016 (cit. on p. 17).

Baldwin, M. P. and T. J. Dunkerton (2001). "Stratospheric harbingers of anomalous weather regimes." In: *Science* 294.5542, pp. 581–584. DOI: 10.1126/science.1063315 (cit. on p. 50).

Bartels, J. (1936). *Aufschlüsse über die Ionosphäre aus der Analyse sonnen-und mondtätiger erdmagnetischer Schwankungen* (cit. on p. 71).

Bartels, J. and H. F. Johnston (1940). "Geomagnetic tides in horizontal intensity at Huancayo." In: *Terrestrial Magnetism and Atmospheric Electricity* 45.3, pp. 269–308. DOI: 10.1029/TE045i003p00269 (cit. on pp. 16, 21, 32, 38, 50, 71, 75).

Beynon, W. J. G. and G. M. Brown (1951). "Geophysical and meteorological changes in the period January–April 1949." In: *Nature* 167.4260, pp. 1012–1014. DOI: 10.1038/1671012a0 (cit. on p. 9).

Butler, A. H. and L. M. Polvani (2011). "El Niño, La Niña, and stratospheric sudden warmings: A reevaluation in light of the observational record." In: *Geophysical Research Letters* 38.13. DOI: 10.1029/2011GL048084 (cit. on p. 64).

Butler, A. H., D. J. Seidel, S. C. Hardiman, N. Butchart, T. Birner, and A. Match (2015). "Defining sudden stratospheric warmings." In: *Bulletin of the American Meteorological Society* 2015. DOI: 10.1175/BAMS-D-13-00173.1 (cit. on p. 50).

Cain, J. C. and R. E. Sweeney (1973). "The POGO data." In: *Journal of Atmospheric and Terrestrial Physics* 35.6, pp. 1231–1247. DOI: 10.1016/0021-9169(73)90021-4 (cit. on p. 17).

Canziani, P. O. (1994). "On tidal variability and the existence of planetary wave-like oscillations in the upper thermosphere–I. Observations of tidal variability." In: *Journal of Atmospheric and Terrestrial Physics* 56.8, pp. 901–912. DOI: 10.1016/0021-9169(94)90153-8 (cit. on p. 9).

Chapman, S. (1919). "The solar and lunar diurnal variations of terrestrial magnetism." In: *Philosophical Transactions of the Royal Society of London. Series A, Containing Papers of a Mathematical or Physical Character* 218, pp. 1–118. DOI: 10.1098/rsta.1919.0001 (cit. on pp. 19, 20).

Chapman, S. (1948). "The abnormal daily variation of horizontal force at Huancayo and in Uganda." In: *Terrestrial Magnetism and Atmospheric Electricity* 53.3, pp. 247–250. DOI: 10.1029/TE053i003p00247 (cit. on p. 16).

— (1951). "The equatorial electrojet as detected from the abnormal electric current distribution above Huancayo, Peru, and elsewhere." In: *Meteorology and Atmospheric Physics* 4.1, pp. 368–390. DOI: 10.1007/BF02246814 (cit. on p. 17).

Chapman, S. and J. Bartels (1940). *Geomagnetism*. Vol. 1. Clarendon Press Oxford (cit. on p. 20).

Chapman, S. and R. S. Lindzen (1970). "Atmospheric Tides: Thermal and Gravitational." In: *D. Reidel, Norwell, Mass* (cit. on pp. 8, 19).

Chapman, S. and K. S. R. Rao (1965). "The H and Z variations along and near the equatorial electrojet in India, Africa and the Pacific." In: *Journal of Atmospheric and Terrestrial Physics* 27.4, pp. 559–581. DOI: 10.1016/0021-9169(65)90020-6 (cit. on p. 21).

Chapman, S. and K. C. Westfold (1956). "A comparison of the annual mean solar and lunar atmospheric tides in barometric pressure, as regards their worldwide distribution of amplitude and phase." In: *Journal of Atmospheric and Terrestrial Physics* 8.1-2, pp. 1–23. DOI: 10.1016/0021-9169(56)90087-3 (cit. on p. 19).

Charlton, A. J. and L. M. Polvani (2007). "A new look at stratospheric sudden warmings. Part I: Climatology and modeling benchmarks." In: *Journal of Climate* 20.3, pp. 449–469. DOI: 10.1175/JCLI3996.1 (cit. on pp. 16, 43, 50).

Chau, J. L., B. G. Fejer, and L. P. Goncharenko (2009). "Quiet variability of equatorial E x B drifts during a sudden stratospheric warming event." In: *Geophysical Research Letters* 36.5. DOI: 10.1029/2008GL036785 (cit. on pp. 12, 70).

Chau, J. L., N. A. Aponte, E. Cabassa, M. P. Sulzer, L. P. Goncharenko, and S. A. González (2010). "Quiet time ionospheric variability over Arecibo during sudden stratospheric warming events." In: *Journal of Geophysical Research: Space Physics* 115.A9. A00G06, n/a–n/a. ISSN: 2156-2202. DOI: 10.1029/2010JA015378 (cit. on p. 70).

Chau, J. L., L. P. Goncharenko, B. G. Fejer, and H.-L. Liu (2012). "Equatorial and low latitude ionospheric effects during sudden stratospheric

warming events." In: *Space Science Reviews* 168.1-4, pp. 385–417. DOI: 10.1007/s11214-011-9797-5 (cit. on pp. 11, 12, 32, 65, 71, 92).

Chau, J. L., P. Hoffmann, N. M. Pedatella, V. Matthias, and G. Stober (2015). "Upper mesospheric lunar tides over middle and high latitudes during sudden stratospheric warming events." In: *Journal of Geophysical Research: Space Physics*. 2015JA020998. ISSN: 2169-9402. DOI: 10.1002/2015JA020998 (cit. on pp. 51, 54, 59–62, 66, 67, 77, 98, 99).

Cho, Y.-M., G. G. Shepherd, Y.-I. Won, S. Sargoytchev, S. Brown, and B. Solheim (2004). "MLT cooling during stratospheric warming events." In: *Geophysical Research Letters* 31.10. L10104, n/a–n/a. ISSN: 1944-8007. DOI: 10.1029/2004GL019552 (cit. on p. 70).

Cowling, T. G. (1932). "Magnetism, solar: The electrical conductivity of an ionised gas in the presence of a magnetic field." In: *Monthly Notices of the Royal Astronomical Society* 93, p. 90. DOI: 10.1093/mnras/93.1.90 (cit. on p. 18).

Coy, L. and S. Pawson (2015). "The major stratospheric sudden warming of January 2013: analyses and forecasts in the GEOS-5 data assimilation system." In: *Monthly Weather Review* 143.2, pp. 491–510. DOI: 10.1175/MWR-D-14-00023.1 (cit. on p. 65).

Doumouya, V., J. Vassal, Y. Cohen, O. Fambitakoye, and M. Menvielle (1998). "Equatorial electrojet at African longitudes: first results from magnetic measurements." In: *Annales Geophysicae*. Vol. 16. 6. Springer, pp. 658–676. DOI: 10.1007/s00585-998-0658-9 (cit. on p. 71).

Egedal, J. (1947). "The magnetic diurnal variation of the horizontal force near the magnetic equator." In: *Terrestrial Magnetism and Atmospheric Electricity* 52.4, pp. 449–451. DOI: 10.1029/TE052i004p00449 (cit. on p. 17).

— (1956). *On the computation of lunar daily variations in geomagnetism: two simple methods*. Det danske Meteorologiske Institut (cit. on p. 32).

Elhawary, R. and J. M. Forbes (2016). "Planetary wave variability of Sq currents." In: *Journal of Geophysical Research: Space Physics*. DOI: 10.1002/2016JA023242 (cit. on p. 10).

Fang, T.-W., T. Fuller-Rowell, R. Akmaev, F. Wu, H. Wang, and D. Anderson (2012). "Longitudinal variation of ionospheric vertical drifts during the 2009 sudden stratospheric warming." In: *Journal of Geophysical Research: Space Physics* 117.A3. A03324, n/a–n/a. ISSN: 2156-2202. DOI: 10.1029/2011JA017348 (cit. on p. 70).

Fejer, B. G., M. E. Olson, J. L. Chau, C. Stolle, H. Lühr, L. P. Goncharenko, K. Yumoto, and T. Nagatsuma (2010). "Lunar-dependent equatorial ionospheric electrodynamic effects during sudden stratospheric warmings." In: *Journal of Geophysical Research: Space Physics (1978–2012)* 115.A8. DOI: 10.1029/2010JA015273 (cit. on pp. 12, 21–23, 25, 32, 70, 79, 80, 98).

Fejer, B. G., B. D. Tracy, M. E. Olson, and J. L. Chau (2011). "Enhanced lunar semidiurnal equatorial vertical plasma drifts during sudden strato-

spheric warmings." In: *Geophysical Research Letters* 38.21. DOI: 10.1029/2011GL049788 (cit. on p. 32).

Fesen, C. G. (1997). "Theoretical effects of tides and auroral activity on the low latitude ionosphere." In: *Journal of Atmospheric and Solar-Terrestrial Physics* 59.13, pp. 1521–1532. DOI: 10.1016/S1364-6826(96)00153-8 (cit. on p. 9).

Forbes, J. M. (1981). "The equatorial electrojet." In: *Reviews of Geophysics* 19.3, pp. 469–504. DOI: 10.1029/RG019i003p00469 (cit. on pp. 17, 71).

Forbes, J. M. (1982). "Atmospheric tide: 2. The solar and lunar semidiurnal components." In: *Journal of Geophysical Research: Space Physics* 87.A7, pp. 5241–5252. DOI: 10.1029/JA087iA07p05241 (cit. on p. 20).

— (1995). "Tidal and planetary waves." In: *The Upper Mesosphere and Lower Thermosphere: A Review of Experiment and Theory*, pp. 67–87. DOI: 10.1029/GM087p0067 (cit. on p. 7).

— (2007). "Dynamics of the thermosphere." In: *Journal of the Meteorological Society of Japan. Ser. II* 85, pp. 193–213 (cit. on p. 10).

Forbes, J. M. and X. Zhang (2012). "Lunar tide amplification during the January 2009 stratosphere warming event: Observations and theory." In: *Journal of Geophysical Research: Space Physics (1978–2012)* 117.A12. DOI: 10.1029/2012JA017963 (cit. on pp. 13, 22, 24, 46, 50, 75, 77, 92).

Forbes, J. M., S. E. Palo, and X. Zhang (2000). "Variability of the ionosphere." In: *Journal of Atmospheric and Solar-Terrestrial Physics* 62.8, pp. 685–693. DOI: 10.1016/S1364-6826(00)00029-8 (cit. on p. 8).

Forbush, S. E. and M. Casaverde (1961). *Equatorial electrojet in Peru*. 620. Carnegie Institution of Washington (cit. on pp. 21, 71).

Fuller-Rowell, T., F. Wu, R. Akmaev, T.-W. Fang, and E. Araujo-Pradere (2010). "A whole atmosphere model simulation of the impact of a sudden stratospheric warming on thermosphere dynamics and electrodynamics." In: *Journal of Geophysical Research: Space Physics* 115.A10. DOI: 10.1029/2010JA015524 (cit. on p. 13).

Fuller-Rowell, T., H. Wang, R. Akmaev, F. Wu, T.-W. Fang, M. Iredell, and A. Richmond (2011). "Forecasting the dynamic and electrodynamic response to the January 2009 sudden stratospheric warming." In: *Geophysical Research Letters* 38.13. DOI: 10.1029/2011GL047732 (cit. on pp. 12, 13).

Funke, B., M. López-Puertas, D. Bermejo-Pantaleón, M. García-Comas, G. P. Stiller, T. von Clarmann, M. Kiefer, and A. Linden (2010). "Evidence for dynamical coupling from the lower atmosphere to the thermosphere during a major stratospheric warming." In: *Geophysical Research Letters* 37.13. L13803, n/a–n/a. ISSN: 1944-8007. DOI: 10.1029/2010GL043619 (cit. on p. 70).

Goncharenko, L. P. and S.-R. Zhang (2008). "Ionospheric signatures of sudden stratospheric warming: Ion temperature at middle latitude."

In: *Geophysical Research Letters* 35.21. L21103, n/a–n/a. ISSN: 1944-8007. DOI: 10.1029/2008GL035684 (cit. on pp. 12, 70).

Goncharenko, L. P., A. J. Coster, J. L. Chau, and C. E. Valladares (2010a). "Impact of sudden stratospheric warmings on equatorial ionization anomaly." In: *Journal of Geophysical Research: Space Physics* 115.A10. DOI: 10.1029/2010JA015400 (cit. on pp. 12, 14, 15, 70).

Goncharenko, L. P., J. L. Chau, H.-L. Liu, and A. J. Coster (2010b). "Unexpected connections between the stratosphere and ionosphere." In: *Geophysical Research Letters* 37.10. DOI: 10.1029/2010GL043125 (cit. on p. 12).

Goncharenko, L. P., A. J. Coster, R. A. Plumb, and D. I. V. Domeisen (2012). "The potential role of stratospheric ozone in the stratosphere-ionosphere coupling during stratospheric warmings." In: *Geophysical Research Letters* 39.8. DOI: 10.1029/2012GL051261 (cit. on p. 13).

Gouin, P. (1960). "Preliminary determination of the lunar diurnal influence on the geomagnetic components H, D, and Z at Addis Ababa." In: *Bull. Geophys. Obs., Univ. Coll. Addis Ababa* 2, pp. 1–8 (cit. on p. 32).

Haldoupis, C., D. Pancheva, and N. J. Mitchell (2004). "A study of tidal and planetary wave periodicities present in midlatitude sporadic E layers." In: *Journal of Geophysical Research: Space Physics* 109.A2. DOI: 10.1029/2003JA010253 (cit. on p. 9).

Hocke, K. (1996). "Tidal variations in the high-latitude E-and F-region observed by EISCAT." In: *Annales Geophysicae*. Vol. 14. 2. Springer, pp. 201–210. DOI: 10.1007/s00585-996-0201-9 (cit. on p. 9).

Hollingsworth, A. (1971). "The effect of ocean and Earth tides on the semi-diurnal lunar air tide." In: *Journal of the Atmospheric Sciences* 28.6, pp. 1021–1044. DOI: 10.1175/1520-0469(1971)028%3C1021:TEOOAE%3E2.0.CO;2 (cit. on p. 19).

Holton, J. R. and G. J. Hakim (2012). *An Introduction to Dynamic Meteorology*. Vol. 88. Academic Press (cit. on p. 9).

Holton, J. R. and H.-C. Tan (1980). "The influence of the equatorial quasi-biennial oscillation on the global circulation at 50 mb." In: *Journal of the Atmospheric Sciences* 37.10, pp. 2200–2208. DOI: 10.1175/1520-0469(1980)037%3C2200:TIOTEQ%3E2.0.CO;2 (cit. on p. 63).

Holton, J. R., P. H. Haynes, M. E. McIntyre, A. R. Douglass, R. B. Rood, and L. Pfister (1995). "Stratosphere-troposphere exchange." In: *Reviews of Geophysics* 33.4, pp. 403–439. ISSN: 1944-9208. DOI: 10.1029/95RG02097 (cit. on p. 16).

Hung, R. J. and R. E. Smith (1979). "Dynamics of severe storms through the study of thermospheric-tropospheric coupling." In: *Journal of Geomagnetism and Geoelectricity* 31.3, pp. 183–194. DOI: 10.5636/jgg.31.183 (cit. on p. 9).

Jadhav, G., M. Rajaram, and R. Rajaram (2002). "A detailed study of equatorial electrojet phenomenon using Ørsted satellite observations." In:

Journal of Geophysical Research: Space Physics 107.A8. DOI: 10.1029/2001JA000183 (cit. on pp. 17, 71).

Jin, H., Y. Miyoshi, D. Pancheva, P. Mukhtarov, H. Fujiwara, and H. Shinagawa (2012). "Response of migrating tides to the stratospheric sudden warming in 2009 and their effects on the ionosphere studied by a whole atmosphere-ionosphere model GAIA with COSMIC and TIMED/SABER observations." In: *Journal of Geophysical Research: Space Physics* 117.A10. DOI: 10.1029/2012JA017650 (cit. on p. 13).

Johnson, C. Y. (1966). "Ionospheric composition and density from 90 to 1200 kilometers at solar minimum." In: *Journal of Geophysical Research* 71.1, pp. 330–332. ISSN: 2156-2202. DOI: 10.1029/JZ071i001p00330 (cit. on p. 5).

Kalnay, E., M. Kanamitsu, R. Kistler, W. Collins, D. Deaven, L. Gandin, M. Iredell, S. Saha, G. White, J. Woollen, et al. (1996). "The NCEP/NCAR 40-year reanalysis project." In: *Bulletin of the American meteorological Society* 77.3, pp. 437–471. DOI: 10.1175/1520-0477(1996)077%3C0437:TNYRP%3E2.0.CO;2 (cit. on p. 34).

Kazimirovsky, E., M. Herraiz, and B. A. De la Morena (2003). "Effects on the ionosphere due to phenomena occurring below it." In: *Surveys in Geophysics* 24.2, pp. 139–184. DOI: 10.1023/A:1023206426746 (cit. on pp. 8, 10).

Kivelson, M. G. and C. T. Russell (1995). *Introduction to Space Physics*. Cambridge University Press (cit. on p. 4).

Kohsiek, A., K. H. Glassmeier, and T. Hirooka (1995). "Periods of planetary waves in geomagnetic variations." In: *Annales Geophysicae* 13.2, pp. 168–176. DOI: 10.1007/s00585-995-0168-y (cit. on p. 10).

Labitzke, K. (1972). "Temperature changes in the mesosphere and stratosphere connected with circulation changes in winter." In: *Journal of the Atmospheric Sciences* 29.4, pp. 756–766. DOI: 10.1175/1520-0469(1972)029<0756:TCITMA>2.0.CO;2 (cit. on p. 70).

— (2005). "On the solar cycle–QBO relationship: a summary." In: *Journal of Atmospheric and Solar-Terrestrial Physics* 67.1, pp. 45–54. DOI: 10.1016/j.jastp.2004.07.016 (cit. on p. 64).

Labitzke, K. and M. Kunze (2009). "On the remarkable Arctic winter in 2008/2009." In: *Journal of Geophysical Research: Atmospheres (1984–2012)* 114.D1. DOI: 10.1029/2009JD012273 (cit. on p. 64).

Labitzke, K. and H. Van Loon (1988). "Associations between the 11-year solar cycle, the QBO and the atmosphere. Part I: the troposphere and stratosphere in the northern hemisphere in winter." In: *Journal of Atmospheric and Terrestrial Physics* 50.3, pp. 197–206. DOI: 10.1016/0021-9169(88)90068-2 (cit. on p. 63).

Laštovička, J. (2006). "Forcing of the ionosphere by waves from below." In: *Journal of Atmospheric and Solar-Terrestrial Physics* 68.3, pp. 479–497. DOI: 10.1016/j.jastp.2005.01.018 (cit. on p. 10).

— (2009). "Lower ionosphere response to external forcing: A brief review." In: *Advances in Space Research* 43.1, pp. 1–14. DOI: 10.1016/j.asr.2008.10.001 (cit. on p. 10).

Limpasuvan, V., D. W. J. Thompson, and D. L. Hartmann (2004). "The life cycle of the Northern Hemisphere sudden stratospheric warmings." In: *Journal of Climate* 17.13, pp. 2584–2596. DOI: 10.1175/1520-0442(2004)017%3C2584:TLCOTN%3E2.0.CO;2 (cit. on p. 50).

Liu, H.-L. and R. G. Roble (2002). "A study of a self-generated stratospheric sudden warming and its mesospheric–lower thermospheric impacts using the coupled TIME-GCM/CCM3." In: *Journal of Geophysical Research: Atmospheres* 107.D23. 4695, ACL 15–1–ACL 15–18. ISSN: 2156-2202. DOI: 10.1029/2001JD001533 (cit. on p. 70).

Liu, H.-L., W. Wang, A. D. Richmond, and R. G. Roble (2010). "Ionospheric variability due to planetary waves and tides for solar minimum conditions." In: *Journal of Geophysical Research: Space Physics* 115.A6. DOI: 10.1029/2009JA015188 (cit. on pp. 12, 13).

Lühr, H., S. Maus, and M. Rother (2004). "Noon-time equatorial electrojet: Its spatial features as determined by the CHAMP satellite." In: *Journal of Geophysical Research: Space Physics* 109.A1. DOI: 10.1029/2002JA009656 (cit. on pp. 17, 71, 74).

Lühr, H., M. Rother, K. Häusler, P. Alken, and S. Maus (2008). "The influence of nonmigrating tides on the longitudinal variation of the equatorial electrojet." In: *Journal of Geophysical Research: Space Physics (1978–2012)* 113.A8. DOI: 10.1029/2008JA013064 (cit. on pp. 37, 54, 75).

Lühr, H., T. A. Siddiqui, and S. Maus (2012). "Global characteristics of the lunar tidal modulation of the equatorial electrojet derived from CHAMP observations." In: *Annales Geophysicae* 30.3, pp. 527–536. DOI: 10.5194/angeo-30-527-2012 (cit. on pp. 32, 36, 37, 50, 54, 74, 85, 86).

Maeda, H. and M. Fujiwara (1967). "Lunar ionospheric winds deduced from the dynamo theory of geomagnetic variations." In: *Journal of Atmospheric and Terrestrial Physics* 29.8, pp. 917–936. DOI: 10.1016/0021-9169(67)90241-3 (cit. on p. 21).

Maeda, K. and V. L. Badillo (1966). "Equatorial spread-F and tropospheric tropical disturbances." In: *Journal of the Atmospheric Sciences* 23.6, pp. 812–815. DOI: 10.1175/1520-0469(1966)023%3C0812:ESFATT%3E2.0.CO;2 (cit. on p. 9).

Manney, G. L., M. J. Schwartz, K. Krüger, M. L. Santee, S. Pawson, J. N. Lee, W. H. Daffer, R. A. Fuller, and N. J. Livesey (2009). "Aura Microwave Limb Sounder observations of dynamics and transport during the record-breaking 2009 Arctic stratospheric major warming." In: *Geophysical Research Letters* 36.12. L12815, n/a–n/a. ISSN: 1944-8007. DOI: 10.1029/2009GL038586 (cit. on pp. 79, 88).

Manoj, C., H. Lühr, S. Maus, and N. Nagarajan (2006). "Evidence for short spatial correlation lengths of the noontime equatorial electrojet

inferred from a comparison of satellite and ground magnetic data." In: *Journal of Geophysical Research: Space Physics (1978–2012)* 111.A11. DOI: 10.1029/2006JA011855 (cit. on pp. 33, 35, 52, 73).

Martineau, P. and S.-W. Son (2013). "Planetary-scale wave activity as a source of varying tropospheric response to stratospheric sudden warming events: A case study." In: *Journal of Geophysical Research: Atmospheres*. ISSN: 2169897X. DOI: 10.1002/jgrd.50871 (cit. on p. 50).

Martyn, D. F. (1952). "Troposphere-ionosphere relationships." In: *Geophys. Res. Papers, USA* 12, pp. 31–33 (cit. on p. 9).

Matsuno, T. (1971). "A dynamical model of the stratospheric sudden warming." In: *Journal of the Atmospheric Sciences* 28.8, pp. 1479–1494. DOI: 10.1175/1520-0469(1971)028%3C1479:ADMOTS%3E2.0.CO;2 (cit. on pp. 16, 32, 50, 70).

Matsushita, S. and H. Maeda (1965). "On the geomagnetic lunar daily variation field." In: *Journal of Geophysical Research* 70, pp. 2559–2578. DOI: 10.1029/JZ070i011p02559 (cit. on p. 20).

Maute, A., M. E. Hagan, V. Yudin, H.-L. Liu, and E. Yizengaw (2015). "Causes of the longitudinal differences in the equatorial vertical E × B drift during the 2013 SSW period as simulated by the TIME-GCM." In: *Journal of Geophysical Research: Space Physics* 120.6. 2015JA021126, pp. 5117–5136. ISSN: 2169-9402. DOI: 10.1002/2015JA021126 (cit. on pp. 92, 93).

Mechtly, E. A. and L. G. Smith (1970). "Changes of lower ionosphere electron densities with solar zenith angle." In: *Radio Science* 5.12, pp. 1407–1412. DOI: 10.1029/RS005i012p01407 (cit. on p. 10).

Meyer, C. K. (1999). "Gravity wave interactions with mesospheric planetary waves: A mechanism for penetration into the thermosphere - ionosphere system." In: *Journal of Geophysical Research: Space Physics* 104.A12, pp. 28181–28196. DOI: 10.1029/1999JA900346 (cit. on p. 10).

Monro, P. E., J. S. Nisbet, and T. L. Stick (1976). "Effects of tidal oscillations in the neutral atmosphere on electron densities in the E-region." In: *Journal of Atmospheric and Terrestrial Physics* 38.5, pp. 523–528. DOI: 10.1016/0021-9169(76)90010-6 (cit. on p. 9).

Newman, P. A., E. R. Nash, and J. E. Rosenfield (2001). "What controls the temperature of the Arctic stratosphere during the spring?" In: *Journal of Geophysical Research* 106.D17, pp. 19999–20010. DOI: 10.1029/2000JD000061 (cit. on p. 64).

Newton, I. (1687). "Philosophiæ naturalis principia mathematica (Mathematical principles of natural philosophy)." In: *London (1687)* (cit. on p. 19).

Oliver, W. L., Y. Otsuka, M. Sato, T. Takami, and S. Fukao (1997). "A climatology of F region gravity wave propagation over the middle and upper atmosphere radar." In: *Journal of Geophysical Research: Space Physics* 102.A7, pp. 14499–14512. DOI: 10.1029/97JA00491 (cit. on p. 10).

Onwumechilli, C. A. (1960). "Lunar daily variation of the magnetic declination at Ibadan, Nigeria." In: *Journal of Geophysical Research* 65.10, pp. 3433–3435. DOI: 10.1029/JZ065i010p03433 (cit. on p. 32).

— (1963). "Lunar effect on the diurnal variation of the geomagnetic horizontal field near the magnetic equator." In: *Journal of Atmospheric and Terrestrial Physics* 25.2, pp. 55 –70. ISSN: 0021-9169. DOI: 10.1016/0021-9169(63)90115-6 (cit. on p. 74).

Onwumechilli, C. A. (1967). "Geomagnetic Variations in the Equatorial Zone." In: *Physics of Geomagnetic Phenomena*. Ed. by S. Matsushita and W. H. Campbell, p. 426 (cit. on pp. 16, 18).

Onwumechilli, C. A. (1998). *Equatorial Electrojet*. CRC Press (cit. on p. 17).

Onwumechilli, C. A. and Alexander N. S. (1959). "Variations in the geomagnetic field at Ibadan, Nigeria—II Lunar and luni-solar variations in H and Z." In: *Journal of Atmospheric and Terrestrial Physics* 16.1, pp. 115 –123. ISSN: 0021-9169. DOI: 10.1016/0021-9169(59)90014-5 (cit. on p. 71).

Pancheva, D. and P. Mukhtarov (2011). "Stratospheric warmings: The atmosphere - ionosphere coupling paradigm." In: *Journal of Atmospheric and Solar-Terrestrial Physics* 73.13, pp. 1697–1702. DOI: 10.1016/j.jastp.2011.03.006 (cit. on p. 12).

Pancheva, D., L. F. Alberca, and B. A. De la Morena (1994). "Simultaneous observation of the quasi-two-day variations in the lower and upper ionosphere over Europe." In: *Journal of Atmospheric and Terrestrial Physics* 56.1, pp. 43–50. DOI: 10.1016/0021-9169(94)90174-0 (cit. on p. 10).

Pancheva, D., N. Mitchell, R. R. Clark, J. Drobjeva, and J. Lastovicka (2002). "Variability in the maximum height of the ionospheric F2-layer over Millstone Hill (September 1998–March 2000); influence from below and above." In: *Annales Geophysicae*. Vol. 20. 11, pp. 1807–1819. DOI: 10.5194/angeo-20-1807-2002 (cit. on p. 10).

Pancheva, D., C. Haldoupis, C. E. Meek, A. H. Manson, and N. J. Mitchell (2003). "Evidence of a role for modulated atmospheric tides in the dependence of sporadic E layers on planetary waves." In: *Journal of Geophysical Research: Space Physics* 108.A5. DOI: 10.1029/2002JA009788 (cit. on p. 10).

Parish, H. F., J. M. Forbes, and F. Kamalabadi (1994). "Planetary wave and solar emission signatures in the equatorial electrojet." In: *Journal of Geophysical Research: Space Physics* 99.A1, pp. 355–368. DOI: 10.1029/93JA02096 (cit. on p. 10).

Park, J., H. Lühr, M. Kunze, B. G. Fejer, and K. W. Min (2012). "Effect of sudden stratospheric warming on lunar tidal modulation of the equatorial electrojet." In: *Journal of Geophysical Research: Space Physics (1978–2012)* 117.A3. DOI: 10.1029/2011JA017351 (cit. on pp. 12, 22, 24, 25, 32, 37, 43, 50, 71, 76).

Paulino, A. R., P. P. Batista, and I. S. Batista (2013). "A global view of the atmospheric lunar semidiurnal tide." In: *Journal of Geophysical Research: Atmospheres* 118.23. DOI: 10.1002/2013JD019818 (cit. on p. 20).

Pedatella, N. M. and J. M. Forbes (2010). "Evidence for stratosphere sudden warming-ionosphere coupling due to vertically propagating tides." In: *Geophysical Research Letters* 37.11. DOI: 10.1029/2010GL043560 (cit. on p. 12).

Pedatella, N. M. and H.-L. Liu (2013). "The influence of atmospheric tide and planetary wave variability during sudden stratosphere warmings on the low latitude ionosphere." In: *Journal of Geophysical Research: Space Physics* 118.8, pp. 5333–5347. ISSN: 2169-9402. DOI: 10.1002/jgra.50492 (cit. on pp. 13, 24, 92, 99, 100).

Pedatella, N. M., H.-L. Liu, A. D. Richmond, A. Maute, and T.-W. Fang (2012). "Simulations of solar and lunar tidal variability in the mesosphere and lower thermosphere during sudden stratosphere warmings and their influence on the low-latitude ionosphere." In: *Journal of Geophysical Research: Space Physics (1978–2012)* 117.A8. DOI: 10.1029/2012JA017858 (cit. on pp. 13, 24, 92).

Polvani, L. M. and D. W. Waugh (2004). "Upward wave activity flux as a precursor to extreme stratospheric events and subsequent anomalous surface weather regimes." In: *Journal of Climate* 17.18, pp. 3548–3554. DOI: 10.1175/1520-0442(2004)017%3C3548:UWAFAA%3E2.0.CO;2 (cit. on p. 64).

Raju, D. G., M. S. Rao, B. M. Rao, C. Jogulu, C. P. Rao, and R. Ramanadham (1981). "Infrasonic oscillations in the F 2 region associated with severe thunderstorms." In: *Journal of Geophysical Research: Space Physics* 86.A7, pp. 5873–5880. DOI: 10.1029/JA086iA07p05873 (cit. on p. 9).

Rao, K. S. R. and K. R. Sivaraman (1958). "Lunar geomagnetic tides at Kodaikanal." In: *Journal of Geophysical Research* 63.4, pp. 727–730. ISSN: 2156-2202. DOI: 10.1029/JZ063i004p00727 (cit. on p. 71).

Rastogi, R. G. (1962a). "Enhancement of the lunar tide in the noon critical frequency of the F2 layer over the magnetic equator." In: *J. Res.(NBS) D* 66, pp. 601–606 (cit. on p. 72).

— (1963). "Lunar tidal variations in the equatorial electrojet current." In: *Journal of Geophysical Research* 68.9, pp. 2445–2451. ISSN: 2156-2202. DOI: 10.1029/JZ068i009p02445 (cit. on p. 71).

Rastogi, R. G. and N. B. Trivedi (1970). "Luni-solar tides in H at stations within the equatorial electrojet." In: *Planetary and Space Science* 18.3, pp. 367–377. DOI: 10.1016/0032-0633(70)90174-1 (cit. on pp. 21, 32, 71).

Rastogi, R.G. (1962b). "Longitudinal variation in the equatorial electrojet." In: *Journal of Atmospheric and Terrestrial Physics* 24.12, pp. 1031 –1040. ISSN: 0021-9169. DOI: 10.1016/0021-9169(62)90158-7 (cit. on p. 72).

Richards, P. G. and David Voglozin (2011). "Reexamination of ionospheric photochemistry." In: *Journal of Geophysical Research: Space Physics* 116.A8. A08307, n/a–n/a. ISSN: 2156-2202. DOI: 10.1029/2011JA016613. URL: http://dx.doi.org/10.1029/2011JA016613 (cit. on pp. 4, 5).

Richards, P. G., J. A. Fennelly, and D. G. Torr (1994). "EUVAC: A solar EUV flux model for aeronomic calculations." In: *Journal of Geophysical Research: Space Physics (1978–2012)* 99.A5, pp. 8981–8992. DOI: 10.1029/94JA00518 (cit. on p. 35).

Rigoti, A., F. H. Chamalaun, N. B. Trivedi, and A. L. Padilha (1999). "Characteristics of the Equatorial Electrojet determined from an array of magnetometers in N-NE Brazil." In: *Earth, Planets and Space* 51.2, pp. 115–128. ISSN: 1880-5981. DOI: 10.1186/BF03352216 (cit. on p. 71).

Rishbeth, H. and M. Mendillo (2001). "Patterns of F2-layer variability." In: *Journal of Atmospheric and Solar-Terrestrial Physics* 63.15, pp. 1661–1680. DOI: 10.1016/S1364-6826(01)00036-0 (cit. on p. 8).

Sabaka, T. J., N. Olsen, and M. E. Purucker (2004). "Extending comprehensive models of the Earth's magnetic field with Ørsted and CHAMP data." In: *Geophysical Journal International* 159.2, pp. 521–547. DOI: 10.1111/j.1365-246X.2004.02421.x (cit. on p. 53).

Sabine, E. (1847). "On the lunar atmospheric tide at St. Helena." In: *Philosophical Transactions of the Royal Society of London* 137, pp. 45–50. DOI: 10.1098/rstl.1847.0005 (cit. on p. 19).

Sandford, D. J., H. G. Muller, and N. J. Mitchell (2006). "Observations of lunar tides in the mesosphere and lower thermosphere at Arctic and middle latitudes." In: *Atmospheric Chemistry and Physics* 6.12, pp. 4117–4127. DOI: 10.5194/acp-6-4117-2006 (cit. on p. 20).

Sathishkumar, S. and S. Sridharan (2013). "Lunar and solar tidal variabilities in mesospheric winds and EEJ strength over Tirunelveli (8.7°N, 77.8°E) during the 2009 major stratospheric warming." In: *Journal of Geophysical Research: Space Physics* 118.1, pp. 533–541. ISSN: 2169-9402. DOI: 10.1029/2012JA018236 (cit. on pp. 25, 91, 92, 99).

Scherhag, R. (1952). "Die explosionsartigen Stratosphärenerwärmungen des Spätwinters 1951/52." In: *Berichte des deutschen Wetterdienstes in der US-Zone* 6.38, pp. 51–63 (cit. on pp. 14, 32, 50, 70).

Schödel, J. P., J. Klostermeyer, J. Roettger, and G. Stielke (1973). "Evidence for tropospheric-ionospheric coupling by atmospheric gravity waves." In: *Zeitschr. Geophys.* 39, pp. 1063–1066 (cit. on p. 9).

Shapley, A. H. and W. J. G. Beynon (1965). "'Winter Anomaly' in Ionospheric Absorption and Stratospheric Warmings." In: *Nature* 206.4990, pp. 1242–1243. DOI: 10.1038/2061242a0 (cit. on p. 11).

Siddiqui, T. A., C. Stolle, H. Lühr, and J. Matzka (2015a). "On the relationship between weakening of the northern polar vortex and the lunar tidal amplification in the equatorial electrojet." In: *Journal of Geophysi-*

cal Research: Space Physics 120.11. 2015JA021683, pp. 10006–10019. ISSN: 2169-9402. DOI: 10.1002/2015JA021683 (cit. on pp. 72, 73, 75, 77, 81).

Siddiqui, T. A., H. Lühr, C. Stolle, and J. Park (2015b). "Relation between stratospheric sudden warming and the lunar effect on the equatorial electrojet based on Huancayo recordings." In: *Annales Geophysicae* 33.2, pp. 235–243. DOI: 10.5194/angeo-33-235-2015 (cit. on pp. 50, 52, 54, 57, 71, 72, 86).

Sridharan, S., S. Sathishkumar, and S. Gurubaran (2009). "Variabilities of mesospheric tides and equatorial electrojet strength during major stratospheric warming events." In: *Annales Geophysicae*. Vol. 27. 11. Copernicus GmbH, pp. 4125–4130. DOI: 10.5194/angeo-27-4125-2009 (cit. on p. 22).

Stening, R. J. (1995). "What drives the equatorial electrojet?" In: *Journal of Atmospheric and Terrestrial Physics* 57.10, pp. 1117–1128. DOI: 10.1016/0021-9169(94)00127-A (cit. on p. 32).

— (2011). "Lunar tide in the equatorial electrojet in relation to stratospheric warmings." In: *Journal of Geophysical Research: Space Physics (1978–2012)* 116.A12. DOI: 10.1029/2011JA017047 (cit. on pp. 32, 50, 57).

Stening, R. J. and R. A. Vincent (1989). "A measurement of lunar tides in the mesosphere at Adelaide, South Australia." In: *Journal of Geophysical Research: Space Physics* 94.A8, pp. 10121–10129. DOI: 10.1029/JA094iA08p10121 (cit. on p. 20).

Stening, R. J., C. E. Meek, and A. H. Manson (1987). "Lunar tidal winds measured in the upper atmosphere (78–105 km) at Saskatoon, Canada." In: *Journal of the Atmospheric Sciences* 44.8, pp. 1143–1151. DOI: 10.1175/1520-0469(1987)044%3C1143:LTWMIT%3E2.0.CO;2 (cit. on p. 20).

— (1996). "Upper atmosphere wind systems during reverse equatorial electrojet events." In: *Geophysical Research Letters* 23.22, pp. 3243–3246. DOI: 10.1029/96GL02611 (cit. on p. 22).

Stening, R. J., J. M. Forbes, M. E. Hagan, and A. D. Richmond (1997). "Experiments with a lunar atmospheric tidal model." In: *Journal of Geophysical Research* 102, pp. 13–465. DOI: 10.1029/97JD00778 (cit. on pp. 20, 22).

Stening, R. J., C. Carmody, and J. Du (2002). "Simulating the lunar geomagnetic variations." In: *Journal of Geophysical Research: Space Physics* 107.A7, SIA 12–1–SIA 12–11. ISSN: 2156-2202. DOI: 10.1029/2001JA000240 (cit. on p. 72).

Stolle, C., C. Manoj, H. Lühr, S. Maus, and P. Alken (2008). "Estimating the daytime Equatorial Ionization Anomaly strength from electric field proxies." In: *Journal of Geophysical Research: Space Physics (1978–2012)* 113.A9. DOI: 10.1029/2007JA012781 (cit. on pp. 34, 53).

Sugiura, M. and J. C. Cain (1966). "A model equatorial electrojet." In: *Journal of Geophysical Research* 71.7, pp. 1869–1877. DOI: 10.1029/JZ071i007p-01869 (cit. on p. 21).

Sugiura, M. and D. J. Poros (1969). "An improved model equatorial electrojet with a meridional current system." In: *Journal of Geophysical Research* 74.16, pp. 4025–4034. DOI: 10.1029/JA074i016p04025 (cit. on p. 21).

Tarpley, J. D. (1970). "The ionospheric wind dynamo–I: Lunar tide." In: *Planetary and Space Science* 18.7, pp. 1075–1090. DOI: 10.1016/0032-0633(70)90109-1 (cit. on p. 20).

Van Bemmelen, W. (1912). "Die lunare variation des Erdmagnetismus." In: *Meteorol. Z* 29, pp. 218–225 (cit. on p. 20).

Van Loon, H. and K. Labitzke (2000). "The influence of the 11-year solar cycle on the stratosphere below 30 km: A review." In: *Space Science Reviews* 94.1-2, pp. 259–278. DOI: 10.1023/A:1026731625713 (cit. on p. 64).

Vial, F. and J. M. Forbes (1994). "Monthly simulations of the lunar semidiurnal tide." In: *Journal of Atmospheric and Terrestrial Physics* 56.12, pp. 1591–1607. DOI: 10.1016/0021-9169(94)90089-2 (cit. on pp. 19, 20).

Vincent, R. A. (1990). "Planetary and gravity waves in the mesosphere and lower thermosphere." In: *Advances in Space Research* 10.12, pp. 93–101. DOI: 10.1016/0273-1177(90)90388-G (cit. on p. 10).

Vineeth, C., T. K. Pant, and R. Sridharan (2009). "Equatorial counter electrojets and polar stratospheric sudden warmings–A classical example of high latitude-low latitude coupling?" In: *Annales Geophysicae: Atmospheres, Hydrospheres and Space Sciences*. Vol. 27. 8, p. 3147. DOI: 10.5194/angeo-27-3147-2009 (cit. on p. 22).

Waugh, D. W., W. J. Randel, S. Pawson, P. A. Newman, and E. R. Nash (1999). "Persistence of the lower stratospheric polar vortices." In: *Journal of Geophysical Research: Atmospheres* 104.D22, pp. 27191–27201. ISSN: 2156-2202. DOI: 10.1029/1999JD900795 (cit. on p. 64).

Yamazaki, Y. (2013). "Large lunar tidal effects in the equatorial electrojet during northern winter and its relation to stratospheric sudden warming events." In: *Journal of Geophysical Research: Space Physics* 118.11, pp. 7268–7271. DOI: 10.1002/2013JA019215 (cit. on pp. 38, 50, 54, 71, 100).

— (2014). "Solar and lunar ionospheric electrodynamic effects during stratospheric sudden warmings." In: *Journal of Atmospheric and Solar-Terrestrial Physics* 119, pp. 138–146. DOI: 10.1016/j.jastp.2014.08.001 (cit. on p. 21).

Yamazaki, Y., K. Yumoto, T. Uozumi, S. Abe, M. G. Cardinal, D. McNamara, R. Marshall, B. M. Shevtsov, and S. I. Solovyev (2010). "Reexamination of the Sq-EEJ relationship based on extended magnetometer networks in the east Asian region." In: *Journal of Geophysical Research: Space*

Physics 115.A9. A09319. ISSN: 2156-2202. DOI: 10.1029/2010JA015339 (cit. on p. 53).

Yamazaki, Y., K. Yumoto, M. G. Cardinal, B. J. Fraser, P. Hattori, Y. Kakinami, J. Y. Liu, K. J. W. Lynn, R. Marshall, D. McNamara, et al. (2011). "An empirical model of the quiet daily geomagnetic field variation." In: *Journal of Geophysical Research: Space Physics* 116.A10. DOI: 10.1029/2011JA016487 (cit. on pp. 19, 21).

Yamazaki, Y., K. Yumoto, D. McNamara, T. Hirooka, T. Uozumi, K. Kitamura, S. Abe, and A. Ikeda (2012a). "Ionospheric current system during sudden stratospheric warming events." In: *Journal of Geophysical Research: Space Physics (1978–2012)* 117.A3. DOI: 10.1029/2011JA017453 (cit. on p. 32).

Yamazaki, Y., A. D. Richmond, and K. Yumoto (2012b). "Stratospheric warmings and the geomagnetic lunar tide: 1958–2007." In: *Journal of Geophysical Research: Space Physics (1978–2012)* 117.A4. DOI: 10.1029/2012JA017514 (cit. on pp. 12, 23, 25, 32, 40, 42, 50, 52, 57, 70, 71, 99).

Yamazaki, Yosuke, Arthur D. Richmond, Astrid Maute, Qian Wu, David A. Ortland, Akimasa Yoshikawa, Isaac Abiodun Adimula, Babatunde Rabiu, Manabu Kunitake, and Takuya Tsugawa (2014). "Ground magnetic effects of the equatorial electrojet simulated by the TIE-GCM driven by TIMED satellite data." In: *Journal of Geophysical Research: Space Physics* 119.4, pp. 3150–3161. ISSN: 2169-9402. DOI: 10.1002/2013JA019487 (cit. on p. 17).

Yiğit, E. and A. S. Medvedev (2015). "Internal wave coupling processes in Earth's atmosphere." In: *Advances in Space Research* 55.4, pp. 983–1003. DOI: 10.1016/j.asr.2014.11.020 (cit. on p. 10).

Yiğit, E., P. K. Knížová, K. Georgieva, and W. Ward (2016). "A review of vertical coupling in the Atmosphere–Ionosphere system: Effects of waves, sudden stratospheric warmings, space weather, and of solar activity." In: *Journal of Atmospheric and Solar-Terrestrial Physics* 141, pp. 1–12. DOI: 10.1016/j.jastp.2016.02.011 (cit. on p. 8).

Zhang, J. T. and J. M. Forbes (2013). "Lunar tidal winds between 80 and 110 km from UARS/HRDI wind measurements." In: *Journal of Geophysical Research: Space Physics* 118.8, pp. 5296–5304. DOI: 10.1002/jgra.50420 (cit. on p. 21).

Zhang, X. and J. M. Forbes (2014). "Lunar tide in the thermosphere and weakening of the northern polar vortex." In: *Geophysical Research Letters* 41.23, pp. 8201–8207. ISSN: 1944-8007. DOI: 10.1002/2014GL062103 (cit. on pp. 26, 50, 51, 54, 55, 57, 59–62, 66, 67, 77, 98).

DECLARATION

I, Tarique Adnan Siddiqui, hereby declare that this thesis titled, 'Long-term investigation of the lunar tide in the equatorial electrojet during stratospheric sudden warmings' and the work presented in it are my own. I confirm that:

- I have fully acknowledged and referenced the ideas and work of others, whether published or unpublished, in my thesis.
- This dissertation has not been submitted for the award of any other degree or diploma in any other institution.

Potsdam, Mai 2017

Tarique Adnan Siddiqui